

Novel Therapeutic Approaches for Neuromuscular Diseases

Inauguraldissertation

zur

Erlangung der Würde eines Doktors der Philosophie

vorgelegt der

Philosophisch-Naturwissenschaftlichen Fakultät

der Universität Basel

von

Ruben Herrendorff

aus Wimmis (BE)

Basel, 2015

Originaldokument gespeichert auf dem Dokumenteserver der Universität Basel

edoc.unibas.ch

Genehmigt von der Philosophisch-Naturwissenschaftlichen Fakultät

auf Antrag von

Prof. Dr. Michael Sinnreich

Prof. Dr. Markus Rüegg

Prof. Dr. Beat Ernst

Basel, den 11. November 2014

Prof. Dr. Jörg Schibler

Dekan

Acknowledgements

“It is good to have an end to journey toward; but it is the journey that matters, in the end.”
(Ernest Hemingway)

On the PhD journey, which I have been pursuing during the last four years, many lovely people accompanied me and I would like to express my sincerest thanks to some of them on this occasion.

I would like to especially thank Prof. Michael Sinnreich for providing me with a very interesting drug discovery project for DM1, for his support, guidance and motivation. I would also like to thank Prof. Beat Ernst and Prof. Andreas J. Steck for initiating the anti-MAG neuropathy project and for having supported me as great mentors since my Master's. I admire the fascination for science and medicine of all three of you. Many thanks also go to Prof. Markus Rüegg for valuable feedback and for taking time to look at my thesis.

I would like to particularly thank all of the members of the Neuromuscular Research group, where is spent most of my PhD time: Dr. Jon Ashley, Dr. Bilal Azakir, Marielle Brockhoff, Dr. Perrine Castets, Dr. Sabrina Di Fulvio, Beat Erne, Frances Kern, Dr. Jochen Kinter, Dr. San Pun, Adeline Stiefvater and Dr. Tatiana Wiktorowicz. Thank you Jochen for supervising my project, for many interesting discussions, and for sharing many valuable insights. Frances, thank you so much for the warm welcome to the Sinnreich group. In addition, I would like to thank all members of the Institute of Molecular Pharmacy, where I started the PhD. You all ensured a stimulating and interesting working environment, many laughs, and a good time.

I would like to thank all our collaborators for making the DM1 project possible: Maria Teresa Faleschini, Prof. Matthias Hamburger, Dr. Olivier Potterat; Prof. David Boykin, Prof. Reto Brun, Dr. Tanja Wenzler; Jacqueline Bezençon and many others who helped and assisted me.

I am incredibly thankful to my friends and family for all their love and support. You're great! Unending thanks go to my dear parents, my sister and her fiancé, my parents-in-law, my godfather, my good old buddies, and also to my lovely wife. You're awesome!

Last but not least I would like to thank the Almighty for his protection, love and mercy. I would like to express my deepest gratitude to you for my life, which is nothing but a gift, with all its opportunities, e.g. the privilege to work in research. May I never forget you and may I never take all this for granted.

Summary

Neuromuscular diseases (NMDs) are a vast group of hereditary or acquired disorders which affect components of the peripheral nervous system (PNS) and / or skeletal muscle. In this thesis, we present new therapeutic approaches towards two diseases from this spectrum of mostly rare, but severe, disorders. The first disease, myotonic dystrophy type I (DM1), is a multisystemic genetic disorder that predominantly affects skeletal and cardiac muscle, but also involves other tissues. The second disease, anti-myelin associated glycoprotein (MAG) neuropathy, is an immune-mediated peripheral neuropathy that affects the peripheral nerve.

DM1 is caused by a mutation in a non-coding region of the dystrophia myotonica-protein kinase (DMPK) gene. The mutation leads to a mutated RNA that binds splicing factors such as muscleblind-like 1 (MBNL1). We developed an *in vitro* screening assay to identify small molecular weight inhibitors of the toxic RNA-MBNL1 interaction. In one screening project, we screened a collection of isolated natural substances and extracts from plants and fungal strains. This screening led to the identification of several alkaloids that improved aspects of the DM1 pathology in a cell model as well as in a mouse model of DM1. In a second screening project, that was based on a previously described DM1 lead compound, the antiprotozoal pentamidine, we screened a library of antiprotozoal small molecules. Here, we identified diimidazolines as a new group of small molecules that improved DM1 disease aspects in a cell model of the disease. Compounds from both screens have therapeutic potential for DM1 and RNA-mediated diseases in general, and could serve as valuable starting points for medicinal chemistry programs.

Anti-MAG neuropathy is an antibody-mediated autoimmune disorder. Immunoglobulin M (IgM) autoantibodies targeting the human natural killer-1 (HNK-1) glycoepitope on the myelin protein MAG are thought to be pathogenic. Based on the structure of the HNK-1 epitope we synthesized small molecular weight HNK-1 mimetics to block the IgM-MAG interaction. These mimetics were tested in an *in vitro* competitive binding assay. The mimetic with the closest structural similarity to the natural epitope displayed the strongest inhibitory activity on IgM autoantibody binding to MAG. Using this mimetic, we synthesized a polymer that presents the epitope in a multivalent fashion. This polymer blocked with high efficiency the pathogenic IgM autoantibodies from patient sera. It is biodegradable and could be used as a new therapeutic agent to deplete autoantibodies in the circulation of affected patients.

Table of Contents

Acknowledgements	I
Summary	II
List of Abbreviations.....	IV
List of Schemes	IX
List of Tables.....	X
List of Figures	XI
Preface.....	XII
1 Introduction to Neuromuscular Diseases	1
2 Myotonic Dystrophy Type I.....	2
2.1 Introduction.....	2
2.2 Molecular Disease Mechanism.....	2
2.3 Current Treatments	6
2.4 New Therapeutic Approaches.....	6
2.4.1 Antisense oligonucleotides	6
2.4.2 Enzymatic degradation of DMPK transcripts.....	7
2.4.3 Gene therapy	8
2.4.4 Small molecules.....	9
2.4.5 Aim of our study.....	9
2.5 Manuscript I.....	10
2.6 Manuscript II.....	39
2.7 Discussion.....	64
2.8 Conclusion and Outlook	69
3 Anti-Myelin Associated Glycoprotein Neuropathy	73
3.1 Introduction.....	73
3.2 Molecular Disease Mechanism.....	75
3.3 Current Therapeutic Approaches.....	80
3.3.1 Aim of our study.....	82
3.4 Manuscript III	82
3.5 Discussion.....	116
3.6 Outlook	119
4 Closing Words.....	120
References	121

List of Abbreviations

AAE	Adeno-associated virus
AICAR	5-Aminoimidazole-4-carboxamide ribonucleotide
AIDP	Acute inflammatory demyelinating polyneuropathy
AMPK	Adenosine monophosphate-activated protein kinase
AON	Antisense oligonucleotide
ASRE	Artificial site-specific RNA endonuclease
ATE1	Arginyltransferase 1
ATP	Adenosine triphosphate
AUC	Area under the curve
BCA assay	Bicinchoninic acid assay
BSA	Bovine serum albumin
C_{avg}	Average (plasma) concentration
CD20	B-lymphocyte antigen CD20 (MS4A2: membrane-spanning 4-domains, subfamily A, member 1)
cDNA	Complementary DNA
CELF1 (=CUGBP1)	CUGBP, elav-like family member 1
CIDP	Chronic inflammatory demyelinating polyneuropathy
CIDP	Chronic inflammatory demyelinating polyneuropathy
CLCN1 / CLC1	Chloride channel, voltage-sensitive 1 Chloride channel 1, skeletal muscle
C_{max}	Maximum (plasma) concentration
CNS	Central nervous system
COSY (NMR)	Correlated spectroscopy (NMR)
CRDs	Carbohydrate recognizing domains
CUGBP1	CUG triplet repeat, RNA binding protein 1
Cy3	Cyanine 3
DAPI	4,6 diamino-2-phenylindole dihydrochloride
DBU	Diazabicycloundecen
DCM	Dichloromethane
DEPC	Diethylpyrocarbonate (diethyl dicarbonate)
DHB	Dihydroberberine

DM1	Myotonic dystrophy type 1
DM2	Myotonic dystrophy type 2
DMAP	4-dimethylamino-pyridine
DMEM	Dulbecco's Modified Eagle's Medium
DMF	<i>N,N</i> -dimethylformamide
DMPK	Dystrophia myotonica-protein kinase
DMSO	Dimethyl sulfoxide
DNA	Desoxyribonucleic acid
DNAse	Desoxyribonuclease
DTT	Dithiotreitol
ECL	Electrochemiluminescence
EDA	Ethylenediamine
ELISA	Enzyme linked immunosorbent assay
EMSA	Electrophoretic mobility gel shift assay
ESI-MS	Electron spray ionization MS
ETR3	Elav-type RNA-binding protein 3
FBS	Fetal bovine serum
FHL1	Four and a half LIM domains 1
FISH	Fluorescence <i>in situ</i> hybridization
FT-IR	Fourier transform IR
Gal	Galactose
GBS	Guillain-Barré syndrome
GlcA	Glucuronic acid
GlcNAc	<i>N</i> -acetylglucosamine
GM1, GM1b, GD1a, GD1b, GT1a, GQ1b, etc. (general: GX _n)	G = ganglioside, X = number of sialic acids, n = characterizes the carbohydrate chain length and the sequence of migration on TLC, x = indicates the type of carbohydrate linkage
GST	Glutathione S-transferase
HEPES	4-(2-hydroxyethyl)-1-piperazineethanesulfonic acid
HIS	Polyhistidin (hexahistidine, His ₆)
HIV	Human immunodeficiency virus
HNK-1	Human natural killer-1
HPLC	High performance liquid chromatography
HRMS	High resolution MS

HRP	Horseradish peroxidase
HSA (LR / SR)	Human skeletal actin (long repeat / short repeat)
HSQC (NMR)	Heteronuclear single quantum coherence (NMR)
IC ₅₀ / Tox IC ₅₀	Half maximal inhibitory concentration / toxicity IC ₅₀
ICNMD	International congress on neuromuscular diseases
IgG	Immunoglobulin G
IgM	Immunoglobulin M
INCAT	Inflammatory neuropathy cause and treatment
INSR	Insulin receptor
IR	Infrared (spectroscopy)
IVIg	Intravenous immunoglobulin
K _D	Dissociation constant
L-MAG	Long MAG
LC-MS	Liquid chromatography-mass spectrometry
LD ₅₀	Median lethal dose
LNA	Locked nucleic acid
log <i>D</i> _{7.4}	Distribution co-efficient at pH 7.4
MAG	Myelin associated glycoprotein
MAO	Monoamino oxidase
MBNL1	Muscleblind-like 1
Me	Methyl
MeCN	Acetonitrile
MGUS	IgM monoclonal gammopathy of unknown significance
minHNK-1 epitope	Minimal HNK-1 epitope
MMN	Multifocal motor neuropathy
MOE	2'- <i>O</i> -Methoxyethyl
mRNA	Messenger RNA
MS	Mass spectrometry
MYOD (=MYOD1)	Myoblast determination protein 1 or myogenic differentiation 1
NMD	Neuromuscular disease
NMR	Nuclear magnetic resonance (spectroscopy)
NP-40	Tergitol-type NP-40, nonyl phenoxypolyethoxylethanol
Nucleobases A, C, T, G, U	Adenine, cytosine, thymine, guanine, uracil
OD	Optical density

<i>p</i> -MeOPh	<i>p</i> -methoxyphenyl
P0	Myelin protein zero
PAMPA	Parallel artificial membrane permeability assay
PBS	Phosphate buffered saline
PCR	Polymerase chain reaction
P_e	Effective permeation
PE	Plasma exchange
pK _a	Negative decadic logarithm of the acid dissociation constant
PKC	Protein kinase C
PL(minHNK-1)x	Polylysine loaded with x% minimal HNK-1 epitope
PMO	Morpholino AON
PMP22	Peripheral myelin protein 22
PNS	Peripheral nervous system
PPB	Plasma protein binding
PPMO	Peptide-linked morpholino AON
PROMM	Proximal myotonic myopathy
PS	Phosphorothioate
Py/pyr	Pyridine
qPCR	Quantitative PCR
RIPA	Radio-immunoprecipitation assay
RNA	Ribonucleic acid
RNAi	RNA interference
RNase H	Ribonuclease H
rt	Room temperature
RT-PCR	Reverse transcription PCR
RT-qPCR	Reverse transcription quantitative PCR
S1	Screening study 1 (natural compounds)
S2	Screening study 2 (synthetic compounds)
SDS	Sodium dodecyl sulfate
SDS-PAGE	Sodium dodecyl sulfate polyacrylamide gel electrophoresis
SERCA1	Sarcoplasmic/endoplasmic reticulum Ca ²⁺ ATPase 1
SGLPG	Sulfoglucuronyl lactosaminyl paragloboside
SGPG	Sulfoglucuronyl paragloboside
shRNA	Small hairpin RNA or short hairpin RNA

Siglec	Sialic acid-binding immunoglobulin-like lectin
S-MAG	Short MAG
SSC	Saline-sodium citrate
TAE	Tris/acetate/EDTA (ethylenediaminetetraacetic acid)
TAR RNA	Trans-activation response element RNA
TBE	Tris/Borate/EDTA (ethylenediaminetetraacetic acid)
TEA	Triethylamine
Tf	Trifluoromethanesulfonyl
TFA	Trifluoroacetic acid
THF	Tetrahydrofuran
TLC	Thin layer chromatography
TMB	Tetramethylbenzidine
TMSOTf	Trimethylsilyl trifluoromethanesulfonate
TNNT2	Cardiac troponin T type 2
TREDS	Triple nucleotide repeat expansion diseases
tRNA	Transfer RNA
Ts	<i>p</i> -toluylsulfonyl
Tween-20	Polyoxyethylene (20) sorbitan monolaurate
UTR	Untranslated region
UV-Vis	Ultraviolet-visible (spectroscopy)
WT	Wild type
ZNF9	Zinc finger protein 9

List of Schemes

Scheme 1 (II 1): Synthesis of DB1796 and DB1973. Reagents and conditions.	62
Scheme 2 (III 1): Synthesis of the minimal HNK-1 epitope in sulfated (1a,b) and unsulfated form (2). Reagents and conditions.	111
Scheme 3 (III 2): Synthesis of the minHNK-1 polymer 25. Reagents and conditions.	112

List of Tables

Table 1 (II 1): Physicochemical and pharmacokinetic parameters of di-imidazolines and the lead compound pentamidine.	63
Table 2: In vivo pharmacokinetic parameters of DB1796 and DB175.	69
Table 3: Diphenylfuran derivatives and their stabilization of poly(A)•(U) and poly(A)•(T) (93).	71
Table 4 (III 1): IC50 values of compounds 1a, 1b, 2 and the minHNK-1 polymer (25) for the four patient sera MK, DP, KH and SJ.	115
Table 5 (III 2): IC50 values of PL(minHNK-1)10-44 for patient sera KH, MK and SJ, and the monoclonal HNK-1 antibody (119).	115

List of Figures

Figure 1: Pathomechanism of DM1.....	3
Figure 2 (I 1): Screening for small molecules of natural origin that disrupt the MBNL1-CUG ₇₈ complex <i>in vitro</i>	30
Figure 3 (I 2): HPLC-based activity profiling of the methanol extract of <i>Peganum harmala</i>	30
Figure 4 (I 3): Representative RT-qPCR and RT-PCR splicing data for WT and DM1 control cells as well as treated DM1 human myoblast cells.....	31
Figure 5 (I 4): FISH detection of CUG _n RNA and immunofluorescence detection of MBNL1 in human WT and DM1 myoblasts.....	34
Figure 6 (I 5): Representative <i>in vivo</i> RT-qPCR splicing data for vehicle treated WT and HSA ^{LR} mice as well as compound treated HSA ^{LR} mice (quadriceps muscle).....	35
Figure 7 (I 6): Western immunoblot detection and quantification of CLCN1 protein levels in mouse quadriceps muscle.....	37
Figure 8 (II 1): Screening for nucleic acid binding small molecules that disrupt the MBNL1-CUG ₇₈ RNA complex <i>in vitro</i>	57
Figure 9 (II 2): Representative RT-qPCR and RT-PCR splicing data for WT and DM1 control cells as well as treated DM1 human myoblast cells.....	58
Figure 10 (II 3): Di-imidazolines do not affect alternative splicing of MBNL1-independently regulated ATE1 and FHL1 pre-mRNAs in treated DM1 myoblasts, compared to untreated WT and DM1 control myoblasts.....	60
Figure 11 (II 4): FISH detection of CUG _n RNA and immunofluorescence detection of MBNL1 in human WT and DM1 myoblasts.....	61
Figure 12: Mean concentration in mouse plasma over time profiles for DB1796 and DB175.....	68
Figure 13: The HNK-1 trisaccharide epitope.....	76
Figure 14: IgM autoantibodies target the HNK-1 epitope on MAG and other myelin components.....	78
Figure 15 (III 1): Representative competitive binding ELISA.....	113
Figure 16 (III 2): A-D: Binding curves for compounds 1a,b and 2 , and polymer 25	114
Figure 17 (III 3): Inhibition curves of PL(minHNK-1) ₁₀₋₄₄ with the HNK-1 reference antibody (119). Inhibitory activity of polymers approaches a maximum with increasing epitope loading.....	114
Figure 18 (III 4): Control polymer PL(minHNK-1) ₀ without minHNK-1 epitope loading does not inhibit IgM antibody binding from patient sera MK, KH, and SJ to MAG.....	115

Preface

“It is an exciting time to work in the field of neuromuscular diseases”. This was one of the closing remarks that Prof. Charles Thornton addressed to the younger researchers in the audience at the International Conference for Neuromuscular Diseases (ICNMD) 2014 in Nice, France during his keynote speech (10.07.2014). Prof. Thornton is an expert for neuromuscular diseases and one of the leading researchers in the field of myotonic dystrophy type I (DM1). Indeed, over the past decades many pathomechanisms have been elucidated for neuromuscular disorders. Thus, new targets for potential therapies have been identified and new therapies are being developed and evaluated in clinical trials.

Neuromuscular disorders are mostly rare, but they often impose a significant socio-economic burden on the patients as well as their families, relatives, friends etc. Therefore, identification of therapies for affected individuals is imperative. Indeed, for both of the here addressed neuromuscular diseases, DM1 and anti-MAG neuropathy, new therapies are needed and for both diseases currently new therapeutic agents are being evaluated in clinical trials.

The aim of this thesis is to evaluate novel therapeutic approaches for both of these diseases. The thesis describes the design and identification of new chemical agents and discusses their therapeutic potential. The work for the DM1 project was performed in the research group of Prof. Michael Sinnreich, Neuromuscular Research Group, Departments of Neurology and Biomedicine, University Hospital Basel. The work for the anti-MAG neuropathy project was performed in the research group of Prof. Beat Ernst, Molecular Pharmacy, University of Basel, and under the supervision of Prof. Andreas J. Steck, Departments of Neurology and Biomedicine, University Hospital Basel.

The thesis is written in a manuscript format. It contains two manuscripts addressing DM1 and one manuscript focusing on anti-MAG neuropathy. The manuscripts are currently unpublished, but ready for submission. A patent on several substances from the DM1 drug discovery project is pending. The anti-MAG neuropathy work has been published in a patent (EP14159528), March 2014. The basic structure of the thesis is given in the following part.

Chapter 1: The introductory part of the thesis gives a definition for neuromuscular diseases and outlines commonly encountered symptoms as well as the overall medical need.

Chapter 2: This chapter gives an introduction to the two known forms of myotonic dystrophy and then focuses on the more common form DM1. Its disease mechanism, clinical features and current therapeutic approaches are outlined. Subsequently, two manuscripts describe our drug discovery efforts for DM1. Manuscript I describes the screening of natural substances and the identification of alkaloids, whereas manuscript II describes the screening of a library of synthetic antiprotozoal small molecules and the identification of di-imidazolines. The therapeutic potential of the identified natural and synthetic small molecules is discussed.

Chapter 3: This chapter is dedicated to anti-MAG neuropathy. First, an introduction to immune-mediated neuropathies is given. Within this group of disorders, anti-MAG neuropathy is outlined in detail with regard to its pathomechanism and clinical aspects. Furthermore, current therapeutic approaches are outlined. Thereafter, manuscript III describes the synthesis and biological evaluation of new therapeutic agents and a new therapeutic approach with a glycopolymer. This new therapeutic approach for anti-MAG neuropathy is then discussed with respect to its potential clinical application.

Chapter 4: This chapter rounds up the described therapeutic approaches with final comments and an outlook into the future of treatments for the two addressed neuromuscular disorders.

1 Introduction to Neuromuscular Diseases

Neuromuscular diseases (NMDs) are a large group of hereditary or acquired disorders which affect the peripheral nervous system and / or the muscle apparatus. These diseases originate in dysfunctions of the peripheral nerves, the neuromuscular junctions, and the skeletal muscle (1, 2).

Degeneration and wasting of peripheral nerve or skeletal muscle tissue can lead to severe disability of affected individuals. In advanced disease states NMD patients often need specialized care. Symptoms frequently associated with NMDs are weakness (when motor neurons or muscles are affected) (1, 3, 4); stiffness and spasticity (when upper motor neurons are affected) (1); numbness, tingling and pain (when sensory nerves are affected) (1, 5); ataxia (when sensory or cerebellar neurons are involved), and a welter of other symptoms (1).

Muscular dystrophies, are characterized by degeneration and weakness of skeletal muscle (6) and muscle loss can cause life-threatening disability in muscular dystrophy patients. Degeneration of respiratory muscles (intercostal and diaphragmatic muscle) and cardiac muscle leads to respiratory and cardiac dysfunction in the two most common forms of muscular dystrophy, i.e. Duchenne muscular dystrophy and myotonic dystrophy type I (DM1). Respiratory failure is the most common cause of death in both of these muscular dystrophies. Another cause of death in DM1 is sudden cardiac failure through heart block or ventricular arrhythmia (7).

With respect to degeneration of peripheral nerve tissue, besides motor neurons also sensory neurons can be affected. Anti-MAG neuropathy is an example for a disorder primarily affecting sensory neurons (8) via an autoimmune attack of the axon-surrounding myelin sheaths.

Even though many NMDs are rare, a fact that dampens economic interest in the development of new therapies, there is a huge medical need in this area, which calls for new and better treatments. The following two chapters describe and discuss novel therapeutic approaches for DM1 and anti-MAG neuropathy, two disorders from the vast spectrum of NMDs.

2 Myotonic Dystrophy Type I

2.1 Introduction

Two types of myotonic dystrophy

There are two types of myotonic dystrophies that can be distinguished on the basis of clinical characteristics and genetic determinants (*loci*). Type I (DM1, Curschmann-Steinert) is caused by CTG triple nucleotide expansion in the 3' untranslated region (UTR) of the DMPK gene (9), whereas type II (DM2, proximal myotonic myopathy, PROMM) is caused by a CCTG expansion in intron 1 of the zinc finger protein 9 (ZNF9) gene (10).

Clinical aspects of DM1

DM1 is the more common form of the two variants and is in fact the most common form of muscular dystrophy among the adult population with an estimated prevalence of 1:8'000. The disease is inherited in an autosomal dominant manner and affects multiple organ systems, most visibly the skeletal muscle with wasting, weakness and an inability to relax (myotonia). Conduction defects in cardiac muscle lead to arrhythmia and may cause sudden death. Besides cataracts, endocrine and gastrointestinal disturbances, as well as insulin resistance, the CNS is also affected, leading to intellectual impairment and daytime somnolence. Compared to other muscular dystrophies, DM1 is somewhat unique with regard to its multisystemic nature, the occurrence of myotonia, and the phenomenon of anticipation. Anticipation means that affected members in succeeding generations show earlier disease onset and have more severe disease courses. Morbidity is high in DM1 with a significant mortality due to respiratory and cardiac dysfunction (7, 11).

2.2 Molecular Disease Mechanism

Location and characteristics of the CTG trinucleotide expansion

In contrast to the majority of genetic diseases, DM1 is not caused by mutated protein(s) but by a toxic effect of an RNA molecule (Fig 1B) (12, 13). A sequence of CTG triplet repeats, located in the 3' UTR of the DMPK gene, is abnormally elongated in patients (9, 14). Disease severity and age of disease onset correlate with the number of triplet repeat expansions (15, 16) (Fig 1A). Thus, four severity grades of DM1 are distinguished, late-onset/asymptomatic,

adult-onset, childhood-onset, and congenital, each correlating with increasing CTG expansion size (11). Germline instability of the genomic CTG expand is thought to be responsible for the anticipation phenomenon. Besides germline repeat expansion, also somatic expansion takes place which over a lifespan leads to a mosaicism, with very long expands occurring in muscle tissue compared to other tissues (17). The expansions probably take place during DNA repair (18).

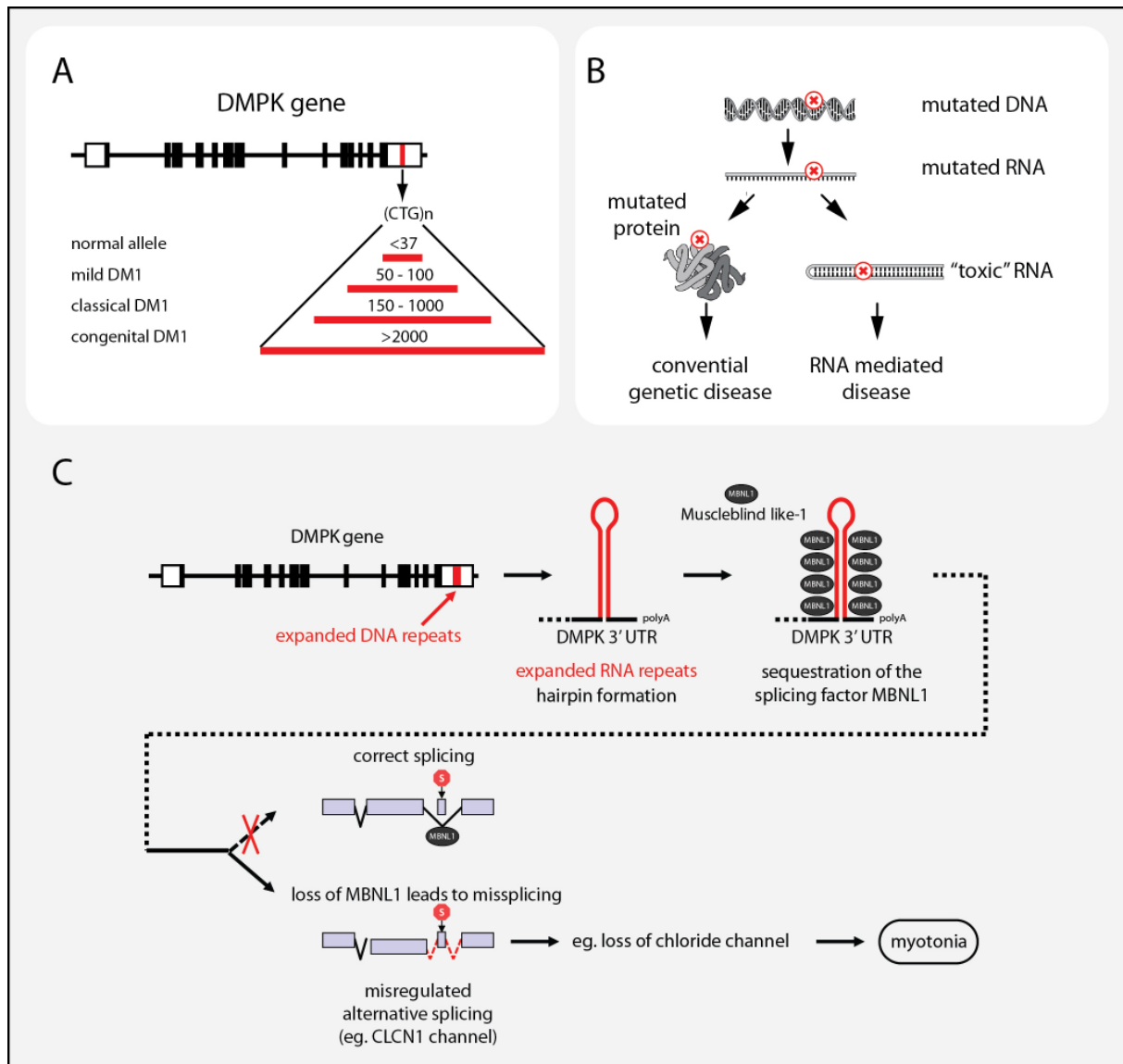


Figure 1: Pathomechanism of DM1. **A)** The molecular basis of DM1 is an expansion of an unstable repeat sequence in the noncoding part of the DMPK gene. Severity of disease is correlated with repeat expansion size. **B)** In DM1 the mutation is located in a noncoding region and does not alter the protein sequence, but leads to toxic RNA hairpins. **C)** Example of a splicing defect in DM1: The sequestration of the alternative splicing factor MBNL1 by toxic RNA leads to altered splicing of the muscle-specific CLCN1 chloride channel. The channel is lost, leading to symptoms of myotonia (Figure courtesy of Dr. J. Kinter).

A new paradigm of RNA toxicity

Although studies showed decreased DMPK levels in DM1 (19), the phenotype of DMPK deficient mice was not reminiscent of the DM1 disease phenotype (20, 21). These mice only developed a late onset and rather mild myopathy, indicating that altered DMPK levels might be responsible at most for a minor part of the DM1 disease features. To determine a potentially direct toxic effect of the DMPK-CUG_n RNA, the group of Prof. Charles Thornton designed and compared two mouse lines with a muscle-specific transgene. The HSA^{LR} mouse line contained a long CTG₂₅₀ repeat within the 3' UTR of a human skeletal actin transgene, whereas the HSA^{SR} contained a shorter CTG₅ repeat (12). The muscle phenotype of these HSA^{LR} mice was shown to recapitulate major features of the DM1 disease phenotype. Interestingly, the disease evocation seemed to be independent of the genetic *locus* of the expanded repeat (HSA instead of DMPK *locus*). These *in vivo* experiments were the first to provide evidence of the toxicity of expanded transcripts such as DMPK-CUG_n RNA in DM1. Subsequently analysis of other mouse models (DM300, DMSXL) showed that expression of expanded DMPK transcripts in the context of the human DM1 locus also recapitulated the skeletal muscle DM1 characteristics, and furthermore recapitulated cardiac, CNS and other DM1 features (22, 23). All of these mouse models—HSA^{LR}, DM300, DMSXL—are suitable for therapeutic studies (23).

Molecular effects of toxic DMPK-CUG_n transcripts

How does this toxic DMPK-CUG_n RNA exert its toxic effect? The CTG_n expansion in the human DM1 locus leads to RNA transcripts with expanded CUG repeats. These fold into double stranded, A-form DNA-like hairpins that sequester splicing factors, such as MBNL1 (24, 25). The mutant DMPK RNA transcripts are retained in the nuclei of DM1 cells where they form aggregates with MBNL1, so-called *foci* (26-28). The resulting lack of available MBNL1, due to RNA sequestration, leads to mis-regulated alternative splicing of a multitude of pre-mRNAs in various tissues, such as the skeletal muscle chloride channel (CLCN1) (29-31) (Fig. 1C), the insulin receptor (INSR) (32, 33), sarcoplasmic/endoplasmic reticulum Ca²⁺ ATPase 1 (SERCA1) (34) and cardiac troponin T type 2 (TNNT2) (35). The multitude of genes mis-spliced in DM1 accounts for the multisystemic nature of DM1 (11).

Correlation of mis-splicing and specific disease symptoms

The mis-splicing of a specific gene and its correlation with a specific disease symptom can be well explained with the example of the chloride channel CLCN1 (Fig. 1C). The chloride channel CLCN1 is developmentally regulated in skeletal muscle, such that fetal muscle cells

do not express this channel (31). The fetal mRNA of CLCN1 includes a “developmental” exon (exon 7a). Inclusion of this exon in the mRNA causes a shift in the open reading frame leading to premature termination of translation and to the translation of a truncated/nonfunctional CLCN1 protein that is sent for degradation. It is only after removal of this “fetal” exon, through developmentally-regulated, MBNL1-dependent alternative splicing, that the CLCN1 transcript can yield a functional protein in mature muscle. In DM1 patients, the splicing factor MBLN1 is sequestered by CUG_n-RNAs and cannot exert its function on target pre-mRNAs, including the pre-mRNA of CLCN1 (29, 30). CLCN1 is present at the plasma membrane of skeletal muscle and is responsible for maintaining the resting potential of the muscle cell at a precise level. Absence of CLCN1 alters the chloride conductance of the muscle plasma membrane and leads to myotonia (36). Along the same lines, the mis-splicing of the insulin receptor pre-mRNA leads to increased expression of a receptor isoform with decreased insulin-sensitivity, which accounts for symptoms of diabetes (32).

MBNL1 and other splicing factors involved in DM1

The importance of MBNL1 sequestration for the DM1 pathomechanism was shown by means of a MBNL1 knockout mouse model (37). The phenotype of this mouse model recapitulated major DM1 defects such as mis-splicing, myotonia, myopathy and faithfully mimicked the multisystemic nature of DM1. Overexpression of MBNL1 in the HSA^{LR} mouse model successfully reversed mis-splicing and myotonia (38). These findings indicate that the toxic effect of expanded DMPK-CUG_n transcripts are mainly mediated through MBNL1 sequestration.

MBNL1 and other members of the MBNL family are major regulators of alternative splicing and are involved in a shift from fetal to post-natal splicing patterns (39). The human MBNL genes are homologous with the *Drosophila muscleblind* gene, which is substantially involved in eye and muscle differentiation (24). Alternative splicing occurs in about 41 – 60% of genes in the human genome and accounts for an enormously rich protein diversity via different splicing isoforms for a specific gene (40). Besides MBNL proteins, other splicing factors involved in the DM1 pathomechanism are members of the CUG-BP and ETR3-like factor (CELF) proteins (31). The CUG binding protein 1 (CUGBP1, CELF1) and MBNL1 work antagonistically in the splicing regulation of the INSR and TNNT2 pre-mRNA (33, 35). The steady-state levels of CUGBP1 are augmented in nuclei of DM1 cells/tissues via PKC-mediated hyperphosphorylation and stabilization of CUGBP1 (41).

The interaction of the toxic DMPK transcripts with splicing factors, the resulting formation of *foci* and disruption of splicing are the best-studied molecular features of DM1. However, the toxic RNA transcripts might affect many other cellular pathways, e.g. the mentioned PKC activation. According to comments of Prof. C. Thornton at the ICNMD 2014, as yet undetected translation products of the CUG_n expansions could contribute to the DM1 pathomechanism.

2.3 Current Treatments

There is no causal treatment available for DM1 patients to date. Patients are currently treated symptomatically, such as with cardiac monitoring with pacemaker implantation, if required, and the removal of cataracts (7, 11). Pain, e.g. muscle or abdominal pain, can be treated with analgesics; diabetic symptoms with anti-diabetic drugs such as glitazones (42). Daytime sleepiness is treated with the CNS stimulant Modafinil in some patients (43).

2.4 New Therapeutic Approaches

Now that the molecular pathomechanism for DM1 is known, it is possible to design causal treatments. The toxic DMPK-CUG_n transcript has been identified as the culprit of the disease and has therefore been the molecular target of interest in most studies evaluating new therapeutic approaches. Therapeutic approaches aimed at either at displacement of splicing factors from the DMPK transcripts, in particular MBNL1, or at the degradation of toxic DMPK RNA transcripts. Seminal therapeutic studies had shown that, either by overexpression of MBNL1 (38) or displacement of MBNL1 from CUG_n-RNA (13), the pathomechanism of DM1 can be reversed. Following this direction, many therapeutic approaches have been investigated and are briefly mentioned in this section.

2.4.1 Antisense oligonucleotides

RNA interference (RNAi) as well as antisense oligonucleotide (AON) therapeutics have been successfully used to interfere with the DM1 pathomechanism in mouse models of the disease. Two RNAi studies showed that RNAi are effective in silencing toxic DMPK transcripts, these studies are discussed in more detail in section 2.4.3 as these studies made use of viral vectors and can thus be regarded as RNAi-based gene therapy (44, 45). AON therapeutics have been

used to either liberate splicing factors from toxic DMPK transcripts (13, 46) or degrade the toxic transcripts (47, 48). The study of Wheeler *et al.* was performed with an intramuscularly injected CAG₂₅ morpholino AON (PMO) in HSA^{LR} mice (13). Splicing, *foci* formation and myotonia was corrected in injected and electroporated muscles. However, PMOs are not suited for systemic delivery due to insufficient cell-permeability. Therefore, a peptide-linked morpholino AON (PPMO) with increased permeability was synthesized. It was delivered systemically (intravenously) to HSA^{LR} mice and successfully restored aspects of the DM1 pathology, i.e. splicing, *foci* and myotonia (46). However, there are unsolved issues regarding toxicity of cationic peptides and suitable peptides have to be screened as clinical candidate compounds.

The degradation of DMPK transcripts is particularly promising as nuclear-retained DMPK CUG_n transcripts (and other nuclear-retained transcripts) were shown to be unusually vulnerable to antisense silencing in studies by Lee *et al.* and Wheeler *et al.* (47, 48). Both studies used gapmer AONs either targeting the CUG_n repeats (47) or targeting DMPK sequences up- or downstream of the CUG_n repeats (48). Gapmer AONs contain modified nucleotides with increased RNA affinity and resistance to nucleases at both ends and a central gap of unmodified nucleotides or RNase H-tolerated phosphorothioate (PS) nucleotides to attract RNase H. RNase H recognizes RNA-DNA duplexes and mediates cleavage as well as decay of the target RNA. Lee *et al.* used locked nucleic acid (LNA) or 2'-*O*-Methoxyethyl (MOE) nucleic acids for the ends and PS nucleotides for the gap. Wheeler *et al.* used MOE nucleotides at the ends, unmodified nucleotides for the gap region and a PS nucleotide at both gap borders.

These and other antisense chemistries are currently being investigated with respect to nuclease resistance and membrane permeability. Delivery of AONs remains a big challenge. A first AON therapeutic, a gapmer, is moving towards clinical trials. ISIS Pharmaceuticals is currently preparing a clinical phase I trial with their ISIS-DMPKRx development candidate. One drawback of AONs and other therapeutic agents designed to degrade the mutant DMPK transcripts is that they also reduce DMPK protein expression, which might cause therapeutic side effect. Nevertheless, DMPK deficient mice have shown only a very mild and late-onset muscle phenotype, thus DMPK might be partly dispensable (20, 21).

2.4.2 Enzymatic degradation of DMPK transcripts

Apart from AON therapeutics designed to degrade the toxic DMPK transcripts, enzymatic degradation approaches have been investigated, i.e. degradation by ribozymes and exonucle-

ases. Ribozyme target sites were detected in the 3'UTR of the DMPK transcript, thus Langlois *et al.* designed a nuclear-retained hammerhead ribozyme, expressed under a tRNAm^{eti} promoter, to cleave DMPK transcripts (49). This approach reduced the DMPK transcript by 63% in transfected DM1 myoblasts and furthermore reduced nuclear *foci*. Following a similar path, Zhang *et al.* designed artificial site-specific RNA endonucleases (ASREs) to bind and cleave the mutant DMPK transcripts (50). This approach resulted in reduction of nuclear *foci* and splicing restoration of several genes in transfected myoblasts. Both ribozymatic and enzymatic degradation of toxic CUG_n RNA present gene therapeutic approaches; they were discussed in this subchapter due to their uniqueness. More gene therapy studies are discussed in the following subchapter.

2.4.3 Gene therapy

Delivery of exogenous MBNL1 is a therapeutic approach which was successfully tested in the HSA^{LR} mouse model (38). Delivery was achieved by intramuscular injection with an adeno-associated virus (AAV). The overexpression of MBNL1 was able to saturate the CUG binding sites of the toxic CUG_n transcripts and excess free MBNL1 reversed the mis-splicing and myotonia in the mouse model. Another study by D. Furling *et al.*, used retroviral *in vitro* transfection of human DM1 myoblasts with an antisense RNA complementary to CUG₁₃ and to 110bp following the repeat tract (44). This study showed that antisense RNA delivery with a retrovirus decreased mutant RNA and ameliorated CUGBP1 levels and aspects of myoblast function. A study by Langlois *et al.* also investigated an RNAi-based gene therapy approach using lentiviral delivery of shRNA to fetal DM1 myoblasts to silence DMPK transcripts (45). Thus, DMPK RNA was successfully down-regulated. At the ICNMD 2014 conference D. Furling presented yet unpublished data on a new gene therapy with an engineered “mini” MBNL1 that displaces native MBNL1 from toxic RNA transcripts. Native MBNL1 can thus perform its proper splicing function.

So far, no such gene therapy has been tested in DM1 patients. Issues with systemic delivery, inadequate transfection efficiency and the immunogenicity of viral vectors still hamper the use of gene therapy in the clinics.

2.4.4 Small molecules

Following in the footsteps of the proof of concept study by Wheeler *et al.* (13), which had initially described the reversibility of the DM1 pathomechanism by displacement of MBNL1 from CUG_n-RNA by means of an AON, several studies aimed to identify small molecules which are able to work similarly as the AON. Small molecules, compared to AONs and gene therapy approaches (e.g. RNAi, MBNL1 overexpression, enzymes to cleave DMPK RNA), have the potential to readily penetrate into a multitude of tissues, including the CNS. A variety of small molecules has been described, which interfere with the MBNL1 CUG_n RNA complex and improve DM1-associated molecular defects *in vitro*, and in some cases also *in vivo*: Several approaches successfully yielded small molecules, such as screening of known nucleic acid binders (51), RNA structure-based rational design of small molecules (52), rational design of oligomers of CUG_n-RNA binders by modular assembly (53, 54), combinatorial chemistry (55, 56), and high throughput screening (57, 58). Furthermore, small molecules have been identified that act on other targets than the MBNL1 CUG_n RNA complex. These molecules include gene transcription modulators (59), kinase modulators (60, 61), or Ras farnesyltransferase inhibitors (62).

The challenge with small molecules is to find compounds with reasonable target selectivity and low toxicity. Targeting RNA is a challenge due to (i) smaller structural variability of RNA and (ii) high flexibility of RNA, both compared to protein targets (63). Besides RNA, other cellular targets, such as kinases, are of interest with respect to DM1 small molecule drug discovery. These protein targets might pose less of a hurdle regarding selectivity and toxicity.

2.4.5 Aim of our study

Our study aimed to identify of novel small molecules to target the MBNL1 CUG_n RNA complex with potential ameliorating effects on DM1-associated defects. We screened small molecules of natural and of synthetic origin. Our first study (manuscript I) is the first to specifically focus on natural compounds drug discovery in the DM1 field and includes the screening of an extract library. The second study (manuscript II) is based on the lead compound pentamidine (51) and describes the screening of synthetic pentamidine-related antiprotozoal compounds. Both studies describe the discovery of new small molecules with therapeutic potential for DM1.

2.5 Manuscript I

Identification of Plant-derived Alkaloids with Therapeutic Potential for Myotonic Dystrophy Type I

Ruben Herrendorff¹, Jochen Kinter¹, Frances Kern¹, Maria Teresa Faleschini², Matthias Hamburger², Olivier Potterat², Michael Sinnreich^{1*}

¹ Neuromuscular Research Group, Departments of Neurology and Biomedicine, University Hospital Basel, Switzerland

² Division of Pharmaceutical Biology, Department of Pharmaceutical Sciences, University of Basel, Klingelbergstrasse 50, CH-4056 Basel, Switzerland

* To whom correspondence should be addressed.

Abstract

Myotonic dystrophy type I (DM1) is a disabling neuromuscular disease affecting multiple organ systems, predominantly skeletal muscle, with no causal treatment available. This disease is caused by expanded CTG triplet repeats in the 3' UTR of the Myotonic Dystrophy Protein Kinase (DMPK) gene, and the disease severity is roughly correlated to the repeat expansion size. On the RNA level these expanded CUG repeats (CUG_n) form hairpin structures, which lead to ribonuclear inclusions. More specifically, the RNA with expanded CUG repeats sequesters splicing-factors, such as muscleblind-like 1 (MBNL1). Lack of available MBNL1 leads to mis-regulated alternative splicing of many target pre-mRNAs, leading to the multisystemic symptoms in DM1.

To date, many studies aiming to identify small molecules targeting the MBNL1-CUG_n complex have been focusing on synthetic molecules. In an effort to identify new small molecules that liberate sequestered MBNL1 from CUG_n-RNAs we focused specifically on small molecules of natural origin. Natural products remain an important source for drug substances and play a significant role in providing novel leads and pharmacophores for medicinal chemistry. In a new DM1 mechanism-based biochemical assay, we screened a collection of isolated natural compounds, and a library of over 2100 extracts from plants and fungal strains. HPLC-based activity profiling in combination with spectroscopic methods were used to identify the active principles in the extracts. Bioactivity of the identified compounds was investigated in a human cell model of DM1, as well as in a mouse model of DM1. We identified several alkaloids, including the beta-carboline harmine and the isoquinoline alkaloid berberine, which rescued certain aspects of the DM1 pathology in these models. Alkaloids as a compound class may have potential for drug discovery in other rare RNA-mediated diseases like myotonic dystrophy type II, fragile-X tremor ataxia syndrome and different types of spinocerebellar ataxias.

Introduction

Myotonic dystrophy type I (DM1) is one of the most common neuromuscular diseases with relatively high prevalence numbers of about 1:8'000 in the adult population (11). This autosomally dominant inherited disease affects multiple organs, most prominently the skeletal muscle, with wasting, weakness and an inability to relax (myotonia) (11). Currently, there is no effective treatment for this disabling disease. The pathomechanism of DM1 is linked to a CTG_n expansion in the 3' UTR of the Myotonic Dystrophy Protein Kinase (DMPK) gene (9, 14) leading to a toxic gain-of-function RNA (12, 13). The mutant DMPK transcript is entrapped within nuclei of affected cells, where it forms aggregates (*foci*) with splicing factors such as muscleblind-like 1 (MBNL1) (26, 27). Bound to mutant DMPK CUG_n RNA, MBNL1 is no longer available for correct splicing of its target pre-mRNAs (24, 25). Thus, the splicing of a multitude of pre-mRNAs is mis-regulated, including the skeletal muscle chloride channel (CLCN1), the insulin receptor (INSR), sarcoplasmic/endoplasmic reticulum Ca²⁺ ATPase 1 (SERCA1) and cardiac troponin T type 2 (TNNT2) pre-mRNA (29, 30, 32, 34, 35, 39, 64). Interestingly, the mis-splicing of some pre-mRNAs can directly be linked to a certain disease symptom, e.g. in the case of the CLCN1 pre-mRNA. It is developmentally regulated by MBNL1; after birth MBNL1 promotes the exclusion of the alternative exon 7a from the CLCN1 pre-mRNA. Hence, MBNL1 sequestration by CUG_n RNA causes inclusion of exon 7a, leading to a shift in the open reading frame and to premature termination of translation (29, 30). As a result of this, functional CLCN1 protein is decreased and resting chloride conductance is reduced, which leads to myotonic discharges characteristic of DM1 (65).

To date, most therapeutic strategies towards DM1 focused either on the development of agents degrading the toxic RNA or blocking its pathogenic interaction with proteins; these strategies are reviewed in ref. (66). Antisense oligonucleotides targeting the DMPK-CUG_n transcripts have been shown to reverse the toxic RNA effect *in vitro* and *in vivo* (13, 47). Viral overexpression of MBNL1 also resulted in a reversal of the toxic RNA effect *in vivo* (38). Compared to the antisense oligonucleotide and gene-therapy approaches, an advantage of a suitable small molecule drug is its potential to penetrate into all tissues affected in DM1 patients, as well as its likely oral bioavailability. A variety of small molecules have been described that interfere with the MBNL1-CUG_n RNA complex and improve DM1 associated molecular defects *in vitro* and in some cases also *in vivo*. Several approaches were successful in identifying small molecules, such as screening of known nucleic acid-binders (51), rational

design of small molecules based on the structure of CUG_n RNA (52), rational design of oligomers of CUG_n RNA binders by modular assembly (53, 54), combinatorial chemistry (55, 56), and high throughput screening (57, 58). Increasingly, molecules are identified that act on other targets than the MBNL1-CUG_n RNA complex. These molecules include gene transcription modulators (59), kinase modulators (60, 61, 67), or Ras farnesyltransferase inhibitors (62).

With respect to the small molecule strategy, most DM1 drug discovery studies have been focusing on synthetic small molecules to target the CUG_n RNA. Only a few small molecules of natural origin have been described to target the toxic repeat RNA, such as neomycin B (51) and lomofungin (57). To our knowledge, our study is the first to focus on small molecules of natural origin and represents the first screening of natural extracts in a DM1 drug discovery effort. Natural products represent a rich source of structurally diverse entities and remain an important source for novel leads and pharmacophores in medicinal chemistry (68). We describe here the screening of isolated natural compounds and extracts from plants and fungal strains in a novel DM1 RNA-MBNL1 inhibition assay, using a DMPK-CUG₇₈ RNA. We identified several alkaloids as MBNL1-CUG_n RNA complex inhibitors. Testing their bioactivity in a human myoblast model of DM1, as well as in the HSA^{LR} mouse model of DM1, showed that the alkaloids ameliorated certain aspects of the DM1 pathology.

Results

Identification of small molecules of natural origin, which disrupt the MBNL1-CUG₇₈ RNA complex *in vitro*

A collection of 70 isolated natural compounds and a library containing 2128 extracts from plants and fungi were screened with a novel *in vitro* CUG₇₈-MBNL1 inhibition assay (Fig. I 1A). For the screening assay we used *in vitro* transcribed CUG₇₈ RNA and purified recombinant MBNL1-HIS (25). Compounds were co-incubated with recombinant MBNL1-HIS in 96-well plates containing immobilized CUG₇₈ RNA, and then MBNL1-CUG₇₈ complex inhibition was measured by antibody detection of RNA-bound MBNL1-HIS. From the compound library we identified the isoquinoline alkaloid berberine (Fig. I 1B) as a complex formation inhibitor with an IC₅₀ of 86.3 ± 5.8 μM (Fig. I 1C). Another alkaloid, isaindigotone, showed weak inhibitory activity at 100 μM concentration. From the extract library we identified 21

extracts that inhibited MBNL1-CUG₇₈ complex formation by at least 40%, as compared to no-compound controls, at a concentration of 100 µg/mL. In order to identify the active principles in the extracts we used an approach referred to as HPLC-based activity profiling. It combines separation of complex mixtures with spectroscopic data recorded on-line, and with biological information obtained in parallel from time-based microfractionation and subsequent bioassay (69). In addition, off-line microprobe NMR analysis was used to fully establish the structure of active compounds. The ten extracts with the strongest inhibitory activity were fractionated using this approach, and the resulting 29 or 30 fractions per extract were retested in the CUG₇₈-MBNL1 inhibition assay. The alkaloid harmine (Fig. I 1B) was identified as an active constituent in a methanolic extract from roots of *Peganum harmala* (Nitrariaceae) (Fig. I 2). Besides, two closely related diterpenquinones, methylenetanshinquinone and 1,2-dihydrotanshinquinone, were detected in the active fractions of an ethyl acetate extract from roots of *Salvia miltiorrhiza* (Lamiaceae). A commercial sample of harmine had an IC₅₀ of 132.4 ± 9.3 µM (Fig. I 1C), whereas the two diterpenquinones, also commercially obtained, showed weak inhibitory activity at 100 µM concentration. The inhibitory activity of the remaining eight extracts could be assigned to tannins, since the activity was lost after filtration of the extracts through a polyamide cartridge (data not shown) (70). Based on the structure of the isoquinoline alkaloid berberine, the most active compound from our screening, we searched for structural analogues with higher inhibitory activity. In this effort, we identified the synthetic alkaloid coralyne (Fig. I 1B), a fully planar berberine derivative, as a strong MBNL1-CUG₇₈ complex inhibitor with an IC₅₀ of 17.8 ± 0.2 µM, (Fig. I 1C). As reference compounds, Hoechst 33258 and neomycin B, two known nucleic acid-binders, were tested and had IC₅₀ values of 195.5 ± 3.0 µM and 5.3 ± 0.6 µM, respectively. Pentamidine, a previously described lead compound for DM1 (51), had no inhibitory effect on complex formation, even at a concentration as high as 500 µM.

Identified alkaloids improve splicing in a human myoblast cell model of DM1

The alkaloids identified in our *in vitro* screening assay were tested for their ability to reverse mis-splicing in human DM1 myoblasts. We investigated the alternative splicing of the insulin receptor (INSR) and cardiac troponin T type 2 (TNNT2) pre-mRNA in two human fibroblast cell lines containing a doxycycline inducible MYOD construct (71). The wild type (WT) cell line contained a CUG₅ repeat in the 3' UTR of the DMPK gene, whereas the DM1 cell line contained a CUG₁₃₀₀ repeat. These cell lines were differentiated into myoblasts by addition of

doxycycline, which induced MYOD expression. As indicators of differentiation, MYOD and desmin expression were confirmed with IHC staining (data not shown). Differentiated DM1 myoblasts were treated for one day with the identified alkaloids, followed by RNA isolation, reverse transcription, and quantitative PCR (qPCR). DMSO-treated WT and DM1 cells served as controls. For the quantification of alternative splicing, a qPCR-based method was developed that makes use of two primer pairs. One primer pair detected all alternative splicing variants of a pre-mRNA and the other primer pair detected only those variants which included an investigated alternative exon. Berberine rescued the splicing of the TNNT2 pre-mRNA but had a negative effect on the INSR pre-mRNA splicing (Fig. I 3A). TNNT2 pre-mRNA splicing was rescued by $62.1 \pm 3.2\%$ (20 μM), $75.1 \pm 2.8\%$ (40 μM) and $86.2 \pm 0.8\%$ (80 μM) through berberine treatment (Fig. I 3A). In contrast to berberine, harmine improved the splicing of the TNNT2 pre-mRNA by $53.3 \pm 3.5\%$ (20 μM), $76.8 \pm 1.6\%$ (40 μM) and $66.1 \pm 1.2\%$ (80 μM) (Fig. I 3B). Furthermore, it also improved splicing of the INSR pre-mRNA by $55.4 \pm 3.3\%$ at a concentration of 80 μM (Fig. I 3B). The synthetic berberine derivative coralyne and the two diterpenequinones, identified together with harmine during the extract screening, showed no effect on splicing in the DM1 cell model (data not shown). The alternative splicing results obtained with the qPCR method were confirmed with classical RT-PCR and visualization of two alternatively spliced isoforms of the INSR and TNNT2 pre-mRNA on 3% agarose gels (Fig. I 3C,D). To investigate the selectivity of berberine and harmine, we tested their effect on alternative splicing of two genes known to be alternatively spliced, but independently of MBNL1, i.e. ATE1 and FHL1 (Fig I 3E,F) (72). We analyzed exon 7 inclusion in the ATE1 pre-mRNA, which was close to 33% for the WT cell line and close to 40% in the DM1 cell line. Exon 5 inclusion in the FHL1 pre-mRNA was close to 0.1 - 0.2% for both the WT and the DM1 cell line. Compared to untreated WT and DM1 control cells, treatment of DM1 cells with berberine and harmine (both at 20 μM and 80 μM) did not show any significant difference in alternative splicing of both genes.

Harmine reduces CUG_n repeat *foci* formation in a human myoblasts cell model for DM1

To examine whether the alkaloids reduced the sequestration of MBNL1 by CUG_n RNA, *foci* formation was investigated in the same human cell lines used in the cellular splicing assay. Immunofluorescence staining in both the WT and the DM1 cell line showed that MBNL1 was mainly localized to the nuclei. In the DM1 cells, punctuate staining of MBNL1 within the

nucleus could be co-localized in *foci* with Cy3-CAG₁₀ probe staining. Upon addition of 80 μ M harmine, we observed a clear reduction in the intensity and quantity of the *foci* (Fig. I 4A). However, 40 μ M concentration of harmine was not sufficient to reduce *foci* formation. Berberine did not reduce *foci* formation, neither at 40 μ M, nor at 80 μ M (Fig I 4A). Quantification of *foci* in a total of 150 randomly chosen nuclei per condition showed a significant decrease in *foci* number for 80 μ M harmine-treated DM1 myoblasts to 0.9 ± 0.2 *foci* per nucleus, compared to DMSO-treated DM1 myoblasts with 4.7 ± 0.3 *foci* per nucleus (Fig. I 4 B). MBLN1 staining gave a rather diffuse, nuclear and cytoplasmic localization, indicative of the release of MBLN1 from the toxic CUG_n RNA and its redistribution. 80 μ M berberine treatment in contrast seemed to increase the number of *foci* to 5.8 ± 0.9 *foci* per nucleus (Fig. I 4B).

Cellular toxicity evaluation of berberine and harmine

Before testing the identified alkaloids *in vivo*, we evaluated their cellular toxicity in a cell viability assay. C2C12 mouse myoblasts were treated with the alkaloids at concentrations ranging from 1 to 900 μ M and the concentrations were determined at which half of the cells remained viable after two days of compound incubation, i.e. toxicity IC₅₀ (Tox IC₅₀) values. Berberine yielded a Tox IC₅₀ value of 212.1 ± 18.3 μ M, whereas harmine gave a value of 123.3 ± 4.6 μ M. The IC₅₀ values from the CUG₇₈-MBNL1 inhibition assay (Fig. I 1A) and the Tox IC₅₀ values were relatively close to each other for both alkaloids. However, both of the compounds showed an effect on alternative splicing in our cell model at concentrations significantly lower than the IC₅₀ and Tox IC₅₀ values, e.g. at 20 μ M (Fig I 3). Mitomycin C was measured as a reference compound and yielded a Tox IC₅₀ of 20.4 ± 1.6 μ M.

Identified alkaloids ameliorate splicing of the CLCN1 pre-mRNA in the HSA^{LR} DM1 mouse model

We treated HSA^{LR} mice, a DM1 model containing a CTG₂₅₀ repeat expressed under an actin promoter, with the identified alkaloids (12). We administered the compounds in a short treatment protocol, consisting of 2 injections at an interval of 12h. 2-4 hours after the second injection, mice were sacrificed, and quadriceps muscle dissected for splicing and protein analysis. Groups of a minimum of three mice were either treated with vehicle or with com-

pounds at two or three dose levels. The compounds were tested for their ability to restore splicing of the CLCN1 (29, 30) and SERCA1 (34) pre-mRNA. MBNL1 promotes the exclusion of the alternatively spliced exon 7a of the CLCN1 pre-mRNA and promotes the inclusion of exon 22 of the SERCA1 pre-mRNA (29, 30, 34). WT mice at the age of 10 to 12 weeks showed a CLCN1 pre-mRNA exon 7a inclusion of $5.0 \pm 0.5\%$, whereas in the HSA^{LR} line the inclusion level was elevated to $40.9 \pm 2.5\%$. The level of SERCA1 pre-mRNA exon 22 inclusion in the WT mice was at $83.9 \pm 2.9\%$. In the HSA^{LR} mice exon 22 inclusion was decreased to $24.8 \pm 2.7\%$. Splicing was analyzed by qPCR, analogously to the splicing analysis in human myoblasts. Compared to vehicle-treated control mice, treatment of HSA^{LR} mice with 20 mg/kg berberine i.p. showed a clear effect on CLCN1 pre-mRNA as well as on SERCA1 pre-mRNA splicing, but was highly toxic to treated mice. Treatment with 5 mg/kg and 10 mg/kg was better tolerated but did not result in any significant splicing improvement (data not shown). We therefore tested two close derivatives of berberine, dihydroberberine (DHB) and palmatine, with higher reported LD₅₀ values, i.e. lower toxicity. DHB improved the splicing of the CLCN1 pre-mRNA at the higher dose of 10 mg/kg by 32.5% ($P=0.0008$, Student's t-test), whereas 5 mg/kg showed no statistical significant effect (Fig. I 5A). The CLCN1 splicing improvement by 10 mg/kg DHB was confirmed by classical RT-PCR and analysis of splicing isoforms on a 3% agarose gel (Fig. I 5D). Palmatine treatment improved the CLCN1 pre-mRNA splicing at a dose of 40 mg/kg by 34.8% ($P=0.0009$), and at a dose of 25 mg/kg by 25.3% ($P=0.0017$), whereas 10 mg/kg did not show a significant effect (Fig. I 5B). Harmine treatment at a dose of 40 mg/kg decreased CLCN1 pre-mRNA exon 7a inclusion by 31.2% ($P=0.0003$) and did not significantly improve splicing at a dose of 20 mg/kg (Fig. I 5C). DHB, palmatine and harmine had no significant effect on SERCA1 pre-mRNA splicing (Fig. I 5). Only the initially tested 20 mg/kg berberine had shown an improvement of SERCA1 pre-mRNA splicing.

CLCN1 protein levels in quadriceps muscle of WT, HSA^{LR}, and treated HSA^{LR} mice.

We examined by Western immunoblot analysis whether the high dose alkaloid treatments, which had ameliorated CLCN1 pre-mRNA splicing, also increased protein levels of functional full-length CLCN1 channel *in vivo*. Using a rabbit polyclonal antibody against the N-terminus of full-length CLCN1 (30), the CLCN1 channel was detected at the expected size of 130 kD in nuclear/membrane fractions of quadriceps muscle of WT and HSA^{LR} mice. As a

protein loading control, we used Lamin B. CLCN1 protein levels in quadriceps muscle of four vehicle-treated HSA^{LR} mice were decreased by $29.1 \pm 12.4\%$ ($p=0.023$, Student's t-test, $n=4$, three immunoblots) compared to four vehicle-treated WT mice (Fig. I 6). Treatment of HSA^{LR} mice with 10 mg/kg DHB raised CLCN1 protein levels by $27.1 \pm 16.1\%$ ($p=0.095$, $n=4$), compared to levels of vehicle treated HSA^{LR} mice (Fig I 6). Although the CLCN1 protein levels of DHB-treated HSA^{LR} mice were close to WT levels, the effect did not reach statistical significance. Both the palmatine and harmine high dose treatments of 40 mg/kg did not increase the CLCN1 protein levels in HSA^{LR} mice (Fig I 6).

Discussion

Drug discovery for RNA targets is an emerging field, and a variety of compounds have been described to bind to specific RNA secondary structural elements (63). Interestingly, many known RNA-binding drugs are of natural origin, such as antibiotics that target the bacterial ribosomal RNA (73). Hence, it is of interest to investigate compounds of natural origin in drug discovery efforts for RNA-mediated diseases such as DM1. Furthermore, as RNA is still a relatively unexploited drug target, natural products present a rich source of new and diverse chemical scaffolds for medicinal chemistry programs (68).

In our *in vitro* screening we identified aromatic alkaloids that inhibited the formation of the MBNL1-CUG₇₈ RNA complex: Berberine, coralyne and harmine. Aromatic alkaloids might be of particular interest for RNA drug discovery as they can interact with RNA via stacking, hydrogen-bonding, or electrostatic interaction (63), and have been previously shown to bind to double stranded RNA (74). To our knowledge, in the context of DM1, no alkaloids have been described hitherto as therapeutic compounds. Although, an *in vitro* screening study by Chen *et. al.* yielded six hits of which four were alkaloids or alkaloid derivatives of the opioid and ergot alkaloid-type, none of these alkaloids could be confirmed in a second screening assay (58). From our three identified alkaloids, berberine and harmine displayed restorative effects in the DM1 models used in this study. Interestingly, both have been described before to bind to specific RNA structures, such as double stranded RNAs, tRNA, and polyA RNA (74-77). In spite of the weak IC₅₀ values in the CUG₇₈-MBNL1 inhibition assay, both compounds ameliorated distinct molecular defects in the human DM1 myoblasts. Berberine strongly improved TNNT2 splicing, however, it worsened the INSR splicing (Fig. I 3A,C) and increased the number of *foci* in the nuclei of DM1 myoblasts (Fig. I 4A,B). Both undesirable effects might be due to compound binding to the natural target pre-mRNAs of MBNL1

and interference with MBNL1 splicing. MBNL1-targeted pre-mRNAs and the toxic DMPK-CUG_n transcripts share the same MBNL1 binding motifs (78). Harmine in contrast improved the splicing of both the TNNT2 and INSR pre-mRNA (Fig. I 3B,D) and nearly completely eliminated *foci* formation in the DM1 myoblasts at 80 μ M concentration.

One major obstacle in RNA drug discovery is to transfer *in vitro* activity into cellular and *in vivo* activity (63). We found that our *in vitro* assay selects for two types of strong *in vitro* complex inhibitors: (i) Highly charged molecules, such as neomycin B, with unfavorable pharmacokinetic profiles that hamper membrane permeation and (ii) unselective nucleic-acid binders such as coralyne. The aminoglycoside neomycin B was identified as a MBNL1-CUG₄ complex inhibitor by Warf *et al.*; it did not show any splicing amelioration in a DM1 cell model (51). We confirmed the strong complex inhibition of neomycin B in our *in vitro* assay (IC₅₀ 5.3 \pm 0.6 μ M). Coralyne also displayed strong complex inhibition in our *in vitro* assay (IC₅₀ 17.81 \pm 0.2 μ M, Fig. I 1B), but failed to improve the splicing in DM1 myoblasts. The fully planar coralyne has been described as a complete intercalator for double stranded RNA and tRNA (74); its insufficient selectivity for the CUG_n RNA might be the reason for its lacking bioactivity in our study. It is understandable that screening hits with (i) low membrane permeability and/or (ii) unselective nucleic acid-binding easily fail to transfer their *in vitro* activity into cellular or *in vivo* activity. Berberine and harmine, despite moderate *in vitro* inhibitory activity, are membrane permeable and also show a degree of selectivity for MBNL1-dependent alternative splicing events (Fig. I 3E,F). Their binding to the CUG_n RNA might, however, involve an intercalative component, as both are rather planar. Indeed, berberine has been described as a partial intercalator for double-stranded RNA (74).

We also tested berberine and harmine in the HSA^{LR} mouse model for DM1. We suggest that the time point of muscle dissection is crucial to detect a potential splicing effect and that the splicing effect is dependent on the pharmacokinetic profile, especially the *in vivo* half-life time, of the tested compound. Performing a short treatment protocol and muscle dissection 2-4 h after the second injection, both alkaloids led to improvement of CLCN1 splicing in HSA^{LR} mice at high doses, i.e. 40 mg/kg harmine (Fig. I 5) and 20 mg/kg berberine. At these doses, both compounds showed side effects. Harmine is described as a tremorogenic substance (79). We indeed observed tremors in the HSA^{LR} mice after administration of harmine, and an adaptation effect after a few repeated doses (80). Berberine was highly toxic to mice treated with 20 mg/kg, we therefore tested it at lower doses (5 and 10 mg/kg) that were better tolerated but no longer improved splicing. Berberine has been described as an inhibitor of

complex I in the mitochondrial respiratory chain (81); hence, decreased metabolic activity might account for the side effects we observed, notably the reduced activity and decreased body temperature. The effect of berberine on thermoregulation in mice has been previously described by Jiang *et al.* (82). Toxicity and off-target effects of berberine- or harmine-type alkaloids will have to be modified by means of medicinal chemistry in future studies. Concerning off-target effects, berberine is a strong AMPK activator (83) and harmine has been described as a DYRK kinase inhibitor (84). Both, berberine and harmine furthermore exert CNS effects, given that both are monoamine oxidase (MAO)-inhibitors (85, 86). On the one hand, this is a side effect that requires modulation; on the other hand, the fact that both alkaloids penetrate the blood brain barrier stirs hope for a future small molecule therapy that also ameliorates the CNS pathology associated with DM1. To address toxicity of berberine we tested less toxic derivatives in HSA^{LR} mice. The structurally similar dihydroberberine (DHB) significantly improved splicing of the CLCN1 pre-mRNA at a dose of 10 mg/kg, as did palmatine at 25 and 40 mg/kg (Fig. I 5). 10 mg/kg DHB treatment furthermore caused a trend towards increased protein levels of correctly spliced CLCN1 channel in quadriceps muscle of HSA^{LR} mice, as shown by Western immunoblot analysis (Fig. I 6). Alkaloids, such as berberine-types, might therefore ameliorate the myotonia caused by CLCN1 pre-mRNA mis-splicing.

In conclusion, we report on the discovery of several plant-derived alkaloids as novel bioactive small molecules with therapeutic potential for DM1. Through inhibition of the CUG_n-MBNL1 complex, presumably by intercalating toxic CUG_n RNA, the alkaloids ameliorate certain aspects of the DM1 pathology. Most interestingly, two alkaloids of the berberine-type and the alkaloid harmine significantly improve the splicing of the CLCN1 pre-mRNA in the HSA^{LR} mouse model. The identified alkaloids are not suited for therapeutic application themselves; the relatively low potency and toxicity are issues that require medicinal chemistry optimization. However, these molecules help to further understand the characteristics of small molecules that interact with toxic CUG_n RNA and provide new chemical scaffolds for medicinal chemistry studies, thus contributing to further progress in small molecule drug discovery for this disabling neuromuscular disease.

Experimental

Compounds

Compounds and extracts screened in this study were part of natural product libraries established at the Division of Pharmaceutical Biology of the University of Basel. One library contained 70 pure natural compounds as 10 mM solutions in DMSO and a second library consisted of 2128 extracts from plants and fungi archived as 10 mg/mL solutions in DMSO (69). Harmine hydrochloride was purchased TCI Europe (#H0002). Berberine chloride (#B3251), palmatine chloride hydrate (#361615), coralyne sulfoacetate (#S424536) were ordered from Sigma Aldrich. Dihydroberberine (#80429) was purchased from PhytoLab GmbH. Methylentanshinquinone (#QP-393) and 1,2-dihydrotanshinquinone (#QP-1166) were obtained from Quality Phytochemicals LLC, East Brunswick, NJ,

MBNL1 preparation

MBNL1 cDNA (isoform with amino acids 1–382) was kindly provided by Maurice Swanson (25), *University of Florida*, USA. The pGEX-6P-MBNL1-N-His (amino acids 1–253) construct used in this study was cloned according to Yuan *et al.* (25). Using BL21 expression cells, protein expression was induced with 0.1 mM isopropyl- β -D-thiogalactosid (IPTG) at an $OD_{600} = 0.8$ –1, for 3–4 h at 30 °C and 180 rpm. Bacteria were pelleted at 7000 rpm for 10 min at 4 °C, the supernatant was discarded and the pellet frozen. The pellet was lysed in lysis buffer (50 mM Tris [pH 8.5], 150 mM NaCl, 5 mM dithiotreitol (DTT) and 10% glycerol) containing 1 mg/mL of lysozyme, 10 μ g/mL DNase, and protease inhibitors 0.5 μ g/mL aprotinin, 1 μ g/mL pepstatin, 2 μ g/mL leupeptin and 1 mM phenylmethanesulfonylfluoride (PMSF). N-octyl- β -D-glucopyranoside was added to a final concentration of 7.3 mg/mL and the lysate was rocked for 15 min at room temperature (rt). After three times of freezing in liquid nitrogen and thawing in hand-hot water, the cell extract was centrifuged at 4 °C for 10 min at 13000 rpm and the supernatant, containing GST-MBNL1-HIS, was collected. GST-MBNL1-HIS protein was bound to His-Select Nickel Affinity Gel beads (Sigma) overnight at 4 °C in equilibration buffer (50 mM Tris [pH 7.4], 150 mM NaCl, 1 mM DTT, 10% glycerol). Beads were washed 1x with equilibration buffer and 1x with equilibration buffer containing

10 mM imidazole. Protein was eluted from beads with elution buffer (equilibration buffer + 500 mM imidazole).

Eluted protein was then bound to Glutathione Sepharose 4B beads (GE Healthcare) by incubation in equilibration buffer for 4 h at 4 °C. Beads were washed 1x with equilibration buffer. MBNL1-HIS was cleaved from beads in cleavage buffer (10 mM Tris [pH 7.4], 50 mM NaCl, 1 mM DTT) overnight at 4 °C with PreScission Protease (GE Healthcare). The eluate was collected, protein concentration determined with the NanoDrop spectrophotometer and a BCA assay (Sigma). The purity of MBNL1-HIS was evaluated by means of SDS-PAGE. MBNL1-HIS aliquots were snap frozen in liquid nitrogen and stored at -70°C.

CUG₇₈ RNA preparation

For this study we used a CAG₇₈ repeat from a blood sample of a patient, who gave informed consent. Genomic DNA was isolated from the patient sample with the Puregene Blood Core Kit B (Qiagen) according to the manufacturer's protocol. A genomic fragment located in the DMPK gene, containing the CAG₇₈ repeat, was PCR amplified with HOT Start DNA Polymerase (Solis BioDyne) by addition of Solution S. The following primers were used for PCR: DMPK forward - 5' CAG CTC CAG TCC TGT GAT CC^{3'} and DMPK reverse - 5' CTG GCC GAA AGA AAG AAA TG^{3'}. The amplicon was agarose gel purified by means of the QIAquick Gel Extraction Kit (Qiagen). The purified DNA fragment was cloned by TA-cloning with the pCR II-TOPO plasmid vector in Dh5α bacterial cells. The plasmid was purified with the QIAprep Spin Miniprep Kit (Qiagen) and used as template for PCR amplification with the following primers: T7 CUG forward - 5' TAA TAC GAC TCA CTA TAG GCA GCT CCA GTC CTG TGA TCC^{3'} and T7 CUG reverse - 5' TAA TAC GAC TCA CTA TAG GCT GGC CGA AAG AAA GAA ATG^{3'}. The amplified DNA was purified with the QIAquick PCR Purification Kit (Qiagen) and the concentration measured with the NanoDrop spectrophotometer. 200 ng of DNA was used as a template for *in vitro* RNA transcription by means of the MEGAscript T7 transcription kit (Ambion). CUG₇₈ RNA was biotin-labeled by addition of 1.875 mM biotin-14-CTP (37.5 nmol), 6.625 mM CTP (112.5 nmol), and 7.5 mM ATP, GTP and UTP to the transcription reaction. RNA quality and purity was tested by visualization of RNA on denaturing 8 M urea/TBE 5% polyacrylamide gels.

Screening assay: CUG₇₈-MBNL1 inhibition assay

All wash steps were performed at rt with 150 μ L wash buffer per well (25 mM Tris [pH 7.4], 80 mM NaCl, 1 mM MgCl₂, 0.5 mM DTT, 0.05% Tween-20, 1.5 mg/mL BSA, DEPC-treated water). The incubation steps were performed with 50 μ L incubation buffer per well (wash buffer + 25 U/mL RNasin) at 30 °C on a BIOSAN plate shaker at 300 rpm. Reacti-Bind NeutrAvidin coated 96-well plates (Pierce) were prewashed once. Wash buffer was removed and of incubation buffer containing 25 ng of biotinylated CUG₇₈ RNA was added per well. After incubation for 1 h the plates were washed twice. Wash buffer was removed and 45 μ L incubation buffer containing 300 ng of MBNL1-HIS was added followed by the addition of 5 μ L of 10x concentrated compound or 5 μ L of DMSO/water for controls. After washing wells twice, mouse anti-HIS antibody (1:2000, GE Healthcare, #27-4710-01) was incubated for 1 h. Another two wash steps preceded 1 h incubation with goat anti-mouse-HRP antibody (1:8000, Jackson ImmunoResearch Laboratories, #115-035-174). After two final wash steps, 70 μ L of TMB substrate (Thermo Scientific) was added to the wells at rt. The colorimetric reaction was performed at 30 °C, 700 rpm for 3 to 5 min and stopped with 70 μ L 0.15 M H₂SO₄ per well. The optical density was read at 450 nm wavelength with a Molecular Devices plate reader. Inhibition curves were fitted with Prism® software and the IC₅₀ values determined.

HPLC-based activity profiling of extracts

HPLC-based activity profiling was performed on a Waters 2695 Alliance Separation Module equipped with a Waters 996 Photodiode Array (PDA) detector and a C18 SunFire column (3.0 x 150 mm; 3.5 μ m; Waters). Mobile phase consisted of 0.1% formic acid in H₂O (A) and MeCN (B), and a gradient of 5 to 95% B in 30 min was applied. The flow rate was 0.5 mL/min. 900 μ g of extract were injected in three portions and time-based microfractions were collected into a deep well 96-well microtiter plate (30 fractions of 60 s each). The microtiter plate was then dried in a Genvac EZ-2 evaporating system at 35 °C overnight. For screening, the dried fractions were taken up in 16 μ L of DMSO, and 1 or 2 μ L were used in the screening assay.

Cell splicing assay

The two used human fibroblast cell lines (WT and DM1) with an inducible MyoD construct for differentiation into myoblasts were kindly provided by Denis Furling, Université Pierre et Marie Curie-Paris, Paris, France (71). These cell lines were grown in monolayers in growth medium (DMEM with GlutaMAX, 10% FBS, 30 mM HEPES, 50 µg/mL gentamycin) at 37 °C under 5% CO₂. 50'000 cells per well were seeded in 0.1% gelatin-coated 6-well plates and grown for 2.5 to 3 days. Cells were washed 1x with DMEM, then differentiation medium (= growth medium + 5 µg/mL Doxycycline) was added. After 24 h of differentiation the cells were washed with DMEM. The myoblast culture was then treated for 24 h with the compounds of interest or DMSO in differentiation medium. The cells were washed 1x with PBS and total RNA was extracted with TRI reagent (Sigma) according to the manufacturer's protocol. The resulting RNA pellet was taken up in 20 µL of RNase free water and the concentration of the isolated RNA was determined with a NanoDrop spectrophotometer. 500 ng of RNA was used for reverse transcription, which was performed with the SuperScript III First-Strand Synthesis System for RT-PCR (Invitrogen) according to the manufacturer's protocol with random hexamer primers. Of the resulting cDNA 1 µL was used as template for PCR, with gene specific primers, with a T_m of 61 °C, and 40 amplification cycles. Two PCR methods were used to quantify the splicing of marker genes:

(1) RT-PCR: In this protocol PCR was performed as described above with the following primer pairs: INSR forward - 5'CCA AAG ACA GAC TCT CAG AT^{3'} and reverse - 5'AAC ATC GCC AAG GGA CCT GC^{3'}; TNNT2 forward - 5'ATA GAA GAG GTG GTG GAA GAG TAC^{3'} and reverse - 5'GTC TCA GCC TCT GCT TCA GCA TCC^{3'}. Amplification was performed with HOT Start DNA Polymerase (Solis BioDyne) and an Applied Biosystems PCR machine. The PCR products were run on 3% agarose gels stained with RedSafe (iNtRON). Gels were imaged with a Gel Doc XR+ (Bio-Rad) and the band densities were quantified with the ImageJ software.

(2) RT-qPCR: In this protocol PCR was performed as described above with two primer pairs for each gene, one primer pair only amplifying those splicing variants which contain an investigated alternative exon (exon) and the other primer pair amplifying all possible splicing variants (pan): INSR forward - 5'GAC CTG GTC TCC ACC ATT CG^{3'} and reverse (exon) - 5'CAC CAG TGC CTG AAG AGG TT^{3'} and reverse (pan) - 5'ACG AAA ACC ACG TTG TGC AG^{3'}; TNNT2 forward - 5'CTG CTG TTC TGA GGG AGA GC^{3'} and reverse (exon) - 5'TCG TCC TCT CTC CAG TCC TC^{3'} and reverse (pan) - 5'CTG CTC CTC CTC CTC GTA

CT^{3'}. As gene expression control β -actin was used with the following primers: forward - 5'CCA ACC GCG AGA AGA TGA^{3'} and reverse - 5'CCA GAG GCG TAC AGG GAT AG^{3'}. Amplification was performed with HOT FIREPol EvaGreen qPCR Mix (Solis BioDyne) on an Applied Biosystems qPCR machine. The amplification efficiencies of the individual reactions were determined via standard curves and the splicing quantification was done with Excel® software.

MBNL1-independent splicing

The effect of the tested alkaloids on MBNL1-independent splicing events was analyzed using the same RT-qPCR protocol (2), with primers for two alternatively spliced genes, ATE1 and FHL1 (72). ATE1 forward - 5'GGG TTT CCA GGC TCA AGG TC^{3'} and reverse (exon) - 5'TGA ACT GCG AAC TTG GTG GA^{3'} and reverse (pan) - 5'TGT GTG ATG CAT TCT CTG GTA A^{3'}. FHL1 forward - 5'ATG CCG ATT GCT TTG TGT GT^{3'} and reverse (exon) - 5'CTG GGT GGC TCA CTC TTG AC^{3'} and reverse (pan) - 5'TCT TGC ATC CAG CAC ACT TCT^{3'}.

FISH and immunofluorescence

Human fibroblasts were seeded on 0.3% gelatin-coated coverslips in 24-well cell culture dishes (15000 cells/well) and grown for up to 24 h in growth medium at 37 °C under 5% CO₂. After a wash step with DMEM, cells were differentiated in differentiation medium for 24 h. Another wash step with DMEM preceded the compound addition in differentiation medium and incubation for 24 h. Cells were washed in PBS and fixed for 10 min in 4% paraformaldehyde phosphate buffered solution. Cells were washed 3x in PBS for 5 min and permeabilized for 5 min in PBS, 0.2% Triton X-100. For the probing with Cy3-CAG₁₀ coverslips were pre-washed in 2xSSC, 30% formamide for 10 min at rt. Hybridization was performed for 2 h at 37 °C with 1 ng/ μ L Cy3-CAG₁₀ in incubation buffer (30% formamide, 2X SSC, 2 μ g/mL BSA, 66 μ g/mL yeast tRNA, 2 mM vanadyl complex, 0.05% Triton X-100). Coverslips were then washed once in 2xSSC, 30% formamide buffer for 30 min at 37°C, once with 1xSSC for 30 min at rt and twice with PBS, 0.05% Triton X-100 for 10 min each.

Coverslips were then incubated for 15 min at rt in blocking buffer (3% BSA, PBS, 0.05% Triton X-100) followed by overnight incubation at 4 °C with 1:5000 diluted MBNL1 antibody (A2764, kind gift from C. Thornton) in PBS, 0.05% Triton X-100 and washed twice in PBS 0.05% Triton X-100 for 10 min. Goat anti-rabbit DyLight 488 antibody (Jackson Immu-

noresearch Laboratories, #111-485-144) was added at a dilution of 1:750 in PBS for 1 h in PBS 0.05% Triton X-100. Coverslips were then washed twice in PBS 0.05% Triton X-100 for 10 min. Cells were stained with 1:20000 DAPI (4,6 diamino-2-phenylindole dihydrochloride) for 5 min in PBS 0.05% Triton X-100 and washed twice in PBS 0.05% Triton X-100 for 10 min. Coverslips were then mounted on glass slides with FluorSave reagent (Calbiochem) and dried for at least one day before imaging. For quantification the amount of *foci* was counted for 150 randomly chosen nuclei from three experiments, 50 nuclei per experiment and condition.

Cell viability assay

C2C12 mouse myoblasts were plated in 96-well plates in growth medium, 4000 cells in 100 μL /well, and grown overnight at 37 °C under 5% CO_2 . 65 μL of medium was removed and 35 μL of 2x concentrated compound in growth medium added and incubated for 48 h. Compound concentrations ranged from 1 to 900 μM . As a reference compound mitomycin C (#M0440, Sigma) was used. After compound incubation 14 μL of CellTiter-Blue reagent (Promega), containing the dye resazurin, was added per well and incubated at 37 °C under 5% CO_2 for 1.5 h. Viable cells convert resazurin to resorufin, which is fluorescent. The fluorescence was then measured by means of an Infinite F500 plate reader (Tecan), with an excitation wavelength of 535 nm and an emission wavelength of 590 nm. Signal-concentration curves were fitted with Prism® software to determine Tox IC_{50} values.

Treatment in mice

HSA^{LR} transgenic mice in line 20b were kindly provided by Charles Thornton, University of Rochester, USA. FVB/N WT control mice were obtained from the animal facility of the Department of Biomedicine, University Hospital Basel, Switzerland. Age- and gender-matched groups of WT or HSA^{LR} mice were treated by intraperitoneal (i.p.) injections of compounds or vehicle. We used male mice at an age of 10 to 12 weeks. Considering the short *in vivo* half-life times of isoquinoline alkaloids such as berberine (87) and beta-carboline alkaloids such as harmine (88), we performed a short *in vivo* treatment protocol with two i.p. injections at an interval of 12 h and sacrificed the mice 2-4 h after the second injection. Harmine hydrochloride was administered in saline, dihydroberberine and palmatine hydro-

chloride in 5% DMSO/PBS. The quadriceps, tibialis anterior and gastrocnemius muscles of mice were dissected for analysis. For splicing and protein analysis quadriceps muscle was powdered after freezing in liquid nitrogen and aliquots stored at -70°C . Animal studies were conducted in accordance with the Animal Research Authorities of the canton of Basel, Switzerland.

Mouse splicing assay

Powdered quadriceps muscle tissue was taken up in TRI reagent (Sigma) and was grinded with a rotor-stator Polytron® (Kinematica) for 30 s at 4°C . Extracellular matrix material and debris was then removed by a centrifugation step at 12000 rpm, 4°C for 10 min. The supernatant was transferred into a new tube and RNA was extracted according to the TRI reagent (Sigma) manufacturer's protocol. Reverse transcription, PCR, and splicing analysis was performed as described earlier for the cell splicing assay. In the RT-PCR protocol (1) the following primers were used: CLCN1 forward - $5^{\prime}\text{GGA ATA CCT CAC ACT CAA GGC C}^3^{\prime}$ and reverse - $5^{\prime}\text{CAC GGA ACA CAA AGG CAC TGA ATG T}^3^{\prime}$; SERCA1 forward - $5^{\prime}\text{GCT CAT GGT CCT CAA GAT CTC AC}^3^{\prime}$ and reverse - $5^{\prime}\text{GGG TCA GTG CCT CAG CTT TG}^3^{\prime}$. In the RT-qPCR protocol (2) the following primer pairs were used: CLCN1 forward (exon) $5^{\prime}\text{GGG CGT GGG ATG CTA CTT TG}^3^{\prime}$ and forward (pan) - $5^{\prime}\text{CTG ACA TCC TGA CAG TGG GC}^3^{\prime}$ and reverse - $5^{\prime}\text{AGG ACA CGG AAC ACA AAG GC}^3^{\prime}$; SERCA1 forward - $5^{\prime}\text{GCC CTG GAC TTT ACC CAG TG}^3^{\prime}$ and reverse (exon) - $5^{\prime}\text{ACG GTT CAA AGA CAT GGA GGA}^3^{\prime}$ and reverse (pan) - $5^{\prime}\text{CCT CCA GAT AGT TCC GAG CA}^3^{\prime}$.

Western immunoblot detection of CLCN1 protein from mouse muscle

Proteins were extracted from powdered mouse quadriceps muscle according to Dimauro *et al.* (89) to obtain the nuclear/membrane fraction. Instead of using the NET buffer from the Dimauro protocol (89), RIPA+ buffer was used (50 mM Tris HCL [pH 8.0], 150 mM NaCl, 1% NP-40, 0.5% sodium deoxycholate, 1% Triton X-100, 0.1% SDS, 10% glycerol), containing protease and phosphatase inhibitor tablets (Roche). Protein concentrations were determined with a BCA assay (Sigma). 10 ug per sample were separated by Tris-glycine SDS-PAGE on a 8% gel and analyzed by Western immunoblot using Protran BA85 nitrocellulose membranes (GE Healthcare), rabbit polyclonal anti-CLCN1 antibody (1:1000, kind gift from Thomas Cooper, Baylor College of Medicine, USA) (30) and HRP-tagged goat anti-rabbit

secondary antibody (1:10000, Jackson Immunoresearch, #11-035-003). To detect Lamin B, goat polyclonal anti-Lamin B antibody (1:1000, Santa Cruz Biotechnology, #sc-6216) and HRP-tagged swine anti-goat antibody (1:10000, Life Technologies, #ACI3404) were used. All antibodies were incubated in TBS, 3% BSA, 0.1% Tween-20, 0.08% SDS. Protein bands were detected with the ECL technique using LumiGLO (KPL) chemiluminescent substrate. Membranes were exposed to Super RX films (Fuji).

Figures and legends

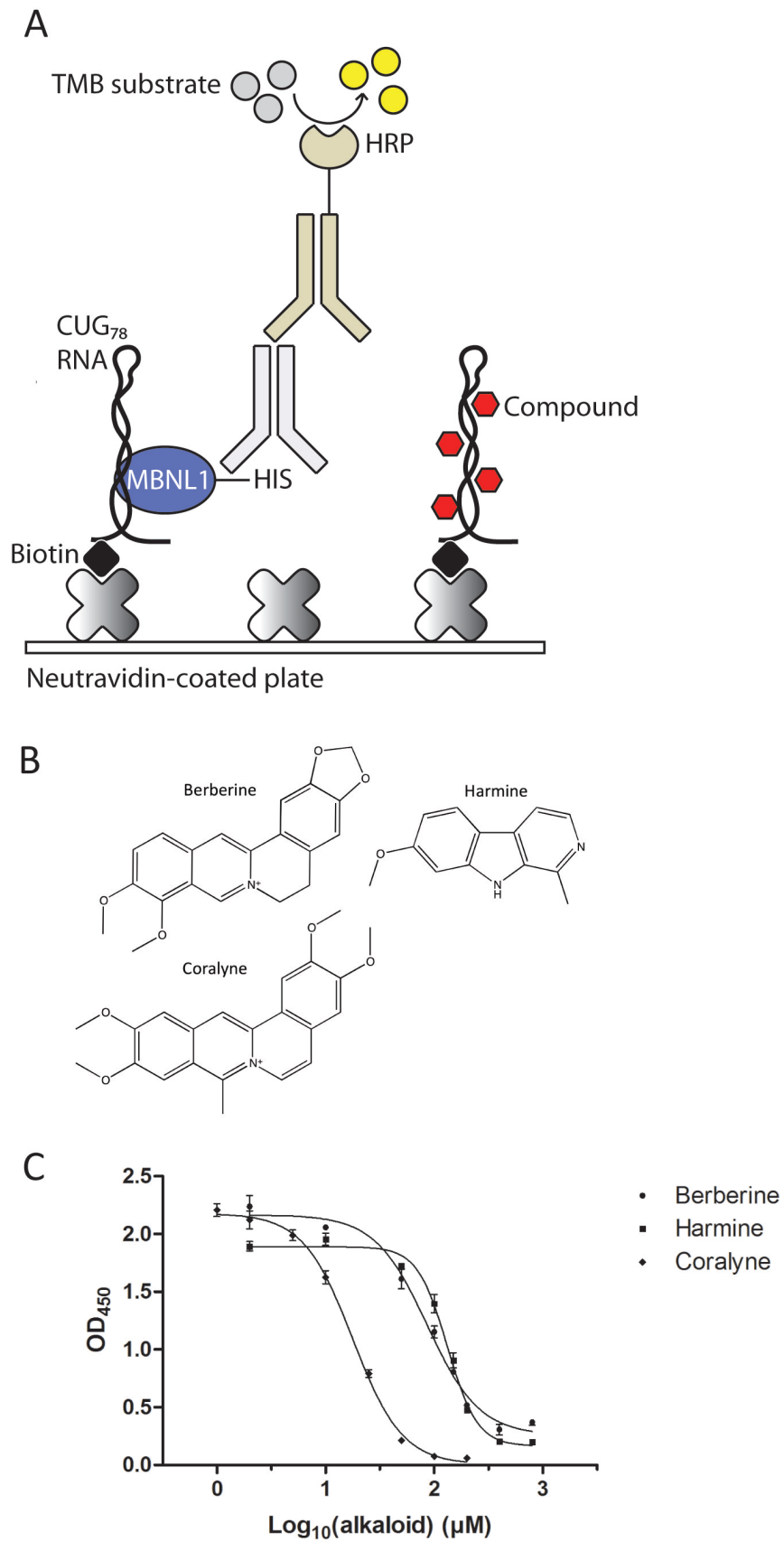


Figure 2 (I 1): Screening for small molecules of natural origin that disrupt the MBNL1-CUG₇₈ complex *in vitro*.

Fig. I 1A: CUG₇₈-MBNL1 displacement screening assay: Biotinylated CUG₇₈ RNA is immobilized and incubated with MBNL1 and compounds. RNA-bound MBNL1 is detected via a primary anti-HIS and a secondary anti-mouse-HRP antibody. A substrate is added to give an optical signal, correlating to the amount of RNA-bound MBNL1. In between all five incubation steps, washing is performed.

Fig. I 1B: Molecular structure of the identified alkaloids berberine, harmine, and coralyne.

Fig. I 1C: MBNL1-CUG₇₈ RNA complex inhibition curves with berberine, harmine, and coralyne.

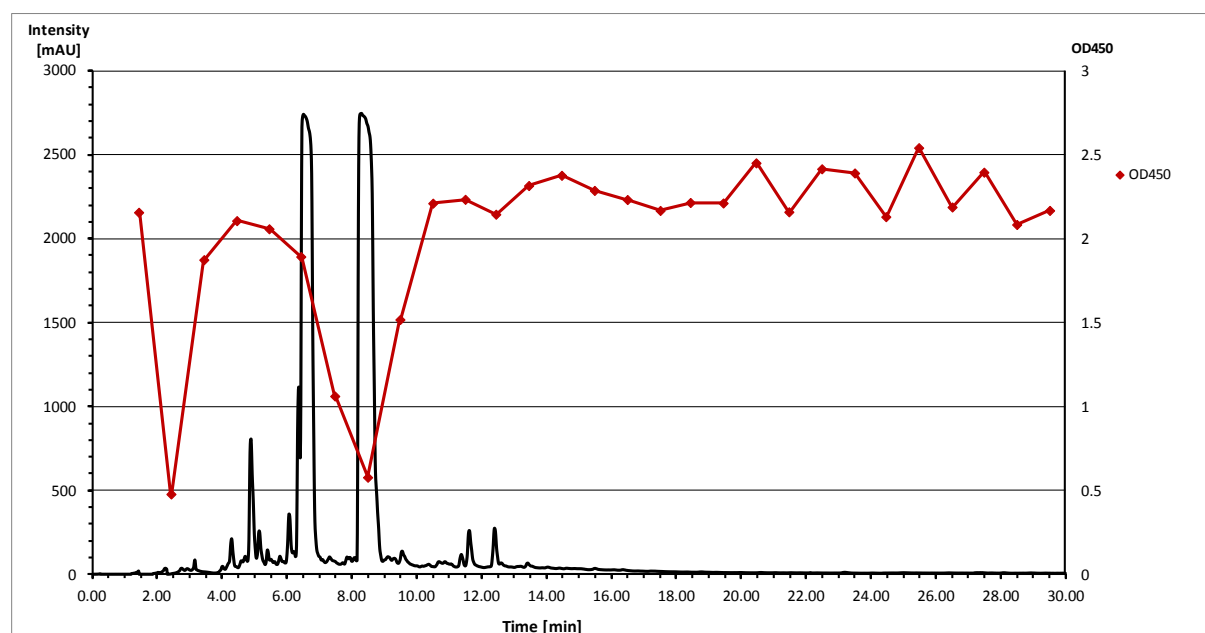


Figure 3 (I 2): HPLC-based activity profiling of the methanol extract of *Peganum harmala*. Shown on the y-axis are the online HPLC-UV trace at 254 nm (black) and the OD₄₅₀ signal from the CUG₇₈-MBNL1 inhibition assay (red) for each of the 29 fractions (min 1 to 30, time on x-axis). The activity of the fractions at minutes 8 and 9 could be assigned to the alkaloid harmine. Based on on-line MS and UV spectroscopic data, the other major peak eluting at 6.6 min was tentatively assigned to harmol. The activity in the early eluting fraction 2-3 min did not correspond to any peak and was not further investigated.

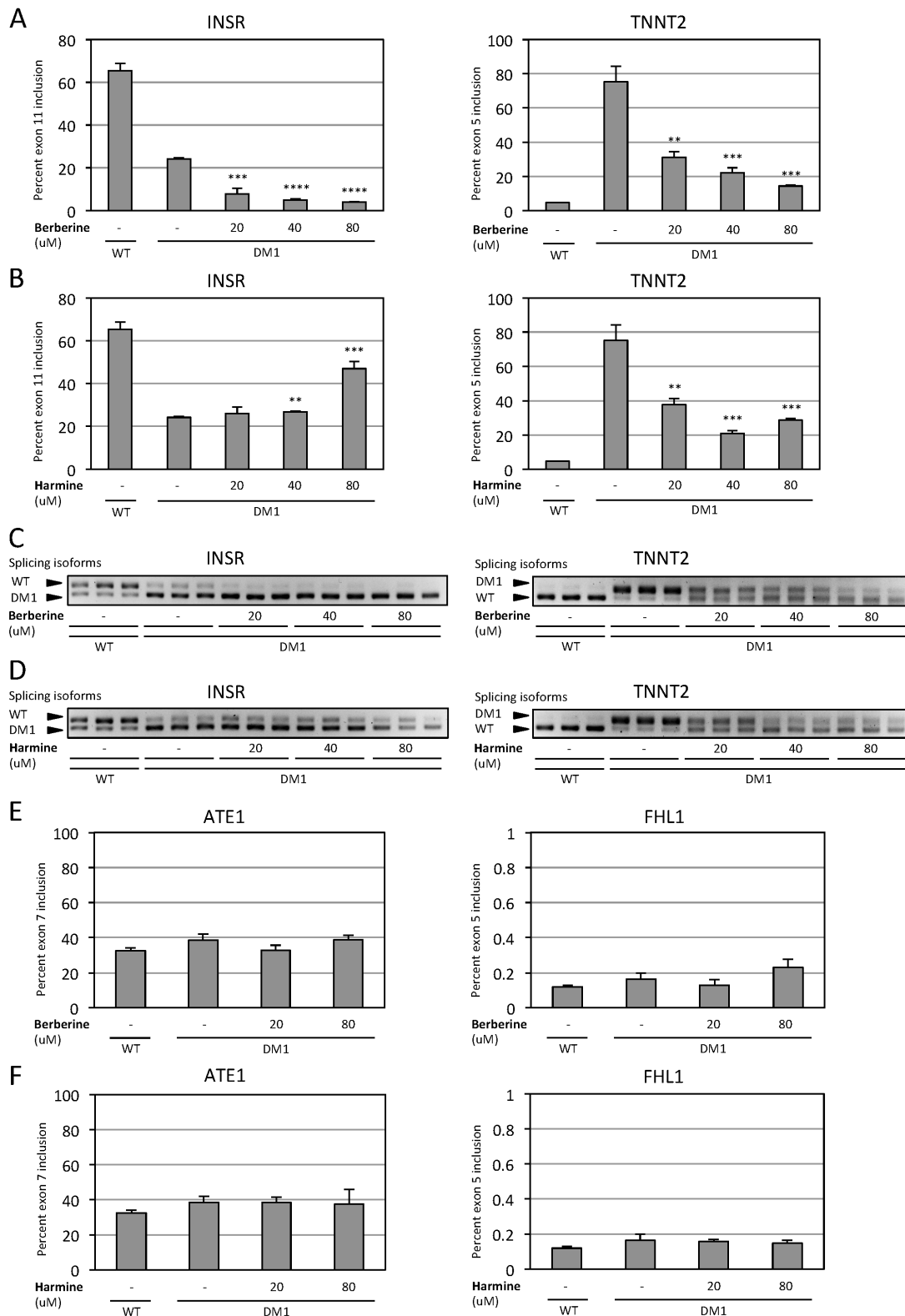


Figure 4 (I 3): Representative RT-qPCR and RT-PCR splicing data for WT and DM1 control cells as well as treated DM1 human myoblast cells.

Fig. I 3A: Berberine improves the splicing of the TNNT2 pre-mRNA but has a detrimental effect on the INSR pre-mRNA splicing.

Fig. I 3B: Harmine improves splicing of the TNNT2 pre-mRNA and also of the INSR pre-mRNA at the highest concentration.

Fig. I 3C,D: Alternative splicing of INSR and TNNT2 pre-mRNA analyzed by RT-PCR and visualized on 3% agarose gels. Shown are the two alternative splicing isoforms for both genes in untreated WT and DM1 control cells and DM1 cells treated with berberine (3 C) and harmine (3 D). The WT splicing isoform represents the predominant mature splicing variant, whereas the DM1 isoform represents the fetal splicing variant.

Fig. I 3E,F: Berberine and harmine do not affect alternative splicing of MBNL1-independently regulated ATE1 and FHL1 pre-mRNAs in treated DM1 myoblasts, compared to untreated WT and DM1 control myoblasts.

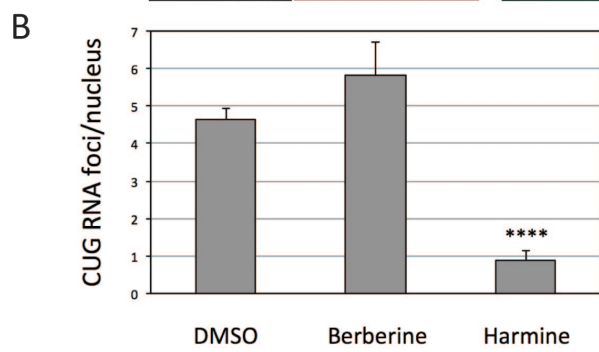
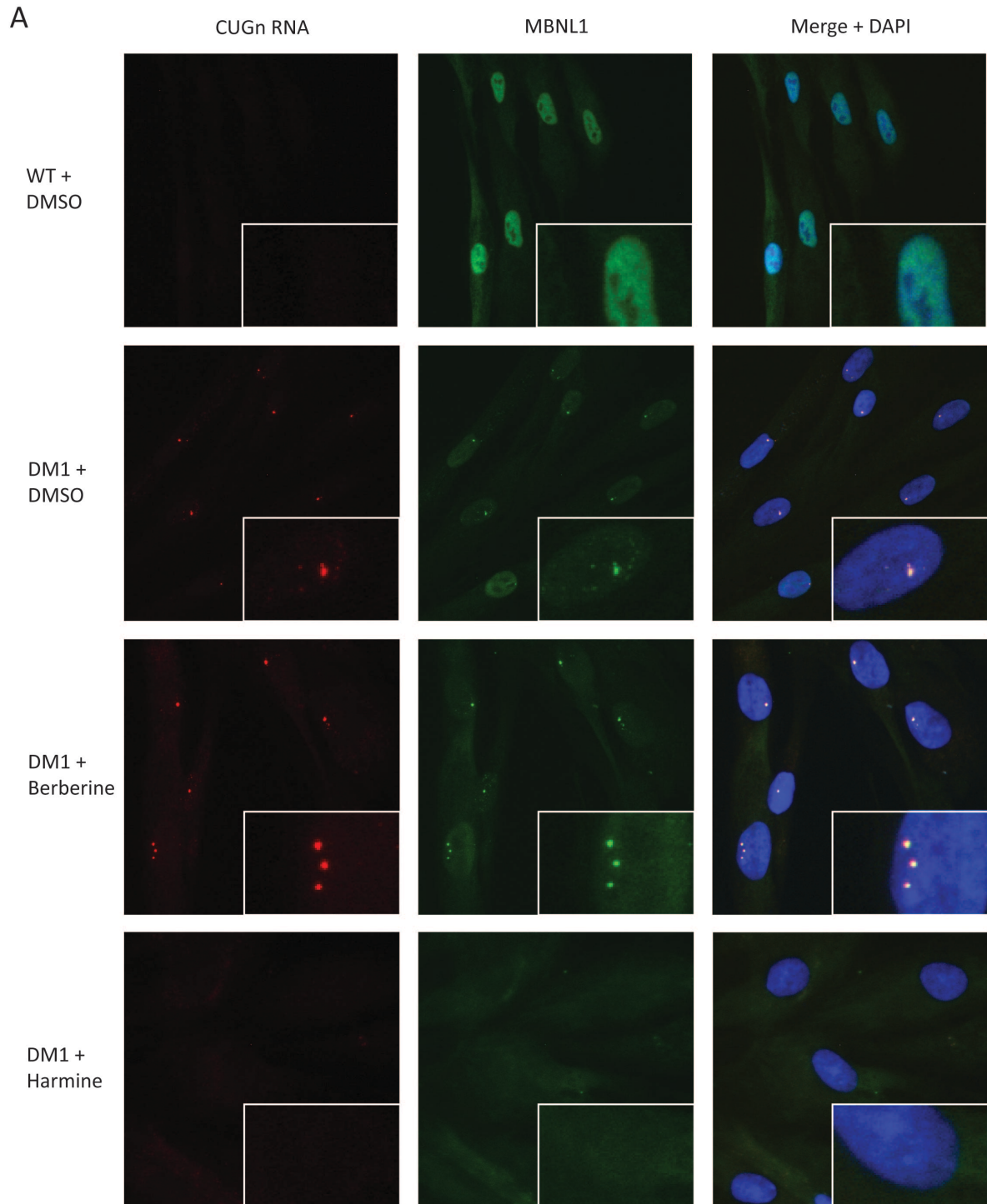


Figure 5 (I 4): FISH detection of CUG_n RNA and immunofluorescence detection of MBNL1 in human WT and DM1 myoblasts.

Fig. I 4A: Harmine reduces the amount and intensity of *foci* at 80 μ M concentration whereas berberine does not reduce *foci*. For each condition a *foci* staining (red), MBNL1 staining (green) as well as a merge of both with a nuclear DAPI staining (blue) is shown. Vehicle treated control WT and DM1 cells as well as compound treated (80 μ M) cells are shown.

Fig. I 4B: Quantification of the number of CUG_n RNA *foci* in human DM1 cells either treated with DMSO or the indicated alkaloids at 80 μ M.

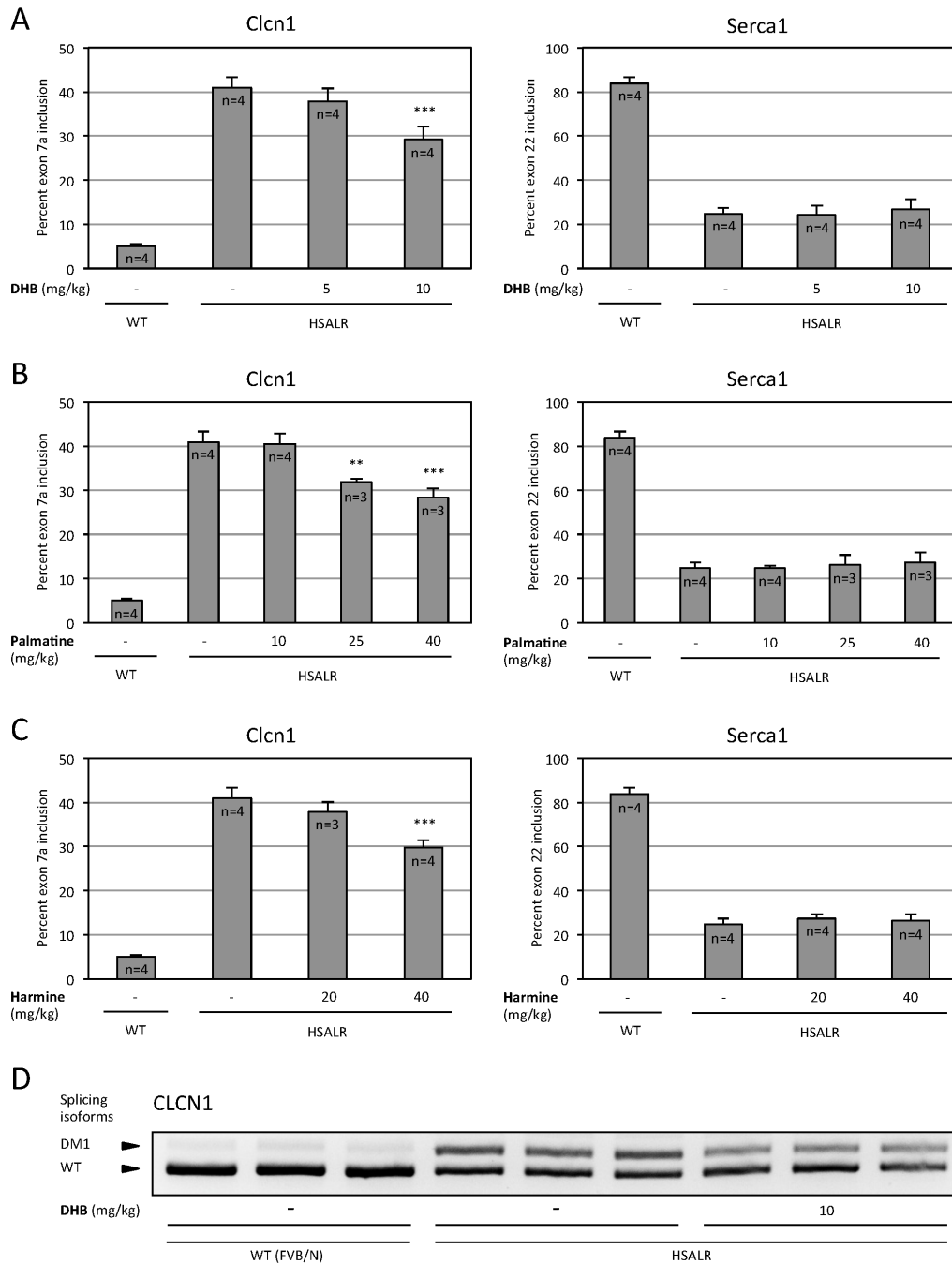


Figure 6 (I 5): Representative *in vivo* RT-qPCR splicing data for vehicle treated WT and HSA^{LR} mice as well as compound treated HSA^{LR} mice (quadriceps muscle). Shown are the splicing of the CLCN1 channel and SERCA1. All three alkaloids improve the splicing of the CLCN1 channel whereas the splicing of SERCA1 is not improved.

Fig. I 5A: Dihydroberberine (DHB) treatment.

Fig. I 5B: Palmatine treatment.

Fig. I 5C: Harmine treatment.

Fig. I 5D: Alternative splicing of the CLCN1 pre-mRNA analyzed by RT-PCR and visualized on 3% agarose gels. Shown are the two alternative splicing isoforms in untreated WT FVB/N and DM1 HSA^{LR} control mice and HSA^{LR} mice treated with 10 mg/kg dihydroberberine (DHB).

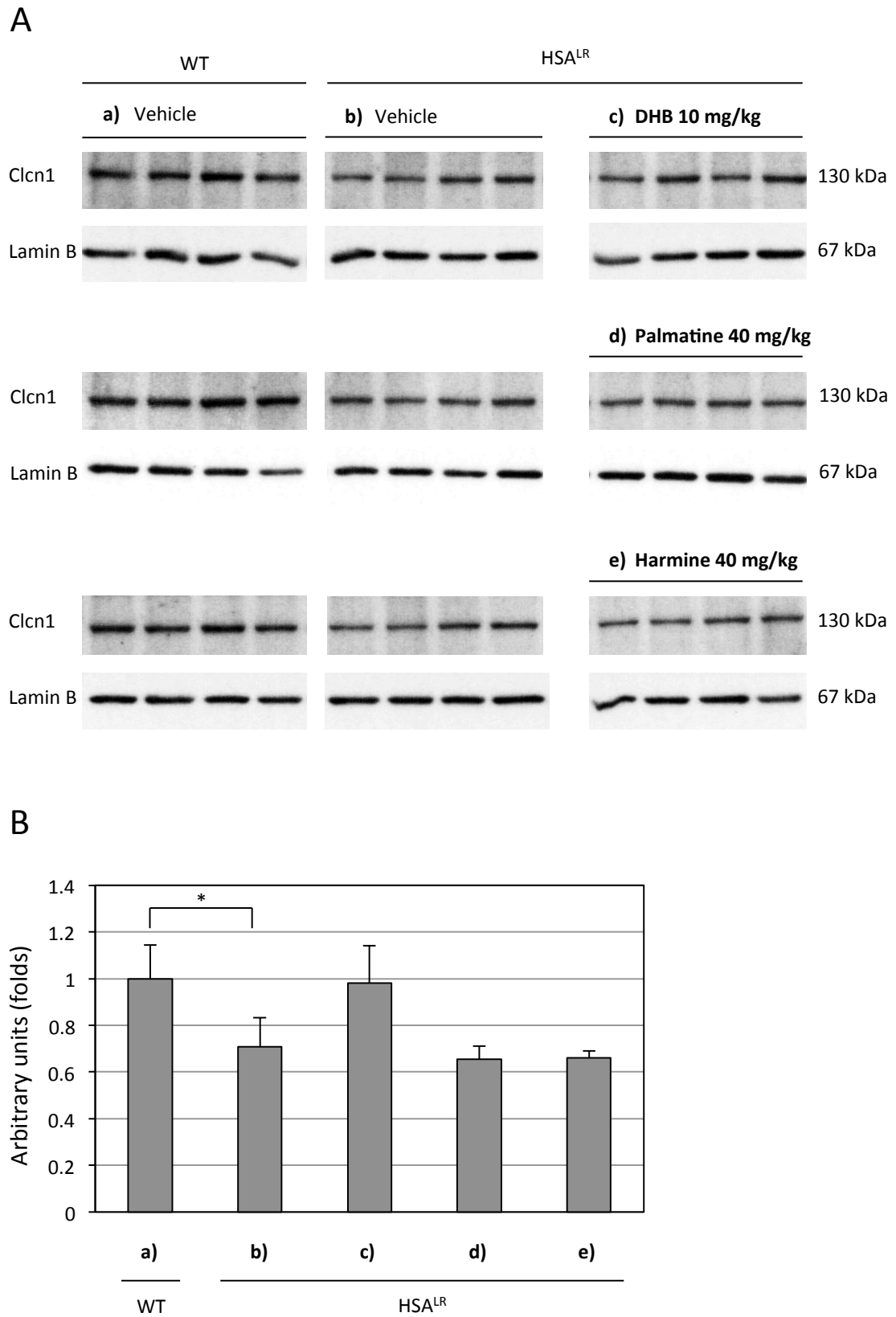


Figure 7 (I 6): Western immunoblot detection and quantification of CLCN1 protein levels in mouse quadriceps muscle.

Fig. I 6A: Western immunoblot showing CLCN1 protein levels of vehicle treated WT mice (a), vehicle treated HSA^{LR} mice (b), and compound treated HSA^{LR} mice (c-e). Lamin B was used as loading control.

Fig. I 6B: Quantification of CLCN1 band intensities normalized to Lamin B. The means of replicates for each condition including the standard deviation are shown.

2.6 Manuscript II

Discovery of Di-imidazoline Small Molecules as Inhibitors of the MBNL1-CUG_n RNA Complex with Therapeutic Potential for Myotonic Dystrophy Type I

Ruben Herrendorff¹, Jochen Kinter¹, Frances Kern¹, Jacqueline Bezençon², Beat Ernst², Tanja Wenzler³, Reto Brun³, Arvind Kumar⁴, Abdelbasset A. Farahat^{4,5}, Martial Say⁴, David W. Boykin⁴, Michael Sinnreich^{1*}

¹ Neuromuscular Research Group, Departments of Neurology and Biomedicine, University Hospital Basel, Switzerland

² Institute of Molecular Pharmacy, Pharmacenter, University of Basel, Switzerland

³ Medical Parasitology & Infection Biology, Swiss Tropical and Public Health Institute, and University of Basel, Switzerland

⁴ Department of Chemistry, Georgia State University, Atlanta, Georgia 30303, USA

⁵ Department of Pharmaceutical Organic Chemistry, Faculty of Pharmacy, Mansoura University, Mansoura 35516, Egypt

* To whom correspondence should be addressed.

Abstract

Myotonic Dystrophy Type I (DM1) is the most common muscular dystrophy among the adult population with a prevalence of about 1:8000. To this date, there is no causal treatment available for this disabling disease. A genetic mutation in the non-coding 3' region of the Myotonic Dystrophy Protein Kinase (DMPK) gene lies at the root of this disease's pathomechanism. A trinucleotide expansion of CTG repeats within this locus leads to a pathogenic CUG_n pre-mRNA that sequesters splicing factors, such as muscleblind-like 1 (MBNL1), leading to mis-regulated alternative splicing of a plethora of pre-mRNAs.

Several studies were performed, which aimed at identifying small molecules that displace MBNL1 from the pathogenic RNA to restore alternative splicing. Pentamidine was described as an inhibitor of the MBNL1-CUG_n RNA complex; it restored molecular defects in a cell model of DM1, and partially in a mouse model of DM1. However, pentamidine is not suited for long-term treatment, mainly due to its toxicity. Our study comprised the screening of 434 pentamidine-related small molecules in an *in vitro* CUG₇₈-MBNL1 inhibition assay. Here, we describe the synthesis, the biological and pharmacokinetic evaluation of three di-imidazolines with improved properties compared to pentamidine. Testing of the di-imidazolines in human DM1 myoblasts led to the identification of a new lead compound DB175, which fully restored the splicing of the INSR and TNNT2 pre-mRNAs, which are both mis-spliced in DM1. Di-imidazolines comprise a new compound class with therapeutic potential for DM1 and possibly other RNA-mediated diseases.

Introduction

Myotonic Dystrophy Type I (DM1) is the most common neuromuscular disorder among the adult population (11). This severe disease currently has no treatment but, due to its relatively well-understood pathomechanism, provides several opportunities for therapeutic intervention. The pathomechanism of DM1 has been linked to a mutation in the non-coding 3' region of the Myotonic Dystrophy Protein Kinase (DMPK) gene (9, 14). The mutant DMPK transcript presents a toxic gain-of-function RNA that binds splicing factors, such as muscleblind-like 1 (MBNL1) (24, 25, 37, 38), which are retained within the nuclei of affected cells (26-28). This leads to mis-regulated alternative splicing of a variety of pre-mRNAs, including the skeletal muscle chloride channel (CLCN1) (29-31), the insulin receptor (INSR) (32), sarcoplasmic/endoplasmic reticulum Ca^{2+} ATPase 1 (SERCA1) (34) and cardiac troponin T type 2 (TNNT2) (35).

Among different therapeutic approaches towards DM1, reviewed in ref. (66), much effort has been put in the search for small molecules as potential therapeutics. Compared to antisense oligonucleotide and gene therapy approaches, the small molecule approach has the advantage of systemic tissue penetration. Several studies led to the identification of small molecules that displaced MBNL1 from the toxic DMPK CUG_n transcript and thus restored DM1-associated molecular defects. Identified small molecules include pentamidine and neomycin B (51), an acridine-triazole conjugate (52), modularly assembled polyvalent derivatives of Hoechst 33258 (53), kanamycin A (90), the antimicrobial lomofungin and its derivative dilomofungin (57), as well as peptides and peptide-derivatives (55, 91). From these compounds pentamidine and the peptide ABP1 have been reported to partially restore splicing *in vivo* (51, 91).

Pentamidine was discovered through screening of a collection of nucleic acid binders in an electrophoretic mobility gel shift assay (EMSA) (51). Parkesh *et al.* employed chemical similarity searching, with pentamidine and Hoechst 33258 as starting points, to find stronger MBNL1-CUG_n RNA complex inhibitors (92). The screening of nucleic acid binders (51) and usage of identified complex inhibitors as chemical starting points for stronger inhibitors (92) has been validated as a drug discovery approach in DM1.

Due to toxicity issues, pentamidine itself is not suited as a drug for DM1 (51). Using the antiprotozoal drug pentamidine as a lead substance, we chose a collection of 434 pentamidine-related compounds from a library of small molecules that was generated during a drug

discovery program for *Trypanosomiasis*. These aromatic, mostly dicationic small molecules were screened in a CUG₇₈-MBNL1 inhibition assay, using a DMPK CUG₇₈ transcript amplified from DNA of a DM1 patient. In this study we identified three di-imidazolines DB1796, DB1973 and DB175 that demonstrated improved properties compared to the lead substance pentamidine with respect to complex inhibitory activity *in vitro*, amelioration of molecular defects in a DM1 cell model, and cellular toxicity. DB1796 and DB1973 have not been described before, we therefore also report their synthesis.

Results

Discovery of di-imidazoline small molecules that disrupt the MBNL1-CUG₇₈ RNA complex *in vitro*

A collection of 434 pentamidine-related small molecules was screened with an *in vitro* CUG₇₈-MBNL1 inhibition assay (Fig. II 1A). Compounds were co-incubated with recombinant MBNL1-His in 96-well plates containing immobilized CUG₇₈ RNA, and then MBNL1-CUG₇₈ complex inhibition was measured. We identified 36 hits at 0.5 μM and 6 hits at 0.125 μM compound concentration (> 80% inhibition of MBNL1 binding to CUG₇₈ RNA). Among the hits were imidazolines, amidines, tetrahydropyrimidines or amines, with the majority of hits being of the di-imidazoline type. The six strongest complex inhibitors comprised the diphenylfuran imidazoline DB60, previously described by Wilson *et al.* (93), three structurally close derivatives thereof, a dibenzimidazolfuran imidazoline and a dibenzimidazolfuran amidine. The CUG₇₈-MBNL1 inhibition assay was used to determine the IC₅₀ values for three most potently bioactive di-imidazolines: DB1796, DB1796 and DB175 (Fig. II 1B). DB 1796 had an IC₅₀ value of $1.5 \pm 0.1 \mu\text{M}$, DB 1973 an IC₅₀ of $6.2 \pm 0.6 \mu\text{M}$ and DB 175 an IC₅₀ of $5.0 \pm 0.1 \mu\text{M}$ (Fig. II 1C). Pentamidine, the lead compound underlying this study, had no inhibitory effect on complex formation whatsoever, even at concentrations as high as 500 μM . As additional reference compounds, we tested Hoechst 33258 and neomycin B, two previously described complex inhibitors (51, 92), which had IC₅₀ values of $195.5 \pm 3.0 \mu\text{M}$ and $5.3 \pm 0.6 \mu\text{M}$, respectively.

Synthesis of the di-imidazolines DB1796, DB1973 and DB175

The synthesis of DB175, a dicationic carbazole, has been described by Patrick *et al.* (94). The syntheses of both DB1796 and DB1973 are outlined in scheme II 1. The first step of the preparation of DB1796 employs a Stille coupling reaction between 2-bromo-5-cyanothiophene and 1-(tert-butoxycarbonyl)-2-(trimethylstannyl)-1H-indole-6-carbonitrile (95), which yielded the coupled product. We detected significant loss of the Boc-protecting group during the reaction and/or work-up; consequently we treated the crude product with Boc-anhydride to simplify the purification by column chromatography. The bis-nitrile was converted into DB1796 using Pinner methodology to form the imidate ester followed by subsequent reaction with ethylene-diamine. The first step in the synthesis of DB1973 involves the oxidative cycloaddition reaction between 3,4-diaminobenzonitrile and 2-cyano-5-formylthiophene using sodium bisulfite as the oxidizing agent to form the corresponding bis-nitrile. We employed the process described for DB1796 to convert the bis-nitrile into DB1973.

Identified di-imidazolines show reversal of mis-splicing of pre-mRNAs in a human myoblast cell model for DM1

We subsequently tested the compounds ability to improve splicing defects in a human myoblast model for DM1 (71). The wild type (WT) cell line contained a short CUG₅ repeat; the DM1 cell line contained a long CUG₁₃₀₀ repeat. DM1 myoblasts were treated for 24 h with the identified compounds, followed by RNA isolation and reverse transcription. DMSO-treated WT and DM1 myoblasts served as controls. For the quantification of alternative splicing, a qPCR-based method was used. This method employs two primer pairs; one primer pair detects all occurring splicing variants of a pre-mRNA and another primer pair only detects those pre-mRNA variants that include an investigated alternative exon. The six strongest complex inhibitors did not improve splicing in the DM1 myoblasts at 20 or 40 μ M concentration; the diphenylfuran imidazoline DB60 and three close derivatives thereof were toxic to the DM1 myoblasts at these concentrations and if tested at lower, more tolerable concentrations the compounds did not show any splicing amelioration (data not shown). Three structurally similar di-imidazolines emerged as the most potently bioactive compounds: DB 1796, DB 1973 and DB 175. All three compounds improved the splicing of two pre-mRNAs, the insulin receptor (INSR) and the cardiac troponin T type 2 (TNNT2) pre-mRNA (Fig. II 2 A-C). In

WT cells close to 60% of INSR transcripts included exon 11, whereas in DM1 cells exon inclusion was reduced to about 10-25%. In WT cells, TNNT2 exon 5 inclusion was around 5%; whereas in DM1 cells inclusion was increased to at least 45% of transcripts. DB 1796 improved the alternative splicing of the INSR pre-mRNA by $20.0 \pm 2.9\%$ (10 μM), $34.7 \pm 1.4\%$ (20 μM) and $13.1 \pm 1.0\%$ (40 μM), whereas the splicing for the TNNT2 pre-mRNA was improved by $14.6 \pm 0.8\%$ (10 μM), $25.7 \pm 0.7\%$ (20 μM) and $64.8 \pm 0.2\%$ (40 μM). Also DB 1973 improved the alternative splicing of the INSR pre-mRNA by $38.8 \pm 2.3\%$ (10 μM), $38.5 \pm 3.8\%$ (20 μM) and $34.6 \pm 3.1\%$ (40 μM), and the splicing for the TNNT2 pre-mRNA was improved by $12.9 \pm 2.5\%$ (10 μM), $17.4 \pm 0.8\%$ (20 μM) and $28.8 \pm 2.3\%$ (40 μM). DB175 effectively improved the splicing of both pre-mRNAs in a concentration-dependent manner and splicing was fully restored at 20 μM concentration. Splicing of the INSR pre-mRNA was improved by $13.2 \pm 2.3\%$ (5 μM), $60.8 \pm 1.3\%$ (10 μM) and $87.8 \pm 6.2\%$ (20 μM), whereas the TNNT2 splicing was improved by $59.9 \pm 1.8\%$ (5 μM), $91.7 \pm 0.4\%$ (10 μM) and $101.2 \pm 0.4\%$ (20 μM). Splicing restoration by DB175 was confirmed with RT-PCR and visualization of the two alternative splicing isoforms of the INSR and TNNT2 pre-mRNA on 3% TAE agarose gels (Fig. II 2D). Pentamidine did not improve splicing of the INSR pre-mRNAs (Fig. II 2C). Only the highest pentamidine concentration used (40 μM) showed a small but significant improvement of $17.4 \pm 3.8\%$ in TNNT2 splicing (Fig. II 2C). To investigate the selectivity of the three identified di-imidazolines, we tested whether they affected MBNL1-independent splicing events in the same DM1 cell line (Fig. II 3A-C). We therefore analyzed the alternative splicing of two genes, ATE1 and FHL1, which are known to be alternatively spliced, but independent of MBNL1 (72). Exon 7 inclusion in the ATE1 pre-mRNA was close to 33% for the WT cell line and close to 48% in the DM1 cell line. Exon 5 inclusion in the FHL1 pre-mRNA was close to 0.1% for both the WT and the DM1 cell line. Compared to the splicing of ATE1 and FHL1 in untreated WT and DM1 control cells the compound-treated DM1 cells did not show any significant difference in alternative splicing of both genes.

Identified di-imidazolines reduce nuclear CUG_n RNA *foci* formation in a human myoblasts cell model for DM1 and change the distribution pattern of MBNL1

Nuclear aggregates of MBNL1 and CUG_n RNA, called *foci*, are a further hallmark of DM1. The identified imidazolines were tested for their ability to reduce *foci* formation (Fig. II 4A) using the same two cell lines that were used for the alternative splicing analysis. Only the DM1 cell line showed CUG_n RNA staining and co-localization with MBNL1 staining. The

MBNL1 staining showed a predominantly nuclear staining in the WT cells, whereas in the DM1 cells MBNL1 was concentrated mainly in nuclear *foci*. At 80 μM concentration of DB1796 and DB1973, the number of *foci* was reduced (Fig. II 4B). MBNL1 staining was more distributed in the nuclei of treated cells, indicating the release of MBNL1 from the toxic CUG_n transcripts. Treatment with DB175 at 40 μM concentration also reduced *foci* formation (Fig. II 4B), resulting in a diffuse MBNL1 staining. MBNL1 was detectable in the nucleus as well as in the cytoplasm of treated cells, indicating increased nuclear export. CUG_n RNA staining was found to be decreased in the nuclei of DB175 treated cells, at the same time the staining was increased in the cytoplasm of treated cells and co-localized partly with MBNL1. DB175 might therefore increase nuclear export of toxic DMPK transcripts and MBNL1, but might also stabilize the RNA transcripts. Quantification of *foci* in a total of 150 randomly chosen nuclei per condition showed a decrease of *foci* number per nucleus, from 4.7 ± 0.3 in DMSO-treated DM1 control cells to 3.1 ± 0.4 (80 μM DB1796), to 2.1 ± 0.3 (80 μM DB1973), and to 3.2 ± 0.1 (40 μM DB175) following compound treatments.

Cellular toxicity of the identified di-imidazolines

A cell viability assay with C2C12 mouse myoblasts was performed to evaluate the cellular toxicity of the three identified di-imidazolines and two reference compounds, pentamidine and mitomycin C. We incubated C2C12 myoblasts with compound concentrations ranging from 1 – 900 μM and determined the toxicity IC₅₀ (Tox IC₅₀) values, whereby half of the cells were still viable after two days of compound incubation. DB1796 had a Tox IC₅₀ of 129.8 ± 3.7 μM , DB1973 had a Tox IC₅₀ of 205.9 ± 10.3 μM and DB175 one of 130.0 ± 1.3 μM . The factor between the activity and toxicity IC₅₀ value (IC₅₀ / Tox IC₅₀) is 86.5 for DB1796, 33.2 for DB 1973 and 26.0 for DB 175. This value can be regarded as a rough selectivity index. Pentamidine had a Tox IC₅₀ of 53.5 ± 0.8 μM . Mitomycin C was measured as a reference compound and gave a Tox IC₅₀ of 20.4 ± 1.6 μM .

In vitro pharmacokinetic analysis of the identified di-imidazolines

To evaluate the di-imidazolines' potential for application *in vivo*, we analyzed their physico-chemical parameters such as lipophilicity (distribution coefficient $\log D_{7.4}$), pK_a values, and permeability (Table II 1). In addition, mouse plasma protein binding (PPB) was determined

(Table II 1). DB1973 was shown to be strongly hydrophilic ($\log D_{7.4} < -1.5$). For estimating the influence of the pK_a on lipophilicity and permeability we experimentally determined the pK_a value for DB1973 by the $^1\text{H-NMR}$ method described in ref. (96). The experimental pK_a values of the two imidazoline groups of DB1973 could not be distinguished and showed a singular pK_a value of 7.83 ± 0.35 ; the pK_a of the benzimidazole was 0.61 ± 0.07 . In addition, the pK_a values for the three di-imidazolines and the reference compound pentamidine were calculated *in silico* (Marvin 5.6.0.2, ChemAxon, 2011). The predicted pK_a values for the imidazoline group (DB1796, DB1973, DB175) were in the range of 7 to 9.5, whereas the pK_a of the more basic amidine group (pentamidine) was above 11.5. This indicates less charge-neutral species of pentamidine at physiological pH 7.4 compared to the di-imidazolines. However, the low lipophilicity (< -1.5 for DB 1973) and the presence of a charged state at the physiological pH explain the low passive permeability through an artificial membrane using the PAMPA (Parallel Artificial Membrane Permeability Assay) (97) for all three di-imidazolines and additionally pentamidine ($\log P_e < -7.3$). Moreover, the *in vitro* mouse PPB for DB1796 (69.5%) and for DB175 (97.1%) were higher than the reported PPB of pentamidine (41%) (98).

Discussion

There is a fast growing interest in RNA as a drug target and DM1 is at the center of attention in the field of RNA drug discovery. Several RNAs, owing to distinct secondary structural elements, have been investigated intensely, e.g. the bacterial ribosome or the TAR RNA of the human immunodeficiency virus type 1 (HIV-1) (63, 99). Also RNA triple nucleotide repeat expansions represent distinct secondary structural elements and are being investigated as drug targets (63, 66, 99). Triple nucleotide repeat expansions are the characteristic molecular hallmark for the group of triple nucleotide repeat expansion diseases (TREDs) including fragile X syndrome, myotonic dystrophy type I and II, Huntington's disease and spinocerebellar ataxias (66). Among the TREDs, DM1 presents a model disease due to its relatively well-studied pathomechanism and the theoretical reversibility thereof by therapeutic intervention, e.g. with suited small molecules that inhibit the disease-characteristic MBNL1-CUG_n RNA complex.

The antiprotozoal drug pentamidine was the first small molecule described as an inhibitor of this complex and it improved molecular defects of in a cell model and a mouse model of DM1 (51). As there are several drawbacks to pentamidine as a DM1 drug, notably its toxicity, the

aim of the present study was to identify pentamidine-related small molecules with improved properties. The screening of 434 antiprotozoal small molecules in an *in vitro* CUG₇₈ MBNL1 inhibition assay yielded three potent di-imidazolines with partly improved properties compared to pentamidine, i.e. DB1796, DB1973 and DB175. Their characteristic imidazoline group is a cyclic and planar derivative of the amidine group, characteristic for the diamidines such as pentamidine. The six strongest complex inhibitors from our screening inhibited the formation of the MBNL1-CUG_n RNA complex at 125 nM concentration. Five of these compounds were di-imidazolines, only one was a diamidine. Interestingly, the strongest complex inhibitor identified in our screening, the diphenylfuran imidazoline DB60, has been described previously as a strong intercalator for double stranded RNA (93, 100). From the six strongest inhibitors the diphenylfuran imidazoline DB60 and three structurally close derivatives were toxic to the DM1 myoblasts at 20 or 40 μM concentration and did not improve splicing at lower concentrations, likely due to unspecific nucleic acid intercalation. The two other inhibitors of the dibenzimidazolfuran type did not improve splicing in the DM1 myoblasts, probably due to their high polarity, with four ionizable groups, and resulting poor membrane permeability. Overall, *in vitro* inhibitory activity of the six strongest MBNL1-CUG_n RNA complex inhibitors did not seem to correlate with a biological effect in our DM1 cell model.

We therefore tested screening hits with lower inhibitory activity (IC₅₀ ~ 1 - 10 μM) in our DM1 myoblast model, which successfully yielded bioactive di-imidazolines. Three of these di-imidazolines with *in vitro* IC₅₀ values in the lower μM range (1.5 – 6.2 μM) showed remarkable effects on splicing and *foci* formation in our DM1 cell model. DB175 fully restored the mis-regulated alternative splicing of the INSR and TNNT2 pre-mRNAs in the DM1 myoblasts at 20 μM concentration and reduced nuclear *foci* at 40 μM. FISH and immunofluorescence showed, that MBNL1 was redistributed in DM1 myoblasts treated with 40 μM DB175. But also CUG_n RNA staining was stronger in the cytoplasm compared to untreated control cells, indicating increased nuclear export of the toxic DMPK transcripts. The increased RNA staining might reflect stabilization, and thus decreased decay of the toxic DMPK transcripts in the cytoplasm of these cells, similar to what has been described for di-lomofungin (57). DB175 treatment however decreased nuclear *foci*, which were greatly increased by di-lomofungin. DB1796 and DB1973 also significantly improved splicing in the DM1 myoblasts and reduced the amount of *foci*. The lower *in vitro* inhibitory activity of these three compounds might be compensated by better membrane permeability or target selectivity.

We found that di-imidazolines not only were the most potent MBNL1-CUG_n RNA complex inhibitors, but also performed better than their diamidine counterparts in the cellular splicing assay. A reason for the stronger biological effect might be better membrane permeability of di-imidazolines compared to diamidines. Indeed, the *in silico* predicted pK_a values of our identified di-imidazolines (pK_a 7 – 9) and the experimentally determined pK_a of the DB1973 imidazoline groups (pK_a 7.83 ± 0.35) indicate a lower pK_a for the imidazoline group compared to the amidine group of pentamidine, (pK_a > 11). Thus, more uncharged species of the imidazolines is present at physiological pH, which can potentially pass the membrane barrier. These findings might be comparable to arylimidamides with pK_a values of 7-8 and better membrane permeability than amidines (101). However, PAMPA (97) experiments show low passive membrane permeability of our di-imidazolines and for pentamidine at pH 7.4, which can be explained by their low lipophilicity (< -1.5 for DB1973) and high presence of charged state at physiological pH. Nevertheless, the compounds have shown biological activity in the DM1 myoblasts and therefore, another major permeability mechanism (e.g. active transport) might be involved in the uptake of these compounds into the myoblast, which needs further investigation.

Another reason for a stronger biological effect might be stronger target RNA binding. The planarity of the imidazoline group has been shown to enable better RNA binding by intercalation than the amidine group, which is not planar (100). For the most part, the three identified di-imidazolines DB1796, DB1973 and DB175 are planar. The planarity of the compounds indicates intercalation as a possible binding mode. The aromatic core of the substances might intercalate into the double stranded CUG_n hairpin RNA, forming stacking interactions with the RNA bases, as well as electrostatic interaction via the imidazoline groups with the negatively charged phosphate backbone of the RNA. The three substances seem to share the same pharmacophore. DB1796 with an indole core and DB1973 with a benzimidazole core are structurally very similar and display the two imidazoline groups in the same fashion. DB175 has a carbazole core and displays the two imidazoline moieties in a similar way compared to the two other DB compounds, but conformationally more restricted, which might be beneficial with respect to smaller entropy cost upon binding to the target RNA.

Comparison of the three newly identified di-imidazolines with the lead compound pentamidine reveals several advantages of the di-imidazolines, but also disadvantages, with respect to suitability as DM1 drugs. The newly identified compounds are much stronger binders of the CUG_n MBNL1 complex compared to pentamidine, as we did not detect any inhibition of

MBNL1-CUG_n RNA complex formation by pentamidine. In fact, another mode of action recently described for pentamidine is transcription inhibition of the toxic DMPK transcripts by DNA binding (59). In our DM1 cell model, the three di-imidazolines performed better than pentamidine. Pentamidine did not improve splicing in DM1 myoblasts, except for a minute improvement at the highest tested concentration of 40 μM , which was already very close to the Tox IC₅₀ concentration of $53.5 \pm 0.8 \mu\text{M}$. Regarding toxicity, all of the three di-imidazolines had higher Tox IC₅₀ values than Pentamidine, all above 120 μM . The three di-imidazolines were less toxic to C2C12 mouse myoblasts and also to human myoblasts. Furthermore, the di-imidazolines showed splicing selectivity, they did not affect the alternative splicing of two MBNL1-independently spliced pre-mRNAs (ATE1 and FHL1). The di-imidazolines, compared to pentamidine, have partly improved pharmacokinetic properties which might lead to better membrane permeability, e.g. the earlier discussed lower pK_a values. However, with respect to the pharmacokinetic profile, the three di-imidazolines will need further improvement by suited chemical modification prior to an *in vivo* application. The log $D_{7.4}$ value of DB1973, lower than -1.5, indicates high polarity of the di-imidazolines. A higher log $D_{7.4}$ of 0.144 ± 0.003 was reported for pentamidine (98). In a recent study heptamidine, a pentamidine derivative with increased lipophilicity, proved to be more active in DM1 models compared to pentamidine (59). A balanced activity-pharmacokinetic profile will eventually be needed for effective small molecules to treat DM1. In this respect, drug discovery on the CUG_n RNA target remains a challenge as high charge is needed for target binding, but unwanted for membrane permeability of compounds. Overall, the di-imidazolines provide a few advantages but also disadvantages compared to pentamidine regarding pharmacokinetic parameters.

In conclusion, we show in this study that aromatic di-imidazolines are an promising group of compounds for DM1 and RNA drug discovery. We have identified three di-imidazoline substances as inhibitors of the CUG_n MBNL1 complex with distinct positive effects on the DM1 pathomechanism in human DM1 myoblasts. The three di-imidazolines could contribute to DM1 drug discovery projects as new medicinal chemistry starting points. Foremost the pharmacokinetic profile of these di-imidazolines will require further medicinal chemistry optimization. Currently, these substances are being evaluated *in vivo*.

Experimental

Compound library

The compound library screened in this study was part of a compound library established at the Division of Medical Parasitology & Infection Biology, Swiss Tropical and Public Health Institute, Switzerland. The compounds were synthesized at the Department of Chemistry, Georgia State University, Atlanta, Georgia 30303, USA and the Department of Pathology & Laboratory Medicine, University of North Carolina, Chapel Hill, NC 27599-7525, USA. Most of the 434 compounds were synthesized during a drug discovery program for *Trypanosomiasis*.

Synthesis

Melting points were determined on a Mel-Temp 3.0 melting point apparatus, and are uncorrected. TLC analysis was carried out on silica gel 60 F254 precoated aluminum sheets using UV light for detection. ^1H and ^{13}C NMR spectra were recorded on a Bruker 400 MHz spectrometer using indicated solvents. Mass spectral data was obtained from the Georgia State University Mass Spectrometry Laboratory, Atlanta, GA. Elemental analysis were performed by Atlantic Microlab Inc., Norcross, GA and are within ± 0.4 of the theoretical values. The compounds reported as salts frequently analyzed correctly for fractional moles of water and/or other solvents; in each case ^1H NMR spectra were consistent with the analysis. All chemicals and solvents were purchase from Aldrich Chemical Co., VWR International, or Combi-Blocks, Inc.

Synthesis of DB1796 and DB1973

1-N^t-butoxycarbonyl-2-(5-cyanothienyl)-6-cyanoindole

Tetrakis(triphenylphosphine)palladium(0) (0.23 g, 0.0002 mole, 4 mole %) was added to a stirred mixture of the 1-(tert-butoxycarbonyl)-2-(trimethylstannyl)-1H-indole-6-carbonitrile (95) (2.02 g, 0.005 mole) and 2-bromo-5-cyanothiophene (0.94 g, 0.005 mole) in deaired dioxane (20 mL) under nitrogen. The reaction mixture was heated at reflux for 24 h (TLC monitored), concentrated under reduced pressure, suspended in 30 mL THF, Boc anhydride

(1.09 g, 0.005 mole) and a few crystals of DMAP were added and stirred for 6 h, concentrated under reduced pressure, ice water was added, the precipitate was filtered, washed with water, dried and chromatographed on silica gel using hexane/ethyl acetate (70/30, v/v) giving a white solid (1.13 g, 65%), mp 274-5 °C dec., ¹H NMR (DMSO-d₆): 8.25 (s, 1H), 8.29 (d, 2H, J = 8.4 Hz), 8.11 (d, 2H, J = 8.4 Hz), 7.79 (d, 1H, J = 3.6 Hz), 7.23 (s, 1H), 7.12 (d, 1H, J = 3.6 Hz), 1.46 (s, 9H); ¹³C NMR (DMSO-d₆): 150.2, 148.1, 138.5, 128.7, 127.8, 126.7, 124.8, 124.7, 119.0, 115.8, 112.8, 112.2, 111.4, 105.9, 85.4, 27.1 ; ESI-MS: 350 (M⁺+1); Anal. Calc. for C₁₉H₁₅N₃O₂S: C, 65.31; H, 4.33; N, 12.03. Found: C, 65.44; H, 4.21; N, 12.13.

2-(5-(2-imidazoliny)-thienyl)-6-(2-(imidazoliny)-1H-indole dihydrochloride (DB 1796)

The imidate ester dihydrochloride (0.349 g, 0.001 mole) from the above dicyano compound and 1,2-diaminoethane (0.18 g, 0.003 mole) in 15 mL dry ethanol was allowed to react and worked up as described for DB 1973 which yielded a pale yellow solid (0.34 g, 83%), mp >320 °C dec., ¹H NMR (DMSO-d₆/D₂O): 8.27 (d, 1H, J = 1.5 Hz), 7.10 (d, 1H, J = 3.9 Hz), 7.67-7.64 (m, 2H), 7.23 (brs, 1H), 7.22 (d, 1H, J = 3.9 Hz) 3.98 (s, 4H), 3.97 (s, 4H); ¹³C NMR (DMSO-d₆/D₂O): 166.3, 154.9, 152.2, 140.5, 137.4, 130.0, 128.1, 123.5, 123.2, 122.8, 114.3, 113.2, 110.3, 103.4, 44.9, 44.7; ESI-MS: 336 (M⁺+1); Anal. Calc. for C₁₈H₁₇N₅S-2HCl-0.25H₂O: C, 52.48; H, 4.77; N, 17.01. Found: C, 52.51; H, 4.59; N, 16.96.

2-(5-(2-cyano)-thienyl)-5(6)-cyan-1H-benzimidazole

Sodium bisulfite (0.78 g, 0.0075 mole) was added to a stirred solution of 2-cyano-5-formyl thiophene (0.685 g, 0.005 mole) and 4-cyano-1,2-phenylenediamine (0.665 g, 0.005 mole) in 8 mL dry DMF. The reaction mixture was heated at 135 °C for 15 h, cooled and triturated with ice-water and the precipitated solid filtered, washed with water and dried in air. The yellow solid was purified by column chromatography on silica gel using hexane/ethyl acetate (70/30, v/v) to yield an off-white solid (0.74 g, 59%), mp 213-214 °C dec., ¹H NMR (DMSO-d₆): 14.0 (s, 1H), 8.19 (s, 1H), 8.09 (d, 1H, J = 4 Hz), 7.97 (d, 1H, J = 4 Hz), 7.79 (d, 1H, J = 8 Hz), 7.65 (d, 1H, J = 8 Hz); ¹³C NMR (DMSO-d₆): 148.2, 141.6, 140.9, 139.2, 132.7, 129.3, 128.7, 126.9, 122.2, 116.1, 114.6, 110.9, 105.7; ESI-MS: 251 (M⁺+1); Anal. Calc. for C₁₃H₆N₄S: C, 62.39; H, 2.42; N, 22.39. Found: C, 62.55; H, 2.61; N, 22.21.

2-(5-(2-imidazoliny)-thienyl)-5(6)-(2-(imidazoliny)-1H-benzimidazole trihydrochloride (DB 1973)

A suspension of the above dicyano compound (0.5 g, 0.002 mole) in 25 mL ethanol was saturated with dry HCl(g) at 0 °C and stirred in a closed flask for 7 days, the solid suspension

was triturated with dry ether and filtered, washed with ether and dried under reduced pressure for 4 h to yield the yellow imidate ester trihydrochloride 0.78 g (86%). 1,2-Diaminoethane (0.18 g, 0.003 mole) was added to a suspension of 0.451 g (0.001 mole) the imidate ester in 15 mL dry ethanol, the reaction mixture was heated at reflux for 12 h, concentrated in reduced pressure, dissolved in water, basified with 2N NaOH, the precipitated solid was filtered, washed with water, dried and converted to HCl salt with ethanolic-HCl to yield a pale yellow solid (0.34 g, 82%), mp >300 °C dec., ¹H NMR (DMSO-d₆/D₂O): 8.10 (s, 1H), 7.87 (brs, 1H), 7.85 (s, 1H), 7.10 (d, 1H, J = 4 Hz), 7.65 (d, 1H, J = 4 Hz), 3.96 (s, 4H), 3.80 (s, 4H); ¹³C NMR (DMSO-d₆): 166.2, 160.0, 148.9, 148.0, 141.1, 136.6, 129.4, 129.0, 125.7, 123.7, 123.6, 116.9, 116.1, 45.1, 41.0; ESI-MS: 337 (M⁺+1); Anal. Calc. for: C₁₇H₁₆N₆S·3HCl·2H₂O·0.25C₂H₆O: C, 42.60; H, 5.00; N, 17.03. Found: C, 42.90; H, 4.71; N, 16.69.

MBNL1 preparation

CUG₇₈ RNA preparation

Screening assay: CUG₇₈-MBNL1 inhibition assay

Cell splicing assay

FISH and immunofluorescence

Cell viability assay

These six procedures were performed according to the experimental section of Manuscript I.

Determination of physicochemical and *in vitro* pharmacokinetic properties

DMSO and 1-octanol were purchased from Sigma-Aldrich (St. Louis, MI, USA). Deuterium oxide was purchased from Armar Chemicals (Switzerland). PRISMA HT universal buffer, GIT-0 Lipid Solution, and Acceptor Sink Buffer were ordered from pIon (Woburn, MA, USA). Acetonitrile (MeCN) and methanol (MeOH) were ordered from Acros Organics (Geel, Belgium).

pK_a determination

Experimental pK_a determination for DB1973 was performed as described in ref (96), using NMR chemical shift measurement of reporter protons close to ionizable centers. 100 μ M solutions of the analyte were prepared in D_2O . The analyte was pre-dissolved in DMSO (10 mM), which was taken as the internal standard (at 3.75 ppm). Plotting chemical shifts of reporter protons against the pH values of several analyte samples (of varying pH), and curve fitting by means of Prism®, yielded the pK_a values at the inflection points of the sigmoidal curves. *In silico* prediction of pK_a values was performed with the MarvinSketch® software (version 5.6.0.2, ChemAxon, 2011).

log D_{7.4} determination

$\log D_{7.4}$ determination was performed as described in ref. (102). For the hydrophilic di-imidazolines two different ratios (volume of 1-octanol to volume of phosphate buffer [0.1 M, pH 7.4]) were used for measurement, i.e. 30:140 and 40:130. The compounds were diluted in saturated buffer to a concentration of 1 μ M and transferred into 96-well plates. The analyte solutions were then covered with saturated 1-octanol according to the chosen volume ratio. The measurements for each ratio were performed in triplicates. After 2 h of incubation with shaking and subsequent centrifugation, the phosphate buffer phase was transferred to a second 96-well plate for analysis of compound concentration by liquid chromatography-mass spectrometry (LC-MS).

LC-MS measurements (log D_{7.4})

Analyses were performed using an 1100/1200 Series HPLC System coupled to a 6410 Triple Quadrupole mass detector (Agilent Technologies, Inc., Santa Clara, CA, USA) equipped with electrospray ionization. The column used was an Atlantis T3 C18 column (2.1 x 50 mm, 3 mm particle size) (Waters Corp., Milford, MA, USA). Solvent A (Ammonium formate buffer,

10 mM, pH 3, 5% MeCN) and solvent B (MeCN, containing 0.1% formic acid, v/v) were both delivered at 0.6 mL/min. The gradient was ramped from 95% A/5% B to 5% A/95% B over 1 min, then held at 5% A/95% B for 0.1 min, and brought back (4 min total). MS parameters were optimized and the molecular ion was followed for each analyte. The concentrations of the analytes were quantified with the Agilent Mass Hunter Quantitative Analysis software (version B.01.04).

Parallel artificial membrane permeability assay (PAMPA)

PAMPA (97) permeability ($\log P_e$) was performed in a 96-well format as described in ref. (102). For each compound, measurements were performed at three pH values (3.0, 5.0, and 7.4) in quadruplicate. Twelve wells of a deep well plate, i.e. four wells per pH-value, were filled with 650 μL of PRISMA HT universal buffer adjusted to pH 3.0, 5.0, and 7.4. Samples (150 μL) were withdrawn from each well to determine the blank spectra by UV-spectroscopy (SpectraMax 190, Molecular Devices, Silicon Valley, CA, USA). DMSO-dissolved analyte was added to the remaining buffer to yield 50 μM solutions. Samples (150 μL) were withdrawn to determine the reference spectra. Further 200 μL were transferred to each well of the donor plate of the PAMPA sandwich (pIon, P/N 110 163). The filter membranes at the bottom of the acceptor plate were infused with 5 μL of GIT-0 Lipid Solution and 200 μL of Acceptor Sink Buffer was filled into each acceptor well. The sandwich was assembled, placed in the GutBoxTM, and left undisturbed for 16 h. Then, it was disassembled and samples (150 μL) were transferred from each donor and acceptor well to UV-plates. Quantification was done by both UV-spectroscopy. Effective permeability ($\log P_e$) was calculated from the compound flux, the filter area, and the initial sample concentration in the donor well with the aid of the PAMPA Explorer Software (pIon, version 3.7).

Plasma protein binding

In vitro PPB analysis of DB1796 and DB175 was performed at Charles River Laboratories (MA, USA). It was performed at a two concentration levels, i.e. 500 ng/mL and 5000 ng/mL. Compounds were diluted (in triplicate) in lithium heparin containing mouse plasma to the indicated concentrations and equilibrated with buffer using rapid equilibrium dialysis at 37 °C. Mouse plasma extraction and LC-MS measurements (see below) of compound concentration in both plasma extract and buffer were performed at three time points, i.e. 2, 4, and 24 h. The ratio of the means (mean buffer/mean plasma) was utilized to calculate the free fraction of compound in %, and from this the plasma protein binding was deduced in %. For plasma extraction 10 μL plasma samples and 10 μL each of control blanks, matrix (mouse plasma in

lithium heparin) blanks and ten matrix calibration standards (containing compounds of interest) were pipetted into 96-well plates. 50 μL of the internal standard atenolol was added to all samples, except the matrix blanks, which were added 50 μL of MeCN. The plate was covered, vortexed, centrifuged for 10 min at 3000 rpm to precipitate proteins, and 40 μL of supernatant was transferred into a new 96-well plate. 40 μL of Milli-Q water was added to each well and the plate was covered and vortexed. LC-MS analysis was performed using a Perkin Elmer Series 200 MicroPump LC system equipped with a Chromolith C18 RP-e (3.0 x 100 mm) column and a Leap CTC PAL autosampler. 1 μL of sample was injected for analysis. The mobile phase consisted of solvent A (0.1 % formic acid in water) and solvent B (0.1 % formic acid in MeCN). A 1.40 min gradient was utilized going from 5% to 98% of solvent B with a total run time of 3.50 min and a flow rate of 1 mL/min. Parent ions of the two analytes and internal standard were followed using a AB Sciex QTRAP 6500 instrument, coupled to the LC system. Concentrations of the analytes and controls (atenolol, naproxen) were then calculated with the help of the calibration standard curves.

Figures, schemes, tables and legends

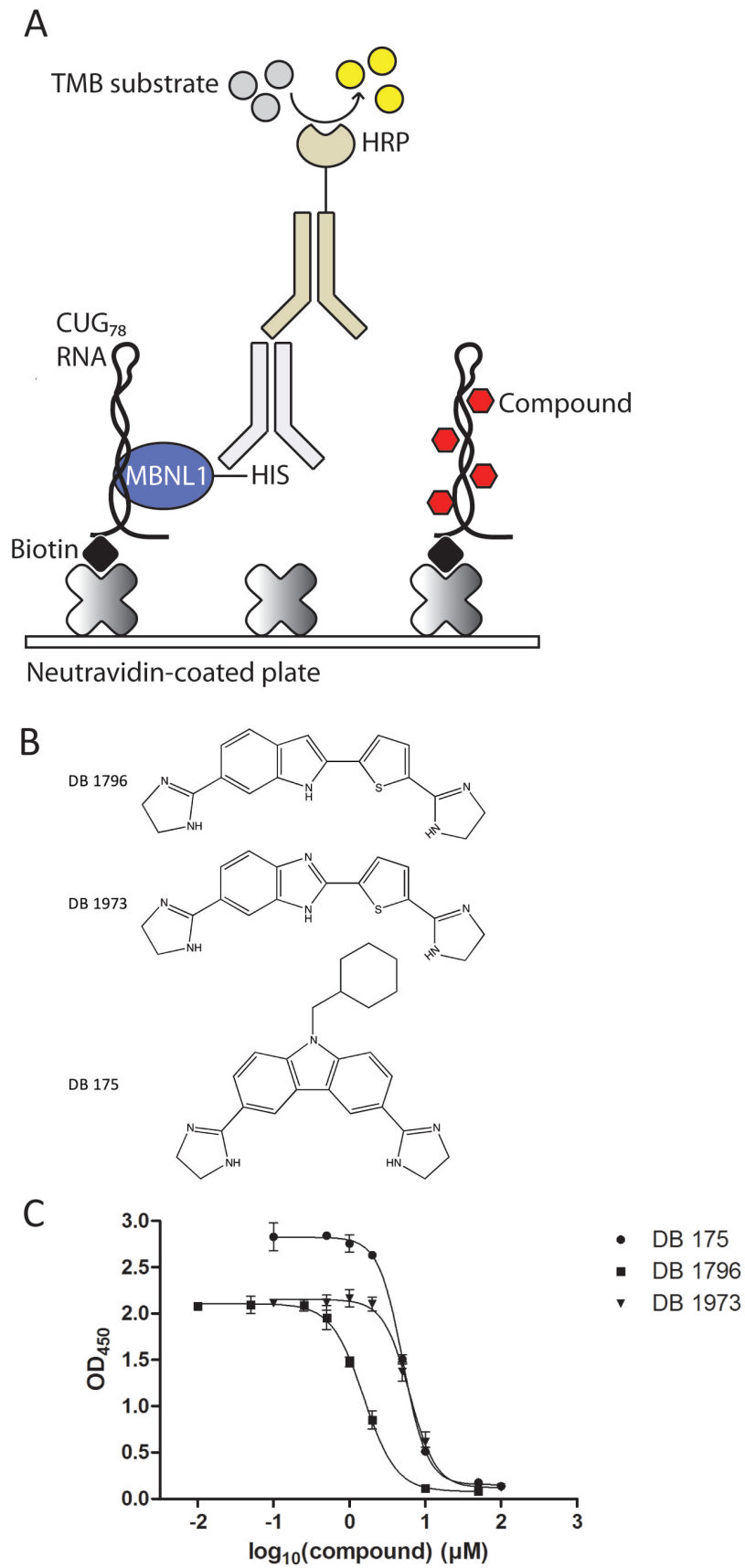


Figure 8 (II 1): Screening for nucleic acid binding small molecules that disrupt the MBNL1-CUG₇₈ RNA complex *in vitro*.

Fig. II 1A: CUG₇₈-MBNL1 inhibition screening assay: Biotinylated CUG₇₈ RNA is immobilized and incubated with MBNL1 and compounds. RNA-bound MBNL1 is detected via a primary anti-His and a secondary anti-mouse-HRP antibody. A substrate is added to give an optical signal, correlating to the amount of RNA-bound MBNL1. In between all five incubation steps, washing is performed.

Fig. II 1B: Molecular structure of the identified MBNL1-CUG₇₈ RNA complex inhibitors DB 1796, DB 1973 and DB 175.

Fig. II 1C: MBNL1-CUG₇₈ RNA complex inhibition curves with DB 1796, DB 1973 and DB 175.

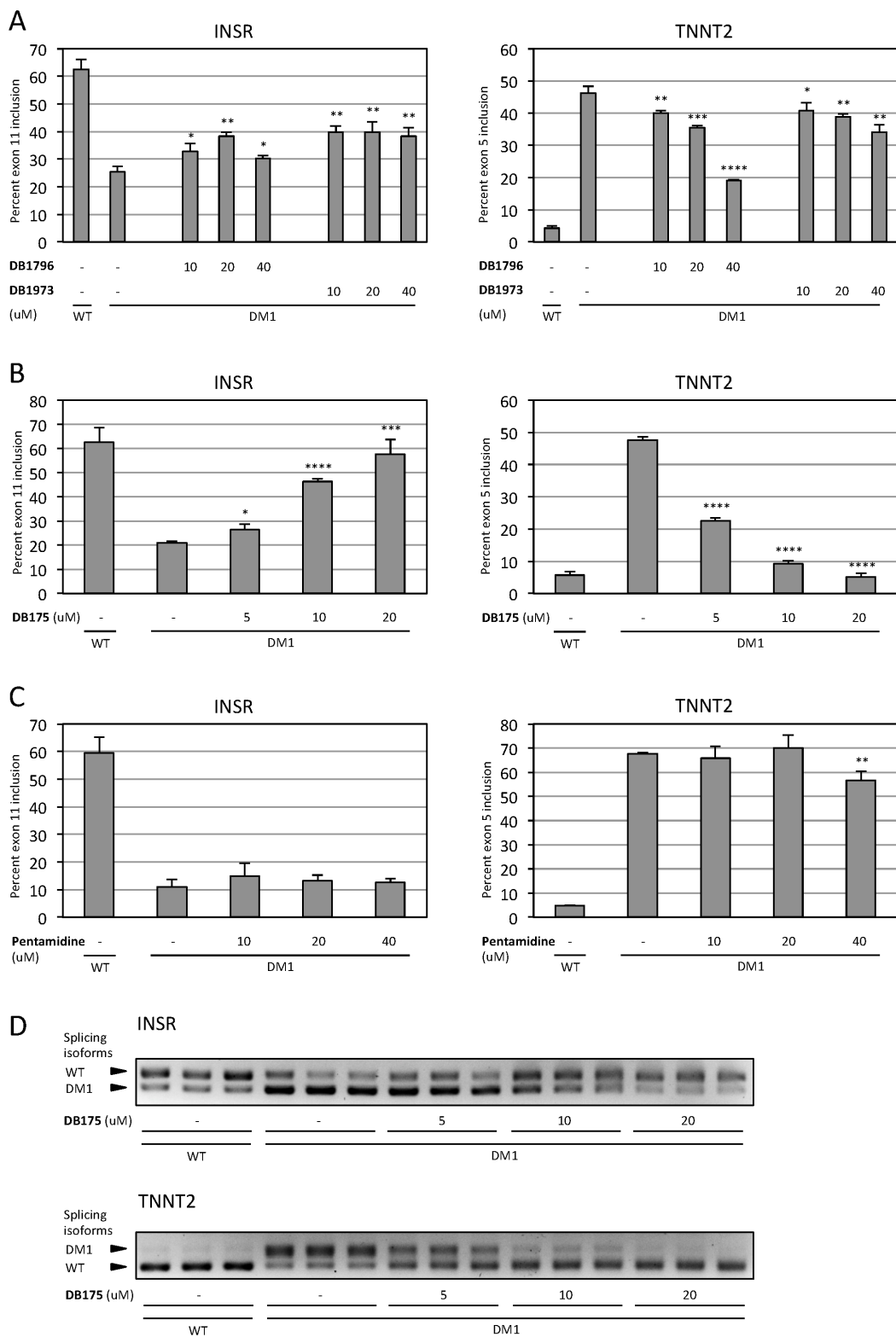


Figure 9 (II 2): Representative RT-qPCR and RT-PCR splicing data for WT and DM1 control cells as well as treated DM1 human myoblast cells.

Fig. II 2A,B: Di-imidazolines improve the splicing of the TNNT2 and INSR pre-mRNA. DB175 fully restores the splicing of both pre-mRNAs at 20 μ M concentration.

Fig. II 2C: Pentamidine has no effect on splicing of the INSR and TNNT2 pre-mRNA, except for an improvement of TNNT2 splicing at the highest concentration of 40 μ M.

Fig. II 2D: Alternative splicing of INSR and TNNT2 pre-mRNA analyzed by RT-PCR and visualized on 3% agarose gels. Shown are the two alternative splicing isoforms for both genes in untreated WT and DM1 control cells and DM1 cells treated with DB175. The WT splicing isoform is the predominant mature splicing variant, whereas the DM1 isoform is the predominant fetal splicing variant.

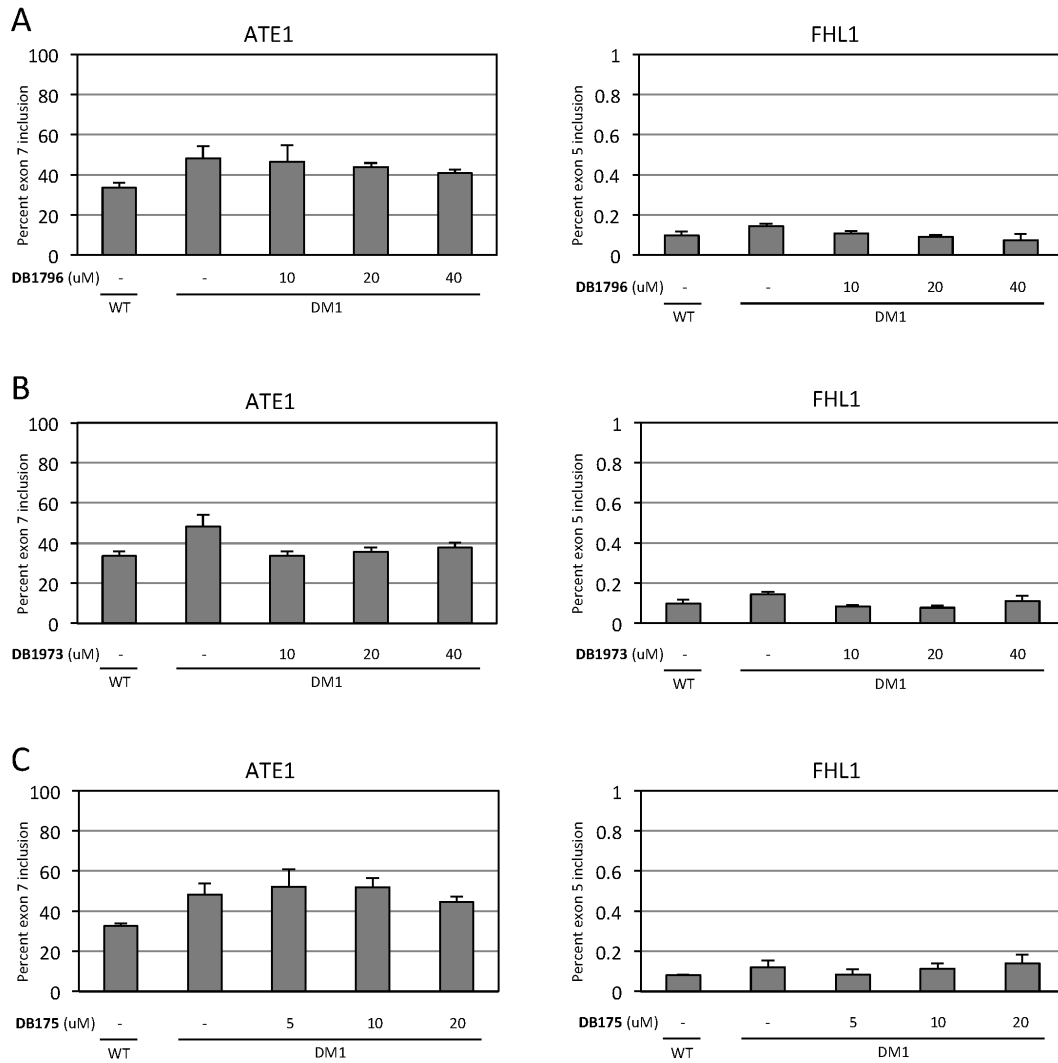


Figure 10 (II 3): Di-imidazolines do not affect alternative splicing of MBNL1-independently regulated ATE1 and FHL1 pre-mRNAs in treated DM1 myoblasts, compared to untreated WT and DM1 control myoblasts.

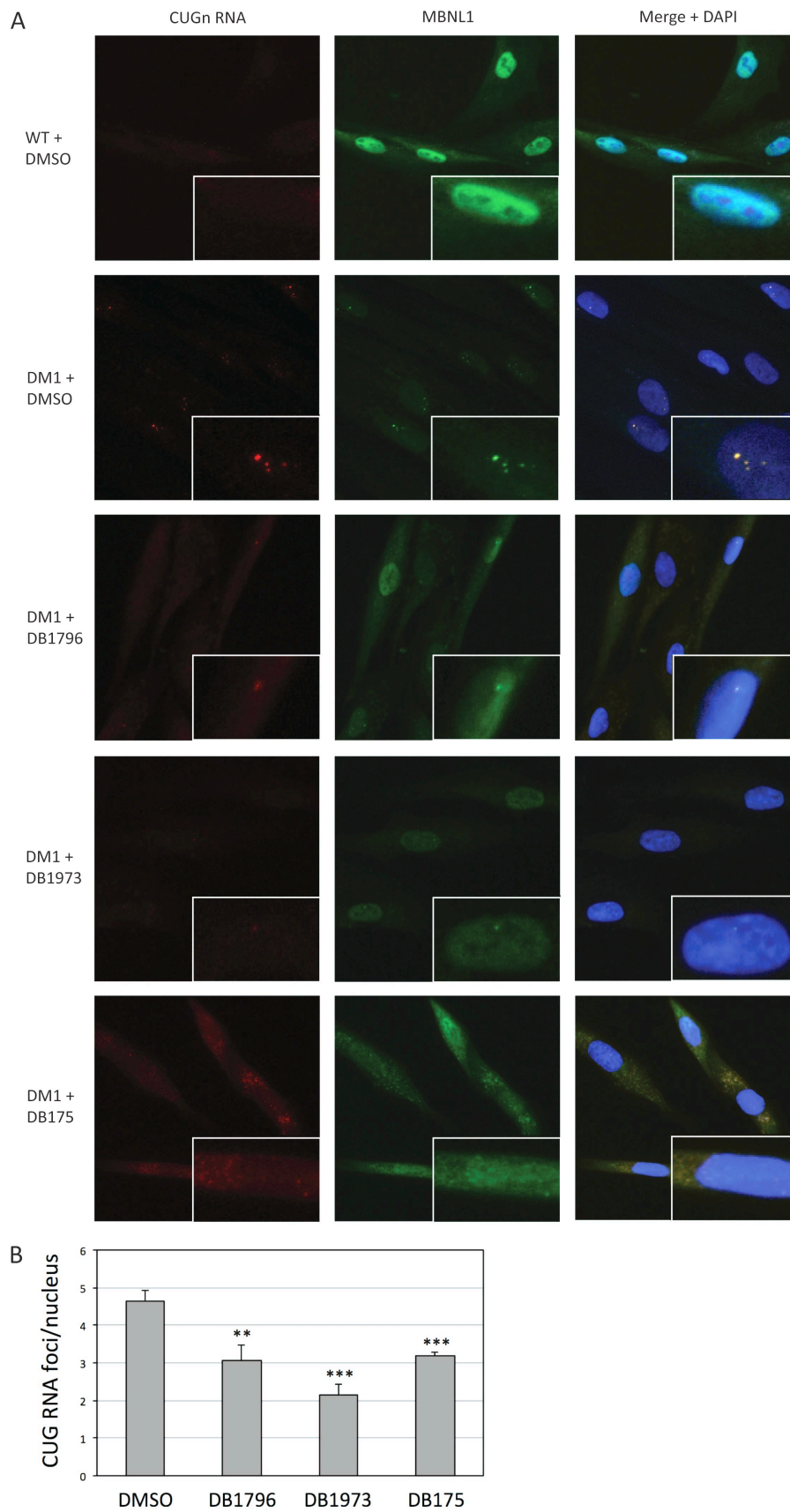
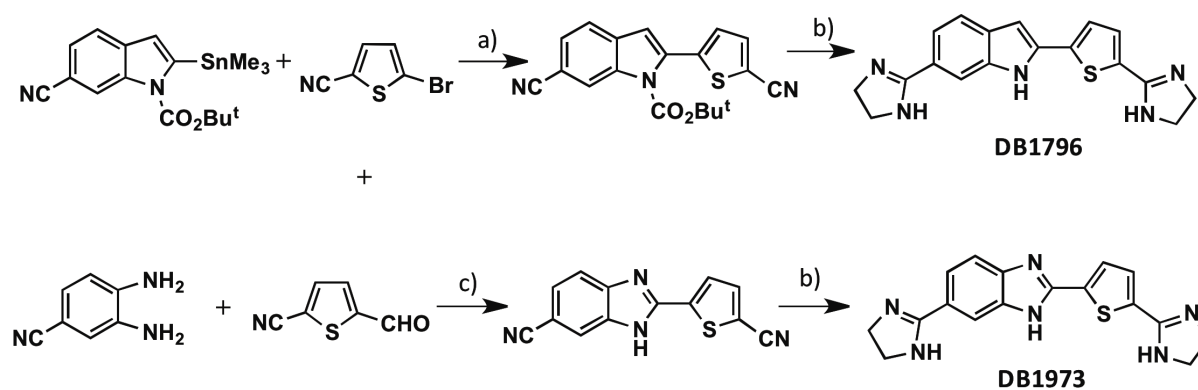


Figure 11 (II 4): FISH detection of CUG_n RNA and immunofluorescence detection of MBNL1 in human WT and DM1 myoblasts.

Fig. II 4A: Di-imidazolines reduce the amount and intensity of *foci* at 40 or 80 μ M concentration. For each condition a CUG_n RNA staining (red), MBNL1 staining (green) as well as a merge of both with a nuclear DAPI staining (blue) is shown. Vehicle treated control WT and DM1 cells as well as compound treated (DB1796 and DB 1973 at 80 μ M, DB175 at 40 μ M) cells are shown. *Foci* are colored yellow in an overlay of CUG_n RNA (red) and MBNL1 (green) staining.

Fig. II 4B: Quantification of the number of CUG_n RNA *foci* in human DM1 cells either treated with DMSO, with DB1796 and DB1973 at 80 μ M, or with DB175 at 40 μ M.



Scheme 1 (II 1): Synthesis of DB1796 and DB1973. Reagents and conditions: a) i: Pd(PPh₃)₄, dioxane, Δ ; ii: THF, DMAP, Boc₂O; b) i: EtOH, HCl; ii: EDA, Ethanol; EtOH, HCL c) NaHSO₃, DMF, Δ .

Table 1 (II 1): Physicochemical and pharmacokinetic parameters of di-imidazolines and the lead compound pentamidine.

Compound	log $D_{7.4}$	pK_a		PAMPA log P_c [log10 ⁻⁶ cm/s] / pH	PPB [%]
		pK_a (<i>in silico</i> , Marvin)	pK_a (<i>experimental</i> , ¹ H-NMR)		
DB1796	n.d.	9.21 7.09	-	-10 ± 0.0 / 3 -7.3 ± 0.5 / 5 -7.5 ± 1.6 / 7.4	69.5
DB1973	< -1.5	9.02 6.63 3.56	7.83 ± 0.35 - 0.61 ± 0.07	-9.4 ± 1.2 / 3 -9.4 ± 1.3 / 5 -9.4 ± 1.3 / 7.4	n.d.
DB175	n.d.	8.85 9.50	-	-9.5 ± 1.1 / 3 -9.3 ± 1.5 / 5 -10 ± 0.0 / 7.4	97.1
Pentamidine	0.144 ± 0.003 (98)	12.13 11.53	-	-9.1 ± 1.1 / 3 -9.2 ± 1.2 / 5 -9.4 ± 0.8 / 7.4	41 ± 5 (98)

2.7 Discussion

As both of our studies are discussed in detail in the individual manuscripts, the scope of this general discussion will be to give an overview over both studies, to compare them, and to draw the main conclusions, while providing some complementary information. In the following, the study with natural compounds (manuscript I) will be referred to as study 1 (S1) whereas the study with synthetic antiprotozoal compounds (manuscript II) will be referred to as study 2 (S2).

Screening assay

The development of a novel *in vitro* CUG₇₈-MBNL1 inhibition assay, using DMPK-CUG₇₈ RNA transcribed from DNA of a DM1 patient and recombinant MBNL1-HIS, permitted successful screening of compound libraries to identify CUG₇₈-MBNL1 complex inhibitors. Initially, we developed a thermal shift assay, based on the Differential Scanning Fluorimetry (DSF)/Thermofluor method (103). MBNL1 thermodenaturation was monitored with an environmentally sensitive fluorescent dye (SYPRO Orange), which becomes fluorescent upon binding to hydrophobic patches of the unfolding protein. CUG₇₈-RNA stabilized MBNL1 and resulted in a shifted MBNL1 thermodenaturation curve of 3 – 4 °C higher T_m values. Successful CUG₇₈-MBNL1 complex inhibitors would decrease MBNL1 ΔT_m values. This assay was eventually deemed unsuitable for screening, because compound-intrinsic fluorescence interfered with the fluorescent readout of the assay. As nucleic acid binders are often aromatic, with extended π -electron systems, they are prone to this kind of interference. We developed an ELISA-type assay instead, i.e. the CUG₇₈ MBNL1-inhibition assay. By washing, compounds were removed before the readout of a photometric signal that correlates to the amount of CUG₇₈-bound MBNL1. Compared to a similar assay described by Pushechnikov *et al.* (53), instead of binding CUG_n RNA to an immobilized capture DNA oligonucleotide (biotinylated), we directly immobilized CUG₇₈ RNA (biotinylated during *in vitro* transcription) to neutravidin plates. Direct immobilization of RNA is simpler and might allow for straightforward assay development for other RNA-protein targets. Besides the CUG₇₈ MBNL1-inhibition assay we also developed an electrophoretic mobility gel shift assay (EMSA), similar to the one used in the screening study of Warf *et al.* (51). The EMSA was based on different electrophoretic mobility in agarose gel of both CUG₇₈-RNA and MBNL1, either in free form or in complexed form. The EMSA was suitable as a secondary assay to confirm complex inhibitors, but not for screening and for quantification of IC₅₀ values.

Screening hits

The S1 screening of natural substances at 100 μM , or extracts at 100 $\mu\text{g/ml}$, yielded a low number of hits compared to the screening of synthetic compounds in S2. This finding makes sense as the library in S2 contained compounds designed to bind to protozoan DNA. Thus, S2 screening at concentrations of 10 μM yielded a high number of hits that bound CUG₇₈ RNA. Lowering the concentration to 1 μM or lower allowed for the identification of the best binders, which inhibited MBNL1 binding to CUG₇₈ RNA at nanomolar concentrations. These were exclusively of the imidazoline or amidine type, predominantly imidazolines. The three di-imidazolines DB1796, DB1973 and DB175, which eventually proved to be the most effective compounds in a DM1 cell model, were not among the best screening hits and had moderate IC₅₀ values between 1 and 6 μM . The weaker inhibitory activity is likely compensated by better membrane permeability or target selectivity. The S1 screening, in contrast, led to the identification of mainly alkaloids, with the best complex inhibitors being berberine and harmine (IC₅₀ values close to 100 μM) and coralyne (IC₅₀ \sim 20 μM). Regarding the biological effect, the weaker *in vitro* complex inhibitory activity is likely compensated by good cell permeability; the two alkaloids are membrane permeable and even pass the blood-brain barrier into the CNS where they inhibit monoamino oxidase (MAO) (85, 86). The results from the two screenings underline the strong influence of the library content, i.e. the type of screened molecules and chemical diversity, on hit number. The library in S1 was of high structural diversity and yielded only a few hits, even though the library was much larger than in S2. Indeed, as the 2128 extracts were compound-mixtures, the actual number of screened molecules was much greater. The screening in S2, in contrast, was a focused screening with molecules belonging to a constricted chemical space, close to the lead compound pentamidine, and thus yielded a high number of hits. In this case stringent selection by lower screening concentrations and further selection in a biological system, such as a DM1 cell model, proved to be of utmost importance.

Evaluation of hits in human DM1 myoblasts and C2C12 myoblasts

Screening hits from both studies were further analyzed for their ability to improve DM1 associated molecular defects, i.e. mis-splicing and nuclear *foci* formation. Our primary assay to test bioactivity was a splicing assay in DM1 myoblasts (DMPK-CUG₁₃₀₀) and wild type control myoblasts (DMPK-CUG₅). We checked whether compound-treated DM1 myoblasts showed a restoration of splicing of the INSR and the TNNT2 pre-mRNA, two MBNL1-regulated alternative splicing events (35). A secondary assay analyzed nuclear *foci* number.

For splicing analysis we developed a new RT-qPCR method, using two primer pairs for an alternatively spliced gene. One primer pair detects all alternative splicing variants of a gene (“pan” primer pair) and the other primer pair detects only those variants including an investigated alternatively spliced exon (“exon” primer pair), by placing either the forward or the reverse primer directly into the alternative exon. Thereby the amount of the exon-containing variant can be quantified relative to the total amount of all variants. Compared to classical RT-PCR, the new method allows for more accurate and convenient quantification of exon inclusion/exclusion by fluorescence readout with a real-time qPCR machine. RT-PCR, as an end-point PCR, is heavily dependent on choosing the optimal PCR cycle number (amplification time), which should lie in the exponential amplification phase for the splicing variants to be analyzed. In addition, analysis of DNA band densities on agarose gels is a source of experimental inaccuracy. Lastly, different amplicons (splicing variants) are amplified with different effectivity, which is not accounted for in classical RT-PCR.

S1 yielded the three alkaloids, berberine, harmine and coralyne as the strongest CUG₇₈-MBNL1 complex inhibitors. The first two partially improved splicing in the DM1 myoblasts whereas coralyne, probably owing to unselective nucleic-acid intercalation, showed no effect on splicing of the INSR and TNNT2 pre-mRNA. Interestingly, the strongest inhibitors from S2, with much lower IC₅₀ values were mostly either not active in the cell-splicing assay or toxic to the DM1 myoblasts. Testing of compounds with intermediate inhibitory activity (1 – 10 μM) led to the identification of the most potent bioactive compounds from S2: DB1796, DB1973 and DB175, three di-imidazolines. DB175 fully restored splicing of both the INSR and TNNT2 pre-mRNA at 20 μM concentration and might be an interesting new lead compound for DM1 drug discovery. Overall, imidazolines were more potent in the splicing assay compared to amidines, e.g. the lead compound pentamidine, which we suggest is due to favorable RNA-binding and favorable pharmacokinetic properties of the imidazoline group compared to amidine (both discussed below). Structure analysis of the strongest inhibitors showed that the *in vitro* screening assay selects strong intercalators such as coralyne (74), with poor target selectivity, and highly charged molecules with poor cell permeability. Such compounds failed to show a splicing effect in DM1 myoblasts. To circumvent the issues linked to our *in vitro* screening assay, high-content cell-based phenotypic screening assays could be used as primary screening assays, to directly select suitable small molecules in cells (60). Some of our identified complex inhibitors were toxic at the concentrations used in cell culture (20, 40 μM), indicating nonselective RNA/DNA binding. Some compounds also showed a worsening effect on alternative splicing, e.g. berberine on INSR splicing, which is

likely caused by their binding to nucleotide sequence motifs shared between the toxic CUG_n RNA and the target pre-mRNAs of MBNL1. MBNL1 binds to pyrimidine-embedded CG motifs (YGCY) present in both types of RNA (78, 104). MBNL1-binding to these motives upstream of an alternative exon promotes exon exclusion, while binding downstream of the alternative exon promotes its inclusion (78, 104). Some compounds might therefore also bind to MBNL1 natural target motifs and interfere with alternative splicing. Selectivity has been best addressed by modular assembly of CUG-binding small molecules, with the resulting oligovalent compounds binding more strongly to the toxic DMPK CUG_n repeats with multiple binding sites compared to MBNL1 target pre-mRNAs with fewer binding sites (90). These polymers are, however, not suitable as therapeutics due to their membrane impermeability *in vivo*. Our identified small molecules were not tested for *in vitro* binding of MBNL1 target pre-mRNAs and other off-target RNA binding. CUG₇₈-MBNL1 complex inhibition by these compounds *in vitro* was not impaired by addition of an excess of yeast tRNA (200 nM). Furthermore, we analyzed the compounds' selectivity for MBNL1-dependent splicing events in the DM1 myoblast model. The alkaloids as well as the di-imidazolines did not affect the alternative splicing of two MBNL1-dependently spliced genes ATE1 and FHL1 (72), compared to both wild-type and DM1 untreated control myoblasts. All of the identified bioactive small molecules from S1 and S2 were furthermore evaluated in a cell viability assay with C2C12 mouse myoblasts to determine Tox IC₅₀ values which were all above 120 μM. The compound concentrations used in the DM1 myoblast splicing assay (20, 40 μM) were below the Tox IC₅₀ values but still relatively close. The rather narrow therapeutic window is an issue with the identified compounds.

Physicochemical and pharmacokinetic properties of identified compounds

The alkaloids berberine, its derivatives palmatine and dihydroberberine, and harmine are cell permeable, even known to cross the blood brain barrier (85, 86). In spite of weaker *in vitro* IC₅₀ values than the di-imidazolines from S2, the alkaloids readily improved molecular defects in the DM1 myoblast model at the same concentrations (20, 40 μM). They apparently make up for their weaker CUG_n RNA affinity with better cell permeability. We therefore did not investigate physicochemical/pharmacokinetic parameters for the alkaloids. Such parameters were investigated for the synthetic compounds from S2, which were more problematic, due to their positive charges. Their *in vitro* analysis revealed little to no cell permeability (low log *P_e* values) and high hydrophilicity (low log *D_{7,4}* values). Still, the lower p*K_a* values of the imidazoline group compared to the amidine group predict a small amount of unprotonated,

cell-permeable species at pH 7.4 as calculated with MarvinSketch® (ChemAxon). Cation transporters might play a role in cellular uptake of di-imidazolines; however, we did not analyze this. The three identified di-imidazolines did not improve splicing in the HSA^{LR} mouse model for DM1. To see whether their *in vivo* pharmacokinetic was the reason for their missing splicing effect, a plasma concentration over time profiling for DB1796 and DB175 was performed (Fig. 12). The study was done at Charles River Laboratories (MA, USA). FVB/N mice were given a single dose of 10 mg/kg i.p. and blood was taken at nine time points. Plasma sample extraction and LC-MS measurement of DB1796 / DB175 compound concentrations (for experimental details see manuscript II; the method is mostly analogous to the one described for the *in vitro* PPB study) revealed reasonable maximal plasma concentrations (C_{max}) at 0.25 h after injection, but very short half-life times ($t_{1/2}$) (Table 2). Parameters were modeled with PKSolver 2.0 (105), and half time was deduced from the first phase (0 – 8 h) in the biphasic decreasing profile. The fast elimination is likely mediated by renal excretion. Interestingly, DB175 shows a slower elimination and three times larger area under the curve AUC_{0-24h} compared to DB1796, which might be linked to its higher PPB, possibly mediated by the lipophilic cyclohexane moiety. The fast elimination and low average plasma concentration (C_{avg}), indicates that the di-imidazolines are not optimal candidates for an *in vivo* application and will require further medicinal chemistry refinement. Their missing splicing effect *in vivo* is probably due to their unfavorable pharmacokinetic profile. Our findings indicate the importance of a balanced compound profile in activity, selectivity and pharmacokinetic parameters.

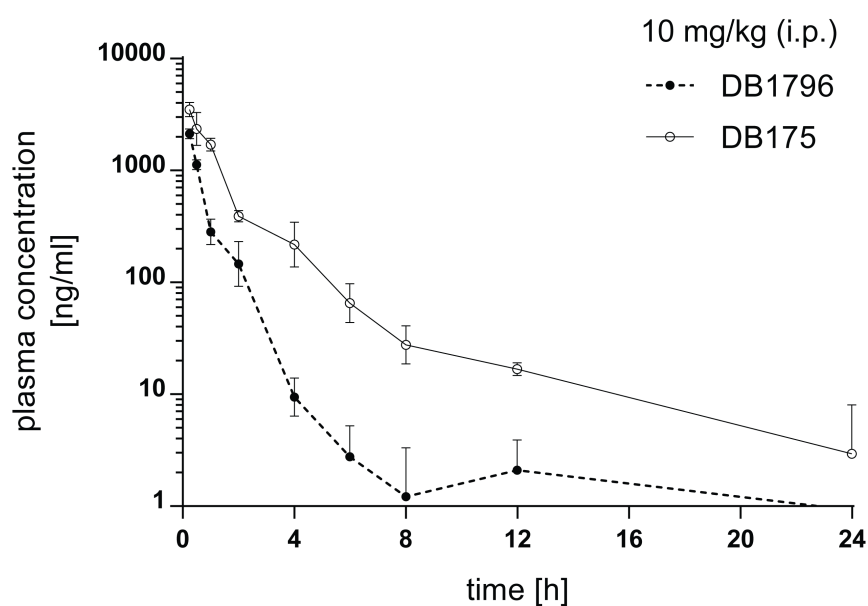


Figure 12: Mean concentration in mouse plasma over time profiles for DB1796 and DB175.

Table 2: *In vivo* pharmacokinetic parameters of DB1796 and DB175.

Compound	AUC _{0-24h} [ng/ml*h]	C _{max} [ng/ml]	C _{avg} [ng/ml]	t _{1/2} [min]	PPB [%]
DB1796	1464.5	2123.3	61.0	28.6	75.7
DB175	4467.8	3513.3	186.2	46.1	92.6

In vivo evaluation of bioactive compounds in the HSA^{LR} mouse model

Three alkaloids from S1 showed a partial improvement of DM1 characteristic mis-splicing of the chloride channel CLCN1 in the HSA^{LR} model, i.e. the two close berberine derivatives dihydroberberine (DHB) and palmatine, as well as harmine. DHB also caused a trend towards increased levels of CLCN1 protein. However, the alkaloids induced toxicity in mice, an issue which will have to be addressed in future studies with these or similar compounds. *In vivo* experiments with the three di-imidazolines from S2 showed no splicing improvement. These findings are in line with the *in vitro* pharmacokinetic analysis, indicating low membrane permeability, and the *in vivo* pharmacokinetic profile for DB1796 and DB175, showing low average plasma concentrations and fast elimination from mouse plasma (Fig. 12).

2.8 Conclusion and Outlook

Our drug discovery effort for DM1 led to the identification of several alkaloids in S1 and di-imidazolines in S2. These compound classes are of interest for future DM1 drug discovery studies and studies in other RNA-mediated diseases. The identified small molecules can serve as valuable starting points for medicinal chemistry programs. In addition, these compounds could be used to synthesize high-affinity/selectivity polymers that account for the repeating structure of the binding sites on CUG_n RNA, as was performed in the study of Lee *et al.* (90). Taken together, the results from both of our studies show that a balanced activity, selectivity (toxicity) and pharmacokinetic profile is key for an interesting lead compound in DM1 and RNA drug discovery in general. As nucleic acid binders often contain positive charges at physiological pH the refinement of the pharmacokinetic profile to allow for cell membrane permeation is crucial. The compounds identified in our studies have therapeutic potential, but also clear deficits that will have to be addressed in future studies.

Alkaloids are an interesting compound class for DM1 drug discovery

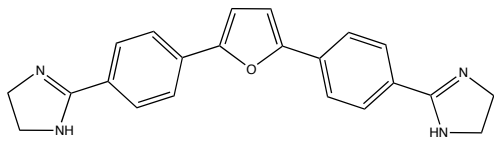
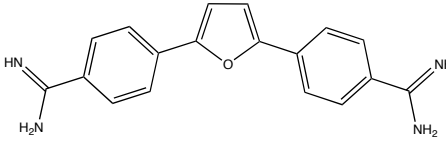
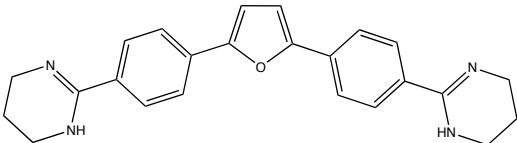
The three strongest MBNL1-CUG₇₈ complex inhibitors identified in the natural compound screening (S1) were alkaloids. berberine, harmine and coralyne have all been described before to bind to certain RNA targets, i.e. tRNA, double stranded RNA, or polyA RNA (74-77). In the context of the DM1 characteristic CUG_n RNA, only the *in vitro* screening study by Chen *et. al.* yielded alkaloids as hits; out of six hits, four were alkaloids or alkaloid derivatives of the opioid and ergot alkaloid type, but none of these alkaloids was confirmed in a second screening assay (58). Altogether, the mentioned findings and our results support the notion that alkaloids are of interest in RNA drug discovery due to certain chemical attributes that enable RNA-binding. Possible interactions include stacking with nucleobases via aromatic groups, hydrogen bonding with the Watson-Crick or Hoogsteen face of nucleic acids, either as acceptors (nitrogen and oxygen groups) or as donors (hydroxyl and amine groups), and electrostatic interaction with the negatively charged phosphate backbone of RNA through positively charged nitrogen groups of the alkaloids. Isochinolin, beta-carboline, indole, opioid and ergot alkaloids etc. might be of considerable valuable for RNA drug discovery, as potential therapeutic molecules or as lead compounds.

Di-imidazolines – an interesting alternative to diamidines

The focused screening of synthetic pentamidine-related substances in S2 led to the identification of three di-imidazolines that outperformed the lead compound pentamidine in several aspects: notably in target RNA binding, bioactivity in the DM1 myoblasts, lower toxicity and probably improved membrane permeation. The imidazoline group seems to enable strong RNA-binding and was superior to amidines, tetrahydropyrimidines, arylimidamides and other related compounds in our *in vitro* and cellular assays. Also Parkesh *et al.* described a few imidazolines as good CUG_n-RNA binders (92). The molecular rationale behind strong RNA binding of the imidazoline group lies in its planarity. Thermal melting studies on poly(A)•(U) RNA with three aromatic diphenylfuran compounds (93), i.e. a diphenylfuran imidazoline (1), a diphenylfuran amidine (2), and a diphenylfuran tetrahydropyrimidine (3) had shown that RNA binding/stabilization, quantified via ΔT_m , was in the order (1) > (2) > (3) (Table 3). Molecular modeling studies with the three compounds and double stranded A₈•U₈ RNA showed that these compounds intercalate via the major RNA groove, and that steric clashes of all three diphenylfuran substituents impaired binding via the minor groove (100). The NCN bond angle was found to be smaller in the five-membered imidazole (1) compared to the torsion angle in compounds (2) and (3). The planar imidazoline (1) slid more deeply into the

intercalation site than the amidine (2) with an NCN torsion angle of 30 – 35° and the six-membered tetrahydropyrimidine (3) with an NCN torsion angle of ~ 30°, all relative to the phenyl group. The torsion angles of the diphenylfuran substituents of compounds (2) and (3) caused steric clashes with the nucleobases at the intercalation site. Hence, both experimental ΔT_m values and *in silico* energy minimization explained stronger RNA binding of the imidazole compared to the amidine and tetrahydropyrimidine groups (93, 100). Interestingly, the strongest complex inhibitor in S2 was the furimidazole DB60, the same compound as (1) described in the study of Wilson *et al.* (93). Three further compounds out of the six best S2 hits were close derivatives of (1), whereas the other two inhibitors were a dibenzimidazolfuran imidazole and a dibenzimidazolfuran amidine, both containing four positive charges at physiological pH 7.4. DB60 fully inhibited MBNL1 binding to CUG₇₈ at 125 nM concentration and apparently is a perfect intercalator for the CUG_n RNA, considering the discussed findings (93, 100). The toxicity and missing splicing effect of DB60 and its close derivatives in the DM1 myoblast model was probably due to target nonselectivity. Certainly, the three identified bioactive di-imidazoles have an intercalative component in RNA binding; DB1796 and DB1973 are fully planar, whereas DB175 is not. Its cyclohexane substituent might convey better target selectivity, which could be the reason for its complete splicing restoration of the TNNT2 and INSR pre-mRNAs in the DM1 myoblast model at 20 μ M concentration.

Table 3: Diphenylfuran derivatives and their stabilization of poly(A)•(U) and poly(A)•(T) (93).

Compound	Structure	ΔT_m poly(A)•(U)	ΔT_m poly(A)•(T)
(1)		14.4	>25
(2)		5.7	24.6
(3)		2.5	26.5

The di-imidazolines DB1796, DB1973 and DB175 provide interesting compounds for RNA targeting and valuable starting points for medicinal chemistry studies. These compounds' selectivity and pharmacokinetic profile pose the biggest challenge for development as potential DM1 drugs. For further studies, we suggest to synthesize analogs of the identified imidazolines, e.g. imidazole, triazole or tetrazole analogs, all with lower pK_a values and thus lower charge and better membrane permeability. Whether RNA binding will be maintained is to be evaluated. A synthesized pyrazole analogue of DB175 (DB2323) was inactive in the DM1 myoblast model, indicating the importance of the H-bond donating NH group of imidazoline. In addition, other lipophilic substituents than cyclohexane should be investigated for the lead compound DB175. Interestingly, DB175 from S2 and harmine from S1 can be regarded as derivatives. Therefore, two different screening studies yielded related compounds.

3 Anti-Myelin Associated Glycoprotein Neuropathy

3.1 Introduction

Anti-MAG neuropathy is a rare disorder of the peripheral nervous system characterized by slowly progressive demyelinating, predominantly sensory neuropathy (8). Patients have high serum levels of monoclonal immunoglobulin M (IgM) autoantibodies that react with the human natural killer 1 (HNK-1) epitope on the myelin-associated glycoprotein (MAG) and on other myelin components. These antibodies are thought to be pathogenic (8, 106). The disease prevalence is not exactly known, but is expected to be similar to the prevalence of a related form of neuropathy called multifocal motor neuropathy (MMN), which affects about 1 – 2 persons in 100'000 people (107). Anti-MAG neuropathy affects mostly men over 50 years old (108). Patients develop sensory loss starting in the toes and fingers, sensory ataxia, and tremor in the hands and legs. As the disease progresses, the tremor becomes more severe and the ataxia steadily worsens. Due to extensive muscle weakness some patients become severely disabled and wheelchair-bound (106).

Classification of anti-MAG neuropathy

The peripheral nerve disorder anti-MAG neuropathy can be categorized as a member of the spectrum of immune-mediated peripheral neuropathies / polyneuropathies. There are acute and chronic types of immune-mediated peripheral neuropathies, whereby anti-MAG neuropathy is of the chronic type. This disease develops in patients with IgM monoclonal gammopathy of unknown significance (MGUS) and is characterized by autoreactivity against a carbohydrate epitope on MAG. Monoclonal gammopathy or paraproteinemia describes the presence of excessive amounts of a monoclonal immunoglobulin. Monoclonality is thought to arise from a somatically hypermutated B cell clone, acquiring IgM secretory activity (109, 110). In the following, a short overview will be given on immune-mediated peripheral neuropathies for which anti-carbohydrate antibodies have been identified that target various components of myelin. This overview is based on a recent review written by three leading experts in the field of peripheral neuropathy: Andreas Steck, Nobuhiro Yuki and Francesc Graus (111).

Acute immune-mediated neuropathies with anti-carbohydrate antibodies

In the group of acute immune-mediated neuropathies, the Guillain-Barré syndrome (GBS) encompasses several disease conditions that often involve autoantibodies against endogenous nerve glycoepitopes. The two major subgroups among GBS are the acute motor axonal neuropathy (AMAN) and the acute inflammatory demyelinating polyneuropathy (AIDP), with AMAN predominantly affecting motor nerves compared to AIDP. Both AMAN and AIDP can involve autoantibodies against gangliosides such as GM1, GM1b, GD1a and GalNAc-GD1a. Another clinically distinct subgroup of GBS is the Fisher syndrome, which is mainly associated with antibodies against the GQ1b or the GT1a epitope. The pathogenic autoantibodies in the group of acute neuropathies are mostly of the IgG isotype (111).

Chronic immune-mediated neuropathies with anti-carbohydrate antibodies

In contrast, in the group of chronic neuropathies, mostly IgM autoantibodies are detected. With a prevalence as high as 9 in 100'000 (112) the chronic inflammatory demyelinating polyneuropathy (CIDP) is the most common form of chronic demyelinating polyneuropathy. CIDP can be considered as the chronic counterpart of the acute GBS. GBS is post-infectious, while CIDP is an autoimmune disorder. CIDP is usually not associated with anti-carbohydrate antibodies. The two other major disease groups among the chronic inflammatory neuropathies are the anti-MAG neuropathy and multifocal motor neuropathy (MMN). The anti-MAG neuropathy mainly involves autoantibodies against the HNK-1 epitope, present on multiple myelin antigens such as MAG, SGPG, SGLPG, P0 and PMP22. MMN patients often show autoantibodies against the ganglioside GM1. Other, less frequent, chronic neuropathies encompass the chronic sensory axonal neuropathy with anti-sulfatide antibodies, the chronic motor neuropathy with GD1a or GD1b antibodies, and the CANOMAD (chronic ataxic neuropathy, ophthalmoplegia, M-protein, agglutination, disialosyl antibodies) with antibodies against disialosyl gangliosides, such as GQ1b and GD1b. Another subgroup of rare chronic neuropathies involves IgM autoantibodies against chondroitin or heparan sulfate (111).

Neuropathies associated with IgM monoclonal gammopathy

Among patients with IgM monoclonal gammopathy (M-protein) the prevalence of neuropathy is estimated to be between 5 to 31% (113, 114). About 50% of IgM antibodies in patients with IgM gammopathy-associated neuropathy react with the HNK-1 epitope; other targets include gangliosides, sulfatide, chondroitin and heparan sulfate (108). IgM monoclonal gammopathy and also neuropathy can be caused by IgM-secreting lympho-proliferative diseases, e.g. Waldenström's macroglobulinemia, lymphoma, myeloma, or chronic lymphocytic leukemia.

However, most neuropathies associated with IgM gammopathy are not linked to one of these lymphoproliferative disorders and are denoted as MGUS (115). In MGUS patients, neuropathy is normally the only clinical symptom caused by the underlying hematologic disorder (108). The IgM antibodies in most of the MGUS patients react with the HNK-1 epitope, implying that anti-MAG neuropathy is the most common form of neuropathy in the MGUS group. Nevertheless, the cause of its underlying lymphoproliferation is not known (8, 116).

3.2 Molecular Disease Mechanism

Discovery of IgM autoantibodies and their antigen on myelin

Anti-MAG neuropathy was first characterized and described as a distinct clinical entity in the early 80s. Back then, it was known that monoclonal IgM autoantibodies from patients with paraproteinemia and peripheral neuropathy react with a myelin protein component of the PNS and an analogous component of the CNS. Studies by Braun *et al.* and Steck *et al.* described for the first time the specific antigen for the monoclonal IgM antibodies: the myelin protein MAG (117, 118). At the same time McGarry *et al.* showed that the HNK-1 antibody, which was raised against a membrane antigen of T cells, cross-reacted with MAG (119, 120). Subsequently, it was shown that the epitope for the patients' IgM antibodies resided in the carbohydrate component of MAG, as shown by loss of antibody reactivity upon deglycosylation of human MAG (121). The same study by Ilyas *et al.* had furthermore described cross-reactivity of patient IgM antibodies with glycolipids in the ganglioside fraction of human peripheral nerve. These glycolipids were later on described to lack sialic acid and to contain 3-*O*-sulfoglucuronic acid (SO₃-3GlcA) as a specific epitope hallmark (122, 123). Finally, the structure of two immunoreactive glycolipids of the peripheral nervous system was described: sulfoglucuronyl paragloboside (SGPG) and sulfoglucuronyl lactosaminyl paragloboside (SGLPG) (124). Interestingly, Chou *et al.* had also shown that both IgM antibodies from neuropathy patients and the HNK-1 antibody bind to these glycolipids (122, 123). Taken together, these findings indicated a shared carbohydrate epitope on MAG, SGPG and SGLPG for IgM antibodies from patients and the HNK-1 antibody.

In 1996, the same carbohydrate epitope was also identified on the myelin glycoprotein zero (P0) and its structure was elucidated from bovine P0 (125). The structural overlap between the pentasaccharide of SGPG, the heptasaccharide of SGLPG and the epitope of P0 was restricted to the terminal trisaccharide at the non-reducing end of these polysaccharides. Hence,

the structure of the HNK-1 epitope was defined as $\text{SO}_3\text{-3-GlcA}(\beta\text{1-3})\text{Gal}(\beta\text{1-4})\text{GlcNAc-OH}$ (Fig. 13).

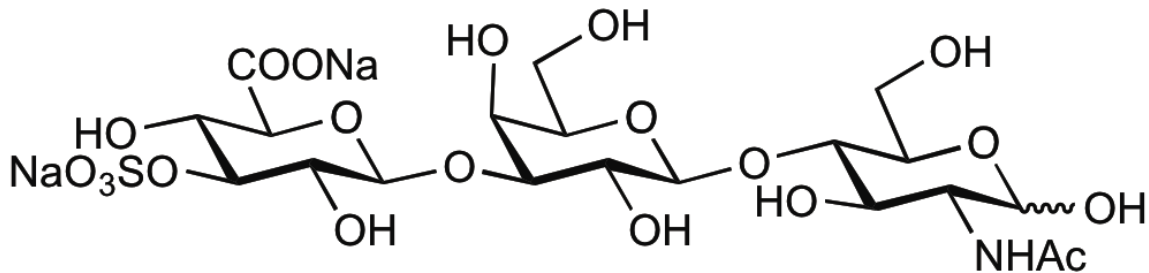


Figure 13: The HNK-1 trisaccharide epitope.

Microheterogeneity of anti-MAG antibodies

Evidence from several studies underline that the specificities of the patient IgM antibodies and the HNK-1 antibody are similar; that is to say that they react with glycoconjugates of peripheral myelin that share the HNK-1 epitope, e.g. the glycoproteins MAG, P0, peripheral myelin protein-22 (PMP22), as well as the PNS-specific glycolipids SGPG and SGLPG (111, 126). Although the HNK-1 epitope is established as the common antigenic determinant for IgM antibodies of patients with anti-MAG neuropathy, there is microheterogeneity in binding strength and structural requirements for binding of anti-MAG antibodies (127). A study by Ilyas *et al.* on IgM antibody binding to SGPG and derivatives thereof had shown previously that the antibodies differ in their structural requirements for binding (128). The study showed that for SGPG binding some anti-MAG IgM antibodies absolutely required the sulfate but not the carboxyl group of the HNK-1 glucuronic acid, whereas for others it was *vice versa*, and a third group of antibodies bound to the glycolipid as long as one of the two negatively charged groups was present. All of the antibodies, including the HNK-1 antibody, bound best to natural SGPG, containing both negatively charged groups (128). Two other studies emphasized the importance of the carbohydrate chain length for antibody binding (129, 130). IgM antibodies were shown to bind more strongly to glycolipids with longer carbohydrate chains. The two terminal sugars $\text{SO}_3\text{-3-GlcA}(\beta\text{1-3})\text{Gal}$ seemed to be the minimum requirement for IgM antibody binding. Whether the additional monosaccharides towards the reducing end of the oligosaccharide chain are involved in binding or merely serve as a spacer could not be determined. Idiotypic heterogeneity is another characteristic of anti-MAG antibodies (131). Therefore, development of an anti-idiotypic antibody for a patients' IgM yielded a therapeutically

effective agent for this specific patient but was ineffective against the IgM antibodies of 20 other patients (131).

Pathogenicity of anti-MAG antibodies

Although the exact role of anti-MAG antibodies in the pathogenesis of neuropathy remains to be clarified, several findings suggest a clear association between anti-MAG antibodies and neuropathy (8, 106). Pathological studies of nerve biopsies from neuropathy patients show demyelination and widening of myelin lamellae, as well as deposits of anti-MAG IgM on myelin (118, 132-134). Localization of IgM antibodies to areas of split myelin indicates a role of the antibodies in myelin disintegration (135). Some studies reported, besides IgM deposits on myelin, the presence of complement proteins (136, 137). These findings indicate a possible involvement of complement activation by IgM antibodies in demyelination. Therapeutic reduction of the anti-MAG IgM antibody levels was shown to lead to clinical improvement of patients in neuropathy symptoms. Such reduction was achieved by treatment with cytostatic agents (138), plasmapheresis (139), and B cell depleting agents such as Rituximab (140, 141). Interestingly, the response of patients to rituximab treatment seems to be correlated to the level of anti-MAG antibody reduction (142) and the level of reduction in non-circulating IgM memory B cells (110). Furthermore, passive transfer (intra-neural or systemic) of the IgM antibodies from patients into healthy experimental animals, including cats (143, 144) and chicks (145), resulted in damage to peripheral nerve myelin and similar pathological characteristics as in human disease (143-146). Active immunization of cats with the glycolipid SGPG induced an ataxic sensory neuropathy, which resembled the human anti-MAG neuropathy (147). All of these findings suggest a pathogenic role of the IgM anti-MAG antibodies in the development of anti-MAG neuropathy (Fig. 14).

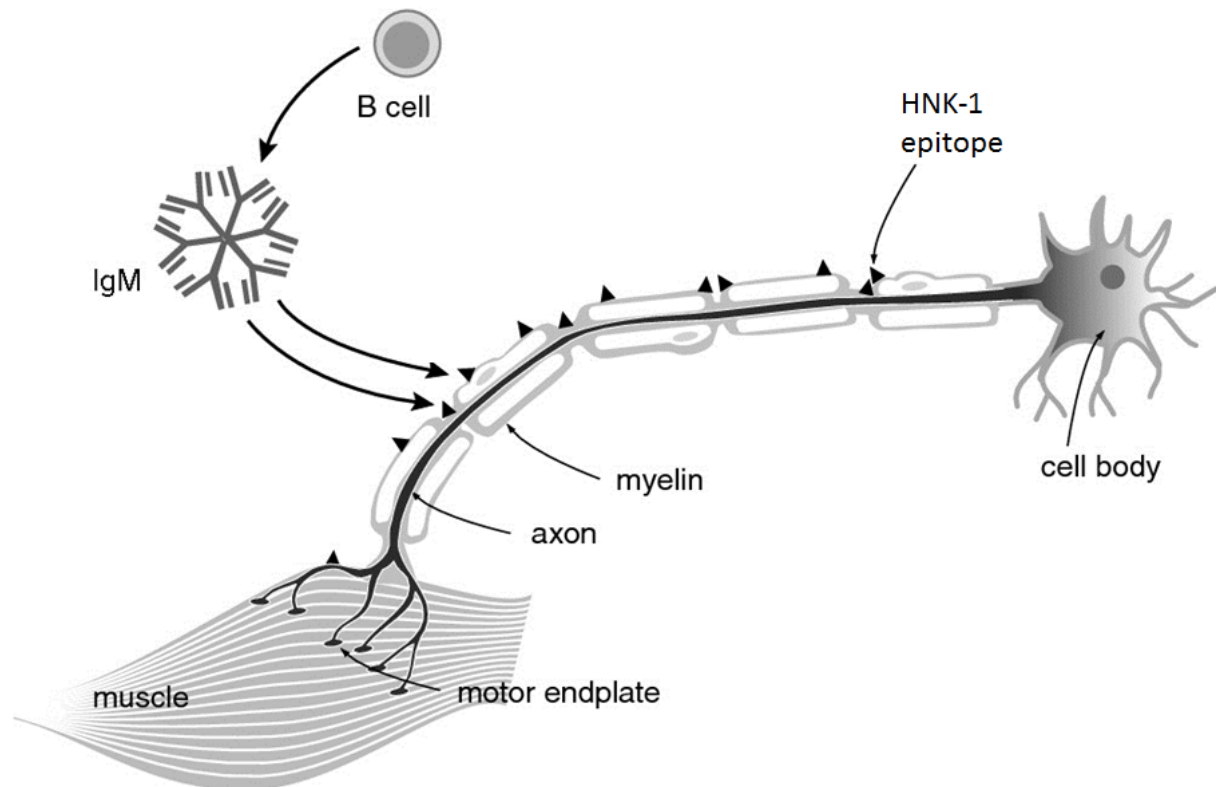


Figure 14: IgM autoantibodies target the HNK-1 epitope on MAG and other myelin components. Graphic modified from Van der Pol WL *et al.*, *J. Clin. Immunol.* **30**, 79-83 (2010).

The role of MAG in anti-MAG neuropathy

The glycoprotein MAG belongs to the family of sialic acid-binding immunoglobulin-like lectins (siglecs) and is classified as siglec-4 (148, 149). It is an I-type lectin, preferentially binding α 2,3-linked *N*-acetylneuraminic acid (Neu5Ac, sialic acid) (126). Besides its capacity to bind carbohydrate receptors, MAG is heavily glycosylated, whereby 30% of the molecule's weight constitutes heterogeneous N-linked oligosaccharides (150). All eight N-glycosylation sites can carry the HNK-1 carbohydrate epitope involved in the anti-MAG neuropathy (151, 152). Of all proteins expressing this epitope, MAG has the highest HNK-1 density, which could explain the strong binding of patients' IgM antibodies compared to other myelin glycoconjugates (153). In accordance, Dalakas reports a 10 to 100 fold stronger binding of IgM antibodies to MAG compared to SGPG, which has implications for diagnostic detection of low-affinity anti-MAG antibodies that can be missed in SGPG-based assays (106). MAG is located mainly in periaxonal membranes of oligodendroglial cells in the CNS and Schwann cells in the PNS (154). Structural details of rat MAG revealed five extracellular immunoglobulin-like domains, a single transmembrane domain and a cytoplasmic domain, which occurs in a short and a long isoform (S-MAG, L-MAG), due to alternative splicing (155-157).

L-MAG is the predominant isoform in the CNS during development, whereas S-MAG is the predominant isoform in the adult CNS and the PNS (158).

In anti-MAG neuropathy, IgM antibodies bind to the S-MAG isoform in the PNS. S-MAG is localized in periaxonal Schwann cell membranes and those of uncompact myelin, e.g. in paranodal loops and Schmidt-Lanterman incisures (158). The intracellular domain of S-MAG has been described to interact with cytoskeletal components of the Schwann cell, e.g. microfilaments and microtubules, emphasizing a role of S-MAG in adhesion processes between the axon and the myelinating Schwann cell (159, 160). MAG is furthermore involved in axon-glia signaling processes, acting on the one hand as a ligand for axonal receptors and on the other hand as a glial receptor for axonal signals (8, 126). MAG has been implicated in a signaling cascade that regulates axonal neurofilament phosphorylation and associated axon diameter (161). MAG is expressed early on in glial cells, indicating a function in early axon-glia interactions, when glial cells wrap around the axon to initiate formation of myelin sheaths (154). MAG knockout mice seem to have relatively normal myelin formation in the PNS, but as they age they develop a neuropathy characterized by decreased axonal caliber, widened periaxonal space, increased neurofilament density, as well as reduced expression and phosphorylation of neurofilaments (162-164). These findings reflect aspects of the nerve pathology of anti-MAG neuropathy patients (161, 165).

Several findings suggest that MAG is the major myelin target for the patients' IgM antibodies: PNS deposits of IgM antibodies co-localize with MAG (166), the IgM antibody titer correlates with selective loss of MAG from myelin (167), the pathology of MAG deficient mice (162-164) shows similarities to the human nerve pathology (161, 165), and MAG exposes probably the highest HNK-1 density of all myelin glycoconjugates, allowing strong IgM antibody binding (153). In conclusion, MAG is involved in the formation and maintenance of myelin sheaths, and furthermore has a regulating effect on axon integrity and function. Anti-MAG IgM antibody binding to MAG interferes with MAGs function, contributing to the pathogenesis of anti-MAG neuropathy. It has been suggested that the axonal atrophy seen in anti-MAG neuropathy patients might be a primary effect of the IgM antibodies binding to MAG (8).

3.3 Current Therapeutic Approaches

Patients with anti-MAG neuropathy are treated with immunosuppressive or immunomodulatory drugs. Treatments aim at reducing IgM antibody titers by either antibody removal or reduction of its production by targeting of the expanded monoclonal B cell clone, or blockage of the assumed effector mechanisms, e.g. complement activation. Paraproteinemic polyneuropathies, such as anti-MAG neuropathy, are potentially treatable, and for some of these diseases there are treatment options (106). For anti-MAG neuropathy, however, to date no treatment has been shown to be satisfactorily effective, hence there is a clear need for new and better treatments. In the following section, a compilation of the evaluated treatments will be given with a specific focus on the currently used therapies.

Chemotherapeutic / cytotoxic drugs

Chemotherapy and cytotoxic drugs have been used since the 80s and a few patients were reported to improve clinically under treatment, whereas the majority of patients were non-responders (138). Cytostatic drugs used in treatment are fludarabine (168) and cladribine (169), which are both purine analogues. Cyclophosphamide has been used in combination with plasma exchange (PE) (170), and in combination with Rituximab (171). In the case of an underlying lymphoproliferative disorder, such as Waldenström's macroglobulinemia, agents like bendamustine, bortezomib and thalidomide-based therapies have been used in combination with Rituximab (172). A general issue with cytostatic therapeutics is their side effects and non-specific immunosuppression; severe and even fatal adverse effects have been reported for some patients (173). There are no controlled trials with any of these treatments (174).

Plasma exchange / plasmapheresis

Plasma exchange (PE) and plasmapheresis has been reported to ameliorate neuropathy in patients either alone or in combination therapy (139, 170). Therapy aims to lower the IgM antibody load by removing circulating antibodies and replacing the patients' plasma with clean substitute plasma. Case reports show benefits lasting from 8 to 36 month, but there are no studies showing a significant benefit of PE (174).

Intravenous immunoglobulin / IVIg

Immunoglobulin of healthy donors has been used in treatment with the aim to "normalize" the immunoglobulin of patients. According to two placebo-controlled trials, one double-blind, there may be a short term benefit of IVIg treatment of a few weeks after infusion (174, 175).

Corticosteroids

Intravenous dexamethasone and oral prednisolone, both immunosuppressive glucocorticoids, have been used in monotherapy, but also in combination therapy with PE or with cytotoxic drugs, e.g. azathioprine, cyclophosphamide, and chlorambucil. There is, however, no data showing statistically significant clinical improvements under corticosteroid treatment (174).

Interferon alpha-2a

Controlled trials with interferon alpha-2a have reported contradictory results. An open trial with an IVIg treated control group had shown a benefit of interferon over IVIg (176). A newer, placebo-controlled, double-blind trial with interferon, however, did not show a significant benefit of interferon (177).

Rituximab

The antibody rituximab has been discussed as being the most promising treatment for anti-MAG neuropathy over the last years; it causes antibody-dependent cell and complement-mediated cytotoxicity of CD20+ B-cells (8, 106, 140). Placebo-controlled trials with rituximab showed marked reduction of CD20+ B-cells and also in the anti-MAG antibody titers. The Dalakas study showed significant clinical improvement. After 8 months, 4 of 13 rituximab-treated patients improved by ≥ 1 INCAT (Inflammatory Neuropathy Cause and Treatment) score compared with 0 of 13 placebo-treated patients ($p = 0.096$). Excluding one rituximab-randomized patient who had normal INCAT score at entry, and thus could not improve, the results were significant ($p = 0.036$). The time to walk 10 meters was significantly reduced in the rituximab group ($p = 0.042$). Clinically, walking improved in 7 of 13 rituximab-treated patients (178). The more recent Leger study failed to show significant improvement in primary outcome measures (179). Nevertheless, significant improvement in secondary outcome measures was reported. Interestingly, clinical improvement has been correlated to the effectiveness of reduction of B cells and IgM antibodies (173), whereas a high load of IgM memory B cells and the persistence of these cells has been correlated with a poor clinical response (110). Clinical worsening has also been described for a few patients treated with rituximab (180, 181). This paradoxical worsening might be linked to an “IgM flare”, a release of paraprotein (anti-MAG IgM) due to rituximab-induced B cell lysis (182). Nevertheless, most patients with anti-MAG neuropathy are currently treated with rituximab. According to comments by Prof. M.C. Dalakas at the ICNMD 2014, it will be crucial to define relevant primary endpoints for future trials with Rituximab or one of its successors, e.g. Eculizumab (Soliris®), Belimumab (Benlysta®), Ocrelizumab, Ofatumumab (Arzerra®), Obinutuzumab

(Gazyvaro/Gazyva®), which might be more efficient in inhibiting B-cells or the complement system. According to comments by J.-M. Leger at the ICNMD 2014, painful paresthesias and sensory ataxia (loss of sensory input in the control of movement) are the most commonly observed disease symptoms, but sensory ataxia is not captured by the scales used in clinical trials, such as INCAT. He suggested better outcome measures to capture improvement in sensory ataxia, e.g. a “time for 10 meters walk” test together with additional biomarkers such as measurement of anti-MAG IgM titers.

3.3.1 Aim of our study

The present work is focused on a new therapeutic and diagnostic approach for the anti-MAG neuropathy, evaluating the first potentially “antigen-specific” therapy. The HNK-1 carbohydrate epitope has attracted considerable interest as a target in anti-MAG neuropathy and compounds binding and blocking specifically the anti-MAG IgM antibodies might be therapeutically of considerable value. Based on the structure of the HNK-1 epitope, carbohydrate mimetics were synthesized that bind to anti-MAG IgM antibodies. Their potential application in the diagnosis, as well as in the treatment, of anti-MAG neuropathy is of considerable medical interest.

3.4 Manuscript III

Anti-MAG Neuropathy - a Carbohydrate Polymer Effectively Blocks Pathogenic Anti-MAG Antibodies

Ruben Herrendorff¹, Fan Yang¹, Nicole Schaeren-Wiemers², Andreas J. Steck², Beat Ernst^{1*}

¹Institute of Molecular Pharmacy, Pharmacenter, University of Basel, Klingelbergstrasse 50, 4056 Basel, Switzerland

²Department of Biomedicine, University Hospital Basel, Hebelstrasse 20, 4031 Basel, Switzerland

* To whom correspondence should be addressed:

To be submitted to *Angewandte Chemie*.

Abstract

Anti-myelin-associated glycoprotein neuropathy is an antibody-mediated demyelinating peripheral neuropathy. The disease is caused by immunoglobulin M (IgM) autoantibodies recognizing the human natural killer-1 (HNK-1) carbohydrate epitope. A specific hallmark of this epitope is an unusual sulfated glucuronic acid. This glyco-epitope is highly expressed in adhesion molecules, such as the myelin-associated glycoprotein (MAG), which is present in myelinated nerve fibers. The pathogenicity of the anti-MAG autoantibodies is well established. Therefore, antagonists that block the antibody binding to MAG are of therapeutic and diagnostic interest.

Our approach was to design carbohydrate ligands that block the IgM antibody binding sites by mimicking the natural epitope. Thus, a minimal HNK-1 epitope, consisting of a sulfated disaccharide, was synthesized. In a competitive binding assay, it successfully inhibited the binding of pathogenic IgM antibodies from patient sera to MAG, although only at micromolar concentrations. A comparison with the unsulfated disaccharide indicated the prerequisite of the sulfate moiety for antibody binding. To mimic the multivalent nature of the MAG - IgM antibody interaction, a polylysine polymer presenting the minimal HNK-1 epitope in a multivalent manner was prepared. Binding affinity was thereby increased by a factor of at least 34000, with inhibitory activity now being in the low nanomolar range. Potential applications of this glycopolymer are in the diagnosis of, as well as the treatment of, anti-MAG neuropathy.

Introduction

Anti-MAG neuropathy is a demyelinating peripheral neuropathy, caused by monoclonal IgM autoantibodies recognizing the antigenic HNK-1 carbohydrate epitope. This epitope is found on MAG and other glycoconjugates of the peripheral nervous system (PNS). The clinical picture is characterized by a slowly progressive demyelinating, predominantly sensory, neuropathy (8, 117, 118). Cardinal clinical symptoms are sensory ataxia with impaired gait, distal muscle weakness, and tremors (106). Evidence is strong for a pathogenic role of the anti-MAG antibodies in demyelination and neuropathy development (8, 106). Histopathological studies on nerve biopsies from patients show demyelinating lesions and widening of myelin lamellae, as well as deposits of anti-MAG IgM within myelin sheaths (118, 132). Localization of anti-MAG IgM antibodies to areas of split myelin indicates a role of the antibodies in myelin disintegration (135). Besides IgM deposits, some studies reported the presence of complement proteins on myelin, suggesting a potential inflammatory element in demyelination (136, 137). Therapeutic reduction of serum anti-MAG IgM antibody serum titers leads to clinical improvement of patients in neuropathy symptoms (106, 140) and therapeutic response seems to be correlated to the level of anti-MAG antibody reduction (142). Passive transfer of patients' anti-MAG antibodies to healthy experimental animals resulted in peripheral nerve myelin damage (143, 145). Active immunization of cats with the HNK-1 containing glycolipid SGPG induced autoantibodies against the HNK-1 epitope and caused an ataxic sensory neuropathy, resembling the human disease (147).

The myelin glycoconjugates that contain the antigenic HNK-1 epitope include the glycoproteins MAG, protein zero (P0), peripheral myelin protein 22, as well as the glycolipids sulfoglucuronyl paragloboside (SGPG) and sulfoglucuronyl lactosaminyl paragloboside (SGLPG) (126). Several observations suggest MAG as the main target for the IgM antibodies: (i) Deposits of patients' antibodies to PNS sites are co-localized with MAG (166), (ii) MAG is selectively lost from PNS myelin in patients with high antibody titers (167), (iii) the pathology of MAG-knockout mice (162, 163) shows similarities to the human nerve pathology (161, 165), and (iv) MAG has the highest HNK-1 epitope density of all myelin glycoconjugates, allowing strong antibody binding (153).

MAG belongs to the family of sialic acid-binding immunoglobulin-like lectins (Siglecs) (148, 149). It is located mainly in periaxonal membranes of oligodendroglial cells in the CNS and Schwann cells in the PNS (154). It is involved in adhesion and signaling processes at the

axon-glia interface, it has been implicated in the formation and maintenance of myelin, and it furthermore shows a regulatory effect on axonal integrity (126). MAG is strongly glycosylated; 30% of its molecular weight are contributed by heterogeneous *N*-linked oligosaccharides (150). All eight *N*-glycosylation sites of MAG can carry the HNK-1 epitope (152). Structural analysis of the HNK-1 epitope from SGPG and SGLPG (123, 124) and from bovine glycoprotein P0 (125) revealed an unusual 3-*O*-sulfoglucuronic acid (SO₃-3GlcA) as a specific epitope hallmark and led to the characterization of the complete epitope structure, which was defined as trisaccharide SO₃-3-GlcA(β1-3)Gal(β1-4)GlcNAc-OH.

Although the anti-MAG IgM antibodies from different patients share the same epitope, there is idiotypic heterogeneity (131) and therefore variability in structural requirements for binding and binding affinity (127). A study with SGPG derivatives showed that the IgM antibodies place different importance on the carboxyl and the sulfate group of GlcA. However, intact SGPG, containing both negatively charged groups, was reported as optimal epitope (128). Other studies analyzed the importance of the carbohydrate chain length for antibody recognition and the SO₃-3-GlcA(β1-3)Gal disaccharide of the HNK-1 epitope was reported to be the minimal requirement for antibody binding (129, 130).

Our study describes the design and biological evaluation of new synthetic carbohydrate ligands that bind to anti-MAG IgM antibodies. The potential applications of these ligands are in the diagnosis as well as in the treatment of anti-MAG neuropathy.

Results

The aim of our study was to design carbohydrate ligands that compete with the endogenous HNK-1 epitope and block the binding sites of anti-MAG IgM antibodies by mimicking the endogenous HNK-1 epitope. We were particularly interested in a potential diagnostic and therapeutic application of carbohydrate ligands that inhibit the antigen-antibody interaction. Based on a study by Tokuda *et al.* (130), reporting that IgM antibodies from anti-MAG neuropathy patients, and also the HNK-1 antibody, bound to SGPG glycolipid derivatives with a minimum of two sugars (SO₃-3-GlcA(β1-3)Gal), we synthesized disaccharide ligands for anti-MAG antibodies of patients. In this effort, we designed the minimal HNK-1 epitope (Scheme III 1, **1a**).

Synthesis of disaccharide HNK-1 mimetics

Disaccharide HNK-1 mimetics were prepared in the sulfated (**1a,b**) and the non-sulfated (**2**) form. The synthesis is depicted in scheme III 1. The selectively protected Gal acceptors **4a,b** (*183*) were glycosylated by trimethylsilyl trifluoromethanesulfonate (TMSOTf)-catalysis with the GlcA trichloro-acetimidate donor **3** (*184*), affording the GlcA(β 1-3)Gal disaccharides **5a,b**. Deprotection of the ester groups with LiOH in tetrahydrofuran (THF)/water (H₂O) yielded **6a,b**. Disaccharide **2** was obtained by catalytic hydrogenation of **6a**. The 3'-OH-unprotected disaccharides **7a,b** were prepared *via* a lactonization/methanolysis procedure (*185*). Subsequent sulfation with the sulfate-pyridine complex (SO₃·Py) in *N,N*-dimethylformamide (DMF) gave 3-*O*-sulfated disaccharides **8a,b**. Catalytic hydrogenation followed by hydrolysis and treatment with Na⁺ cation-exchange resin afforded disaccharides **1a,b**.

Biological evaluation of disaccharide HNK-1 mimetics

The synthesized compounds **1a,b** and **2** were tested in the anti-MAG ELISA kit sold by Bühlmann Laboratories AG, (Schönenbuch, Switzerland). This kit is used for the measurement of anti-MAG antibody titers in patient serum samples for the purpose of diagnosis or therapy monitoring. We applied this ELISA as a competitive binding assay, to test the inhibitory activity of the synthesized HNK-1 mimetics on anti-MAG antibody binding to MAG (Fig. III 1). The synthesized compounds and patient serum samples, containing anti-MAG IgM antibodies, were co-incubated in MAG-coated 96 well plates. Thus, the endogenous HNK-1 epitopes on MAG and the synthesized HNK-1 mimetics competed for binding to the anti-MAG IgM antibodies. After a wash step, MAG-bound IgM antibodies were detected with a horseradish peroxidase-labeled anti-human IgM antibody, followed by a colorimetric reaction. Successful competition of the synthesized compounds with MAG led to diminished MAG-binding of patients' IgM antibodies and therefore to a decrease in measured OD_{450 nm} (OD: optical density) compared to no-compound controls. Serum samples from four patients (MK, DP, KH, SJ), with an anti-MAG neuropathy diagnosis and confirmed high anti-MAG IgM antibody titers, were chosen for our study. In preliminary experiments we determined appropriate serum dilutions, to give OD_{450 nm} values close to 1.0 during standard assay procedure. Serum dilutions used were: DP 1:2500, KH 1:3000, SJ 1:7500, and MK 1:23000. Two sera from patients without anti-MAG neuropathy served as controls and showed no binding to

MAG at a dilution of 1:1000. Dilution series of the synthesized compounds were co-incubated with the appropriately diluted patient sera to determine IC_{50} values (IC_{50} : half maximal inhibitory concentration). The HNK-1 mimetic **1a** inhibited antibody binding to MAG in the micromolar range with the following IC_{50} values: MK: $124.2 \pm 9.5 \mu\text{M}$, DP: $536.1 \pm 23.5 \mu\text{M}$; KH: $614.2 \pm 20.1 \mu\text{M}$ and SJ: $793.1 \pm 24.0 \mu\text{M}$. IC_{50} values are listed in table III 1, and inhibition curves are shown in figure III 2A. The non-sulfated analogue **2** inhibited antibody binding in the millimolar range with following IC_{50} values: MK: $29.0 \pm 0.5 \text{ mM}$ and SJ: $10.0 \pm 1.0 \text{ mM}$ (Fig. III 2B). For curve fitting we included an artificial high concentration of 500 mM with assumed 0% antibody binding because even at the highest tested concentration of **2** (50 mM) the inhibition of antibody binding was not complete. Suspecting a potential role of the terminal *para*-methoxyphenyl group of compounds **1a** and **2** in binding to the pathogenic anti-MAG antibodies, we synthesized and tested the non-aromatic analogue of compound **1a**, i.e. the methyl-analogue **1b**. The IC_{50} values for compound **1b** in the ELISA were $860.0 \pm 58.2 \mu\text{M}$ for serum MK and $1237.0 \pm 56.0 \mu\text{M}$ for serum SJ (Fig. III 2C). Consequently, we defined the best binding HNK-1 mimetic **1a** as the minimal HNK-1 (minHNK-1) epitope.

Synthesis of minHNK-1 polymers

Having confirmed the inhibitory activity of the minHNK-1 epitope **1a** on antibody binding to MAG, we hypothesized that its multivalent presentation might substantially increase binding affinity to the pathogenic antibodies, given that the IgM antibody – MAG interaction is multivalent in nature (153). To test our hypothesis, we synthesized the minHNK-1 carbohydrate polymer **25**, using polylysine as a backbone. The synthesis is outlined in scheme III 2. We had to introduce a linker, which enabled the coupling of the minHNK-1 epitope to the polymer backbone. 4-(2-azidoethyl)phenol (**9**) was obtained by amine-azide interconversion (186) from tyrosine. It was galactosylated with the trichloro-acetimidate donor **10** (187), affording galactoside **11**. Deacetylation under Zemplén conditions (\rightarrow **12**), followed by the formation of the 3,4-isopropylidene derivative **13**, dibenylation under phase transfer catalysis using 50% aqueous NaOH/DCM and 18-crown-6 ether (\rightarrow **14**), acid-catalyzed cleavage of the acetonide (\rightarrow **15**), and mono-benzoylation yielded the selectively protected galactoside **16**. To obtain disaccharide **21**, we used a reaction procedure analogous to the one described above for **1a,b**. The amino group of **21** was reacted with thiobutyrolactone and triethylamine (TEA) in DMF to give the linker-containing minHNK-1 epitope **22**, ready for coupling to the polylysine polymer *via* its thiol group. Commercially available polylysine polymer **23**, with an average

degree of polymerization n around 250 and MW of 50 kDa, was acylated (\rightarrow **24**) before it was coupled to a substoichiometric amount of **22** (0.4 eq) (188). To improve the water solubility of the glycosylated polylysine polymer, the remaining chloroacetamide groups were capped with an excess of thioglycerol (188). For the purification, ultrafiltration was used (Sartorius Stedim Vivaspin 6, MW cutoff, 5000), which yielded the glycopolymer **25**. To evaluate the influence of minHNK-1 epitope density on anti-MAG antibody binding, we subsequently synthesized polylysine polymers with various degrees of carbohydrate epitope (**22**) loading and gave them the nomenclature PL(minHNK-1) x , with x defining the percentage of epitope loading in %. Polymers with $x=10, 25, 31,$ and 44% were prepared and tested in the ELISA with the same three patient sera that polymer **25** was tested with. PL(minHNK-1) $_0$ with 0% epitope loading was prepared as a control polymer and was also tested with the same three sera.

Analysis and biological evaluation of minHNK-1 polymers

Carbohydrate loading of the polylysine polymer **25** was determined by ^1H NMR spectroscopy. According to spectral analysis, approximately 50% of the lysine side chains were coupled to the minHNK-1 epitope. We then tested the minHNK-1 polymer **25** in the competitive ELISA assay, using the sera from patients KH, MK and SJ (Fig. III 2D). The polymer **25** inhibited antibody binding to MAG in the low nanomolar range with the following IC_{50} values: MK: 2.5 ± 0.1 nM, KH: 18.3 ± 2.2 nM and SJ: 14.8 ± 0.6 nM (Table III 1). The IC_{50} values for the polymers PL(minHNK-1) $_{10-44}$ were determined with the sera of patients MK, KH and SJ and the monoclonal mouse HNK-1 IgM antibody (119) (Table III 2). The data showed that increasing epitope loading correlated with higher binding affinity towards the anti-MAG antibodies (Fig. III 3). The control polymer PL(minHNK-1) $_0$ did not inhibit the binding of anti-MAG antibodies from patient sera KH, MK and SJ to MAG, even at concentrations as high as 10 mM (Fig. III 4).

Discussion

The concept of anti-MAG neuropathy as an antibody-mediated autoimmune disease is well established and therapies are aimed at reducing the autoantibody levels or the levels of autoantibody-producing B cell clones (8, 106). Conventional immunosuppressive therapy is how-

ever a heavy burden to patients with respect to treatment side effects, thus therapies that modulate the immune system more selectively are desired.

Intrigued by the idea of an antibody-specific treatment, Page *et al.* raised an anti-idiotypic antibody against the variable regions of a monoclonal IgM antibody of an anti-MAG neuropathy patient (131). This antibody successfully inhibited the binding of the individual patients' IgM antibodies to MAG *in vitro*; however, it was ineffective at inhibiting the binding of 20 other patients' IgM antibodies to MAG, indicating idiotypic heterogeneity among patient autoantibodies. Furthermore, variable binding affinities of antibodies from different patients to MAG have been described (127). The fact that antibodies from different patients share the same trisaccharide HNK-1 epitope, despite their microheterogeneity, suggests that all antibodies might be targeted by mimetics of their shared epitope. Fully recreated antigenic HNK-1 containing molecules, e.g. the penta- and heptasaccharide glycolipids SGPG/SGLPG, could be used to target the antibodies. The full synthesis of these two glycolipids has been described by Nakano *et al.* (189). Interestingly, glycolipids with shorter carbohydrate chains have been shown to retain binding affinity to the anti-MAG antibodies of patients, with a minimum requirement of two sugars ($\text{SO}_3\text{-3-GlcA}(\beta\text{1-3})\text{Gal}$) for binding (130). In addition, pure carbohydrates without ceramide aglyca have been prepared, such as the full $\text{SO}_3\text{-3-GlcA}(\beta\text{1-3})\text{Gal}(\beta\text{1-4})\text{GlcNAc}$ trisaccharide HNK-1 epitope (190) and also its $\text{SO}_3\text{-3-GlcA}(\beta\text{1-3})\text{Gal}$ disaccharide fragment (185). Tsvetkov *et al.* studied the binding of an HNK-1 pentasaccharide, analogous to the glycon part of SGPG, to the monoclonal HNK-1 antibody (119) by saturation transfer difference (STD) NMR (190). Not surprisingly, the terminal trisaccharide $\text{SO}_3\text{-3-GlcA}(\beta\text{1-3})\text{Gal}(\beta\text{1-4})\text{GlcNAc}$, defined as the HNK-1 epitope, had the strongest interaction with the HNK-1 antibody, whereas the terminal disaccharide $\text{SO}_3\text{-3-GlcA}(\beta\text{1-3})\text{Gal}$ was the most important moiety for binding. Besides the synthesis of full or partial HNK-1 carbohydrate epitopes, also non-carbohydrate, glycomimetic compounds have been described, such as a cyclic peptide (191) or a HNK-1 receptor antagonist described by Nelson *et al.* (192). Overall, the HNK-1 carbohydrate epitope and mimetics thereof have attracted considerable interest as potential therapeutic agents.

Based on the findings of Tokuda *et al.* (130), and Tsvetkov *et al.* (190), pointing out the importance of the terminal HNK-1 disaccharide for antibody binding, we synthesized the disaccharide ligands **1a**, **1b** and **2** (Scheme III 1). Their binding to anti-MAG antibodies of patients was evaluated in a competitive ELISA (Fig. III 1). Results showed variable affinities of four different patients' anti-MAG antibodies to our ligands, confirming their microheterogeneity

(127). Furthermore, the sulfated disaccharide **1a** bound more strongly to the pathogenic antibodies than the unsulfated analogue **2** (Table III 1), which is in line with previous findings with SGPG derivatives (128). Our data indicates the crucial role of the sulfate group; it was required for ligand binding to all four patients' IgM antibodies at micromolar concentration. Nevertheless, it is not equally important to all sera. Serum MK showed a high requirement for the sulfate with an approximately 230-fold weaker binding to the unsulfated disaccharide **2**, compared to **1a**; whereas serum SJ only showed a 12.6-fold decrease in binding affinity to the unsulfated disaccharide **2** (Table III 1). Furthermore, we found that the aromatic *para*-methoxyphenyl group at the reducing end of disaccharide **1a** provided better binding to the pathogenic IgM autoantibodies. Upon exchange of the *para*-methoxyphenyl group with a methyl group (**1b**), the compounds' affinity for serum MK dropped by a factor of 6.9 and for serum SJ by a factor of 1.6 (Table III 1). The aromatic moiety might act as a mimetic of the third GlcNAc sugar belonging to the HNK-1 epitope. This might be achieved by imitating the hydrophobic face (193) of GlcNAc and by potential cation- π interaction or π - π stacking in the antibody binding sites. Aromatic HNK-1 mimetics such as **1a** have not been described before. A nice example of terminal (reducing-end) aromatic groups, adding substantially to binding affinities of disaccharides, was illustrated with galectin inhibitors (194). We therefore postulated that compound **1a** is a pseudotriscaccharide, mimicking the natural triscaccharide, and we termed **1a** "minHNK-1 epitope".

Due to the hurdle that the synthesis of complex carbohydrates poses, a minimal structure like compound **1a**, which is easier to prepare than the whole epitope and retains affinity to the IgM antibodies, is advantageous. However, a problem with natural carbohydrates is their low affinities to their binding partners. Polyvalent display of carbohydrates—or of the carbohydrate recognizing domains (CRDs) of carbohydrate-binding proteins—potentiates binding affinity (195). This is also the case for the interaction between HNK-1 epitopes on MAG and patients' anti-MAG IgM antibodies. MAG presents up to eight HNK-1 epitopes on its extracellular domains (151, 152), whereas the pentameric IgM antibodies are decavalent ligands. The multivalent nature of the antibody-antigen interaction for MAG and the IgM antibodies was previously shown (153). Ogino *et al.* measured dissociation constants (K_D) in the range of 2.5×10^{-10} M and 2.1×10^{-7} M for the binding of IgM antibodies to MAG in solution. Digestion of MAG into monovalent HNK-1 glycopeptides or the breakdown of anti-MAG IgM pentamers into their monomers, led to substantially decreased binding affinity due to the loss of the multivalent binding effect. The outlined findings were the rationale underlying our next step: the preparation of glycopolymer **25**, which displayed the minHNK-1 pseudotriscaccha-

ride **1a** multivalently. Polylysine was chosen as polymer backbone as it is biodegradable and therefore suitable for therapeutic application (188). The synthesized minHNK-1 polymer **25** (Scheme III 2), with approximately 50% epitope loading, showed a massive increase in binding affinity towards the pathogenic anti-MAG IgM antibodies (Table III 1). The inhibitory activity, now being in the low nanomolar range, was increased by a factor of at least 34000 compared to the monomer (serum KH). The affinity increase obtained for serum MK and SJ was approximately 50000. These findings clearly demonstrated the multivalent nature of the antigen-antibody interaction. We furthermore showed that the amount of epitope loading (epitope density) strongly affects the inhibitory activity of the polymer. This was tested with four polymer analogues with minHNK-1 loadings ranging from 10 to 44%, using sera from anti-MAG neuropathy patients or the monoclonal HNK-1 antibody (119). Inhibitory activity of the polymers on antibody binding to MAG approached a maximum inhibition with increasing epitope density (Fig. III 3, Table III 2). This is best exemplified with serum MK, for which maximum binding is reached with 31% loading. Too dense epitope loading would likely result in reduced antibody binding.

Glycopolymers, such as compound **25**, might be used as therapeutic agents to deplete pathogenic anti-carbohydrate antibodies *in vivo*. A proof of concept for this therapeutic approach has been performed *in vitro* and *in vivo* for the glycopolymer GAS914 (188). GAS914 and the minHNK-1 polymer **25** use the same polylysine backbone, but are loaded with different carbohydrate epitope warheads. GAS914 carries the $\alpha(1,3)$ -galactosidic carbohydrate epitope. In a non-human primate animal model, xenoantibodies against this antigenic carbohydrate epitope were successfully depleted by immuneapheresis with GAS914 or by i.v. injection. Interestingly, upon injection a sustained antibody down-regulation was caused by the glycopolymer, which was attributed to its binding to antibody-producing B cells. As these were xenoantigenic antibodies, it will be interesting to see whether the same concept also works for autoantigenic antibodies *in vivo*, such as anti-MAG antibodies. The minHNK-1 polymer **25**, or a similar glycopolymer, are therefore of considerable clinical interest as a potential diagnostic and therapeutic agent. In fact, polymer **25** has been successfully immobilized on microtiter plates and reliably detected anti-MAG antibodies in patient sera (data not shown). Regarding its therapeutic use, we can reasonably assume that the minHNK-1 carbohydrate polymer **25** could (i) deplete circulating anti-MAG antibodies and (ii), upon binding to the anti-MAG antibody producing B cells, could furthermore lead to sustained down-regulation of anti-MAG antibody production. It would be the first antigen-specific treatment agent for anti-

MAG neuropathy. In a next step, the polymer **25** will have to be evaluated in an animal model for anti-MAG neuropathy.

Experimental

General methods

NMR spectra were obtained on a Bruker Avance DMX-500 (500 MHz) spectrometer. Assignment of ^1H and ^{13}C NMR spectra was achieved using 2D methods (COSY and HSQC). Chemical shifts are expressed in ppm using residual CHCl_3 , CHD_2OD or HDO as references. Optical rotations were measured on a Perkin-Elmer polarimeter 341. IR spectra were recorded using a Perkin-Elmer Spectrum One FT-IR spectrometer. Electron spray ionization mass spectra (ESI-MS) were obtained on a Waters micromass ZQ. HRMS analysis was carried using an Agilent 1100 LC equipped with a photodiode array detector and a Micromass QTOF I equipped with a 4 GHz digital-time converter. Reactions were monitored by TLC using glass plates coated with silica gel 60 F₂₅₄ (Merck) and visualized by using UV light and/or by charring with mostain (a 0.02 M solution of ammonium cerium sulfate dihydrate and ammonium molybdate tetrahydrate in aq 10% H_2SO_4). Column chromatography was performed on silica gel (Fluka C60 40/60) or RP-18 (Merck LiChroprep® RP-18 40/60). Methanol (MeOH) was dried by refluxing with sodium methoxide and distillation. Pyridine was dried over activated molecular sieves (4 Å). Dimethylformamide (DMF) was purchased from Acros (99.8%, extra dry, over molecular sieves). Dichloromethane (DCM), toluene and hexane were dried by filtration over Al_2O_3 (Fluka, type 5016A basic). Molecular sieves (4 Å) were activated in vacuo at 500 °C for 1h immediately before use. Centrifugations were carried out with an Eppendorf Centrifuge 5804 R.

Patient sera

The sera of four patients (three men and one woman) with positive anti-MAG activity were used in the competitive binding assay (see below). They all were tested positive for a monoclonal IgM gammopathy and were diagnosed with anti-MAG neuropathy at the University Hospital of Basel (Basel, Switzerland). Serum anti-MAG antibody titers were determined by an ELISA assay (Bühlmann Laboratories, Schönenbuch, Switzerland). Sera from two patients

with a monoclonal IgM gammopathy and negative anti-MAG activity served as negative control in the competitive binding assay. Use of sera was approved by the ethics committee of the University Hospital of Basel.

Competitive binding assay

For the biological evaluation of all synthesized compounds we used the anti-MAG ELISA kit sold by Bühlmann Laboratories AG (Schönenbuch, Switzerland). The assay was performed according to the protocol of the manufacturer. The kit provided all buffers, antibodies, the tetramethylbenzidine/hydrogen peroxide substrate and the 0.25 M sulfuric acid stop solution. The 96 well plates, coated with purified MAG from human brain, were washed four times with washing buffer (300 μ l/well) before adding a dilution series of the synthesized carbohydrate ligands (0.05 - 50 mM for the monomers **1a** and **2**, 0.02 - 20 mM for the monomer **1b**, and 0.05 - 5000 nM for the polymer **25** (25 μ l/well). The patient sera containing anti-MAG IgM antibodies were added in the following dilutions (25 μ l/well): DP 1:2500, KH 1:3000, SJ 1:7500, MK 1:23000. The two sera that served as negative controls were used at a dilution of 1:1000. The mouse HNK-1 antibody (119) was diluted 1:1000. The plate was covered with a plate sealer and incubated for 2 h at 5 °C. The wells were washed four times with washing buffer (300 μ l/well) before the anti-human IgM antibody conjugated to horseradish peroxidase was added (100 μ l/well). The mouse HNK-1 antibody was detected with a 1:10000 diluted anti-mouse horseradish peroxidase-labeled anti-mouse IgM antibody (Sigma Aldrich, A 8786) (100 μ l/well). The plate was incubated for 2 h at 5 °C. After washing the wells four times with washing buffer (300 μ l/well), a substrate solution of tetramethylbenzidine and hydrogen peroxide was added (100 μ l/well) and the plate incubated for further 30 min at 800 rpm and room temperature (rt), protected from light. The colorimetric reaction was stopped by the addition of a 0.25 M sulfuric acid (100 μ l/well) and the optical density (OD) was measured at 450 nm with a microplate reader (Spectramax 190, Molecular Devices, California, USA). The IC₅₀ values (half maximal inhibitory concentration) for the tested compounds were calculated using Prism® software (GraphPad Software, Inc, La Jolla, USA). The measurements for each compound were repeated at least three times.

Synthesis

4-Methoxyphenyl (methyl 2,3,4-tri-O-benzoyl- β -D-glucopyranuronate)-(1 \rightarrow 3)-4-O-benzoyl-2,6-di-O-benzyl- β -D-galactopyranoside (5a).

Under argon **3** (1.12 g, 1.68 mmol), **4a** (800 mg, 1.40 mmol) and activated 4 Å molecular sieves (1.2 g) were suspended in DCM (30 mL). The mixture was stirred for 1 h at rt and then cooled to 0 °C. TMSOTf (38.1 μ L, 0.21 mmol) was added dropwise. The reaction mixture was allowed to warm to rt overnight, and was then neutralized with TEA (100 μ L) and concentrated. The residue was purified by chromatography (petroleum ether/EtOAc, 9:1 to 7:3) to yield **5a** (1.21 g, 1.13 mmol, 81%) as a white solid.

$[\alpha]_{\text{D}}^{20} +28.4$ (c 1.01, CHCl_3); $^1\text{H NMR}$ (500 MHz, CDCl_3): δ 3.59 (dd, $J = 7.2, 10.1$ Hz, 1H, H-6a), 3.65 (s, 3H, OMe), 3.69 (dd, $J = 4.8, 10.1$ Hz, 1H, H-6b), 3.74 (s, 3H, OMe), 3.93 (dd, $J = 7.8, 9.5$ Hz, 1H, H-2), 3.96 (dd, $J = 5.1, 6.9$ Hz, 1H, H-5), 4.12 (d, $J = 9.8$ Hz, 1H, H-5'), 4.20 (dd, $J = 3.5, 9.6$ Hz, 1H, H-3), 4.46 (A, B of AB, $J = 11.5$ Hz, 2H, CH_2Ph), 4.51, 4.90 (A, B of AB, $J = 10.5$ Hz, 2H, CH_2Ph), 4.94 (d, $J = 7.8$ Hz, 1H, H-1), 5.36 (d, $J = 7.5$ Hz, 1H, H-1'), 5.44 (dd, $J = 7.5, 9.2$ Hz, 1H, H-2'), 5.66 (t, $J = 9.6$ Hz, 1H, H-4), 5.72-5.79 (m, 2H, H-3', H-4'), 6.76, 7.00 (AA', BB' of AA'BB', $J = 9.1$ Hz, 4H, C_6H_4), 7.19-7.44, 7.47-7.51, 7.54-7.61, 7.75-7.78, 7.87-7.91, 8.03-8.08 (m, 30H, 6 C_6H_5); $^{13}\text{C NMR}$ (126 MHz, CDCl_3): δ 52.88, 55.64 (2 OMe), 69.07 (C-6), 70.01 (C-4), 70.05 (C-4'), 71.76 (C-2'), 72.17 (C-3'), 72.90 (C-5'), 73.54 (C-5), 73.72, 75.23 (2 CH_2Ph), 76.16 (C-3), 79.86 (C-2), 100.29 (C-1'), 102.73 (C-1), 114.57, 118.19 (4C, C_6H_4), 127.69, 127.78, 128.00, 128.09, 128.30, 128.37, 128.43, 128.59, 128.71, 128.89, 129.05, 129.58, 129.77, 129.82, 129.92, 130.11, 132.91, 133.08, 133.27, 133.39, 137.88, 137.90 (36C, 6 C_6H_5), 151.33, 155.33 (2C, C_6H_4), 164.45, 165.00, 165.52, 165.63, 167.15 (5 CO); ESI-MS: m/z : calcd for $\text{C}_{62}\text{H}_{56}\text{NaO}_{17}$ $[\text{M}+\text{Na}]^+$: 1095.35, found: 1095.48.

Methyl (methyl 2,3,4-tri-O-benzoyl- β -D-glucopyranuronate)-(1 \rightarrow 3)-4-O-benzoyl-2,6-di-O-benzyl- β -D-galactopyranoside (5b).

Donor **3** (916 mg, 1.38 mmol) and acceptor **4b** (660 mg, 1.38 mmol) were dissolved in dry DCM (10 mL) in a flask containing activated 4 Å molecular sieves (1.2 g) with the protection of argon. The mixture was stirred for 1 h at rt and then cooled to 0 °C. TMSOTf (30.0 μ L, 0.166 mmol) was added dropwise. The reaction mixture was allowed to warm to rt overnight and was then neutralized with TEA (0.1 mL), concentrated and the residue was purified by

flash chromatography (petroleum ether/EtOAc 10:0 – 7:3) to yield disaccharide **5b** (1.13 g, 1.15 mmol, 83.5%) as a white solid.

$[\alpha]_D^{20} +31.9^\circ$ (*c* 1.0, EA); $^1\text{H-NMR}$ (500 MHz, CDCl_3): δ 8.04 (d, *J* = 7.9, 2H, Ar), 7.90 (d, *J* = 7.9, 2H, Ar), 7.78 (d, *J* = 8.0, 2H, Ar), 7.37 (m, 25H, Ar), 5.75 (m, 2H), 5.67 (t, *J* = 9.5, 1H), 5.42 (m, 1H), 5.39 (d, *J* = 7.5, 1H), 4.78 (d, *J* = 10.7, 1H), 4.48 (m, 2H), 4.42 (d, *J* = 10.7, 1H), 4.35 (d, *J* = 7.7, 1H), 4.14 (m, 2H), 3.87 (t, *J* = 6.0, 1H), 3.62 (m, 9H); $^{13}\text{C-NMR}$ (125 MHz, CDCl_3): δ 167.19, 165.63, 165.46, 164.99, 164.40, 138.21, 137.87, 133.34, 133.21, 132.97, 132.77, 130.07, 129.80, 129.76, 129.55, 129.10, 128.95, 128.77, 128.55, 128.40, 128.28, 128.22, 127.97, 127.85, 127.71, 104.77, 100.26, 80.26, 75.93, 74.95, 73.74, 73.11, 72.92, 72.22, 71.78, 70.16, 70.10, 69.02, 57.34, 52.81. ESI-MS calcd for $\text{C}_{56}\text{H}_{52}\text{NaO}_{16}^+$ $[\text{M}+\text{Na}]^+$: 1003.32, Found: 1003.39.

4-Methoxyphenyl (β-D-glucopyranuronate)-(1→3)-2,6-di-O-benzyl-β-D-galactopyranoside (6a).

Compound **5a** (810 mg, 0.76 mmol) was suspended in THF (7 mL) and the suspension was cooled to -10 °C. Then 2 M aq LiOH (5 mL) was added dropwise. The reaction mixture was stirred overnight and allowed to warm to rt. The solvents were evaporated, the residue was taken up in THF/H₂O (2:3, 8 mL) and treated with TFA (4 mL) for 30 min. The mixture was evaporated to dryness and the residue was purified by reversed-phase chromatography (RP-18, MeOH/water, 0:1 to 2:1) to give **6a** (0.47 g, 0.73 mmol, 97%) as a white solid.

$[\alpha]_D^{20} -43.2$ (*c* 1.00, MeOH); $^1\text{H NMR}$ (500 MHz, CD_3OD): δ 3.30-3.41 (m, 2H, H-2', H-3'), 3.49 (t, *J* = 8.9 Hz, 1H, H-4'), 3.66 (s, 3H, OMe), 3.68 (d, *J* = 5.9 Hz, 2H, H-6a, H-6b), 3.72 (d, *J* = 9.7 Hz, 1H, H-5'), 3.76 (d, *J* = 5.9 Hz, 1H, H-5), 3.79 (dd, *J* = 3.3, 9.9 Hz, 1H, H-3), 3.87 (m, 1H, H-2), 4.00 (d, *J* = 2.7 Hz, 1H, H-4), 4.48 (s, 2H, CH_2Ph), 4.70 (d, *J* = 7.4 Hz, 1H, H-1'), 4.84 (d, *J* = 7.7 Hz, 1H, H-1), 4.87 (s, 2H, CH_2Ph), 6.73, 6.97 (AA', BB' of AA'BB', *J* = 9.0 Hz, 4H, C_6H_4), 7.17-7.28 (m, 8H, 2 C_6H_5), 7.38 (d, *J* = 7.1 Hz, 2H, 2 C_6H_5); $^{13}\text{C NMR}$ (126 MHz, CD_3OD): δ 56.10 (OMe), 70.37 (C-4), 70.72 (C-6), 73.35 (C-4'), 74.37 (CH_2Ph), 74.85 (C-2'), 75.00 (C-5), 76.22 (C-5'), 76.46 (CH_2Ph), 77.35 (C-3'), 80.11 (C-2), 82.20 (C-3), 103.87 (C-1), 105.59 (C-1'), 115.58, 119.23 (4C, C_6H_4), 128.66, 128.76, 128.79, 129.31, 129.41, 129.77, 139.76, 139.96 (12C, 2 C_6H_5), 153.05, 156.67 (2C, C_6H_4), 173.01 (CO); ESI-MS: *m/z*: calcd for $\text{C}_{33}\text{H}_{38}\text{NaO}_{13}$ $[\text{M}+\text{Na}]^+$: 665.23, found: 665.23.

4-Methyl (β -D-glucopyranuronate)-(1 \rightarrow 3)-2,6-di-O-benzyl- β -D-galactopyranoside (6b).

Disaccharide **5b** (1.26 g, 1.28 mmol) was suspended in THF (7 mL) and the suspension was cooled to -10 °C, then 2M LiOH_{aq} (5mL) was added dropwise with the protection of argon. The reaction mixture was stirred overnight and allowed to warm to rt. The solvents were evaporated, and the residue was taken up in THF/H₂O (2:3, 8 mL) and treated with TFA (4 mL) for 30 min. The mixture was evaporated to dryness and the residue was purified by reversed-phase chromatography (RP-18, MeOH/water 0:1 – 2:1) to give **6b** (650 mg, 1.10 mmol, 86%) as a white solid.

$[\alpha]_D^{20}$ -23.5° (*c* 0.3, MeOH:H₂O 3:2); ¹H-NMR (500 MHz, CD₃OD): δ 7.32 (m, 10H, Ar), 4.82 (d, *J* = 10.5, 1H), 4.77 (d, *J* = 10.4, 1H), 4.71 (d, *J* = 7.6, 1H), 4.57 (m, 2H), 4.30 (d, *J* = 7.7, 1H), 4.03 (d, *J* = 3.3, 1H), 3.73 (m, 5H), 3.63 (dd, *J* = 9.6, 7.8, 1H), 3.54 (s, 3H), 3.50 (t, *J* = 9.3, 1H), 3.38 (t, *J* = 9.0, 1H), 3.34 (d, *J* = 7.6, 1H); ¹³C-NMR (125 MHz, CD₃OD): δ 172.97, 140.10, 139.67, 129.58, 129.41, 129.22, 128.83, 128.69, 128.62, 106.06, 105.48, 101.39, 82.07, 80.31, 77.34, 75.89, 74.87, 74.57, 74.41, 73.31, 70.53, 70.31, 57.34; ESI-MS calcd for C₂₇H₃₄NaO₁₂⁺ [M+Na]⁺: 573.19, Found: 573.08.

4-Methoxyphenyl (sodium β -D-glucopyranuronate)-(1 \rightarrow 3)- β -D-galactopyranoside (2).

Compound **6a** (205 mg, 0.31 mmol) and Pd(OH)₂/C (42 mg, 20%) were suspended in MeOH/H₂O (10:1, 5 mL) under argon. The mixture was stirred overnight under an atmosphere of hydrogen (1 atm), then the catalyst was filtered off through a pad of Celite. The Celite was washed with a MeOH/H₂O gradient (6 \times 10 mL, 10:0, 8:2, 6:4, 4:6, 2:8, 0:10). The filtrate was concentrated and passed over a Dowex 50X8 (Na⁺) ion-exchange column. After concentration the residue was purified by reversed-phase chromatography (RP-18, water) followed by P2 size-exclusion chromatography to give **2** (148 mg, 0.31 mmol, 96%) as a white solid.

$[\alpha]_D^{20}$ -40.7 (*c* 1.00, H₂O); ¹H NMR (500 MHz, D₂O): δ 3.43 (t, *J* = 8.3 Hz, 1H, H-2'), 3.48-3.56 (m, 2H, H-3', H-5'), 3.67-3.81 (m, 7H, H-5, H-6, H-4', OMe), 3.83 (dd, *J* = 2.9, 9.8 Hz, 1H, H-3), 3.90 (dd, *J* = 8.0 Hz, 1H, H-2), 4.22 (d, *J* = 2.5 Hz, 1H, H-4), 4.68 (d, *J* = 7.7 Hz, 1H, H-1'), 4.95 (d, *J* = 7.9 Hz, 1H, H-1), 6.94, 7.09 (AA', BB' of AA'BB', *J* = 9.0 Hz, 4H, C₆H₄); ¹³C NMR (126 MHz, D₂O): δ 55.71 (OMe), 60.70 (C-6), 67.94 (C-4), 69.63 (C-2), 71.73 (C-3'), 73.09 (C-2'), 75.05 (C-5'), 75.25 (C-5), 76.18 (C-4'), 82.37 (C-3), 101.29 (C-1),

103.61 (C-1'), 114.96, 118.10, 150.84, 154.61 (6C, C₆H₄), 175.92 (CO); HRMS: *m/z*: calcd for C₁₉H₂₆NaO₁₃ [M + H]⁺: 485.1271, found: 485.1276.

4-Methoxyphenyl (methyl 2,4-di-O-acetyl-β-D-glucopyranuronate)-(1→3)-4-O-acetyl-2,6-di-O-benzyl-β-D-galactopyranoside (7a).

A solution of **6a** (470 mg, 0.73 mmol) in Ac₂O (10 mL) was stirred at 80 °C for 90 min and then cooled to rt. Pyridine (6 mL) and DMAP (15 mg) were added and the reaction mixture was stirred for 3 d. The solvents were co-evaporated with toluene (5 × 5 mL). The residue dissolved in DCM (50 mL) and extracted with brine (50 mL) and water (50 mL). The organic phase was dried over Na₂SO₄ and filtered through cotton wool. After evaporation of the solvent the residue was dissolved in dry MeOH (14 mL) and anhydrous NaOAc (90 mg) was added. The mixture was stirred overnight, neutralized with Amberlyste 15 (H⁺) ion-exchange resin and filtered. The filtrate was concentrated and the residue purified by flash chromatography (petroleum ether/EtOAc, 2:1 to 1:1) to yield **7a** (334 mg, 0.43 mmol, 57%) as a yellowish solid.

[α]_D²⁰ +34.3 (*c* 1.00, CHCl₃); ¹H NMR (500 MHz, CDCl₃): δ 1.92, 2.01, 2.04 (3s, 9H, 3 OAc), 3.48 (dd, *J* = 7.1, 10.1 Hz, 1H, H-6a), 3.55 (dd, *J* = 4.8, 10.1 Hz, 1H, H-6b), 3.60 (m, 1H, H-3'), 3.66, 3.69 (2s, 6H, 2 OMe), 3.77 (dd, *J* = 5.4, 7.0 Hz, 1H, H-5), 3.80 (d, *J* = 9.8 Hz, 1H, H-5'), 3.83 (dd, *J* = 7.6, 9.7 Hz, 1H, H-2), 3.89 (dd, *J* = 3.5, 9.7 Hz, 1H, H-3), 4.43 (A, B of AB, *J* = 11.6 Hz, 2H, CH₂Ph), 4.64 (A of AB, *J* = 11.5 Hz, 1H, CH₂Ph), 4.81 (d, *J* = 7.6 Hz, 1H, H-1), 4.83-4.87 (m, H-1', H-2'), 4.97 (B of AB, *J* = 11.5 Hz, 1H, CH₂Ph), 5.06 (t, *J* = 9.5 Hz, 1H, H-4'), 5.36 (d, *J* = 3.2 Hz, 1H, H-4), 6.72, 6.96 (AA', BB' of AA'BB', *J* = 9.1 Hz, 4H, C₆H₄), 7.18-7.31 (m, 10H, 2 C₆H₅); ¹³C NMR (126 MHz, CDCl₃): δ 20.72, 20.76, 20.80 (3 COCH₃), 52.81, 55.63 (2 OMe), 68.95 (C-6), 69.33 (C-4), 71.87 (C-4'), 72.54 (C-5), 73.04 (C-5'), 73.26 (C-3'), 73.70 (CH₂Ph), 73.79 (C-2'), 75.31 (CH₂Ph), 77.24 (C-3), 79.26 (C-2), 100.15 (C-1'), 102.65 (C-1), 114.56, 118.24 (4C, C₆H₄), 127.76, 127.83, 127.98, 128.04, 128.41, 128.53, 137.87, 138.00 (12C, 2 C₆H₅), 151.35, 155.35 (2C, C₆H₄), 167.46, 170.15, 170.36, 170.38 (4 CO); ESI-MS: *m/z*: calcd for C₄₀H₄₆NaO₁₆ [M+Na]⁺: 805.28, found: 805.34.

4-Methyl (methyl 2,4-di-O-acetyl-β-D-glucopyranuronate)-(1→3)-4-O-acetyl-2,6-di-O-benzyl-β-D-galactopyranoside (7b).

A solution of **6b** (560 mg, 0.73 mmol) in Ac₂O (10 mL) was stirred at 80 °C for 90 min with the protection of argon and then cooled to rt. Dry pyridine (6 mL) and DMAP (15 mg,

0.123mmol) were added and the reaction mixture was stirred for 72 h with the protection of argon. The solvents were co-evaporated with toluene (5 x 5 mL) at 30 °C. The residue was taken up in DCM (50 mL) and extracted with satd aq NaCl (50 mL) and water (50 mL). The organic phase was dried over Na₂SO₄ and filtered through celite. After evaporation of the solvent at 30 °C the residue was dissolved in dry MeOH (14 mL) and anhydrous NaOAc (90 mg) was added with the protection of argon. The mixture was stirred overnight, followed by neutralization with Amberlyste 15 (H⁺) cation-exchange resin. The resin was then filtered off, the filtrate was concentrated in vacuum and the residue was purified by flash chromatography (petroleum ether/EtOAc 2:1 – 1:1) to yield **7b** (250 mg, 0.362 mmol, 49.6%) as an off-white solid.

$[\alpha]_D^{20}$ -30.5° (*c* 0.67, EA); ¹H-NMR (500 MHz, CD₃CN): δ 7.37 (m, 10H, Ar), 5.30 (d, *J* = 3.3, 1H, H-Gal-4), 4.91 (d, *J* = 8.1, 1H, H-Glu-1), 4.86 (t, *J* = 9.2, 1H, H-Glu-4), 4.84 (d, *J* = 10.2, Bn), 4.73 (dd, *J* = 9.5, 8.1, 1H, H-Glu-2), 4.65 (d, *J* = 11.0, 1H, Bn), 4.51 (q, *J* = 11.8, 2H, Bn), 4.34 (d, *J* = 7.8, 1H, H-Gal-1), 3.90 (dd, 1H, *J* = 9.6, 3.6, H-Gal-3), 3.89 (d, *J* = 10.0, H-Glu-5), 3.80 (t, *J* = 6.0, 1H, H-Gal-5), 3.77 (d, *J* = 5.3, 1H, Glu-OH), 3.69 (m, 1H, H-Glu-4), 3.67 (s, 3H, COOMe), 3.51 (s, 3H, 1-OMe), 3.50 (m, 3H, H-Gal-6a, H-Gal-6b, and H-Gal-2), 2.05 (s, 3H, OAc), 2.03 (s, 3H, OAc), 1.95 (s, 3H, OAc); ¹³C-NMR (125 MHz, CD₃CN): δ 169.55 (C=O in Ac), 169.48(C=O in Ac), 169.06(C=O in Ac), 167.47(C=O in COOH), 138.54(tert-C in Bn), 138.18(tert-C in Bn), 127.98(Ar), 127.93(Ar), 127.43(Ar), 127.23(Ar), 127.18(Ar), 116.98(C-Gal-1), 103.95(C-Glu-1), 99.78, 99.63, 79.30, 76.91, 74.10, 72.60, 72.53, 71.88, 71.71, 71.48, 71.25, 69.19, 68.34, 56.04(1-OMe), 51.82(COOMe), 19.79(Ac), 19.59(Ac); ESI-MS calcd for C₃₄H₄₂NaO₁₅⁺ [M+Na]⁺: 713.24, Found: 713.27.

4-Methoxyphenyl (methyl 2,4-di-O-acetyl-3-O-sulfo-β-D-glucopyranuronate)-(1→3)-4-O-acetyl-2,6-di-O-benzyl-β-D-galactopyranoside, sodium salt (8a).

Compound **7a** (334 mg, 0.43 mmol) was dissolved in DMF (5 mL) and SO₃·Py (370 mg, 2.34 mmol) was added. The mixture was stirred for 2 h at rt, then the reaction was quenched by stirring with NaHCO₃ (320 mg, 3.77 mmol) for 2 h. The solid was filtered off and the filter was washed with MeOH. The filtrate was passed over a Dowex 50X8 (Na⁺) ion-exchange column, concentrated and the residue was purified by flash chromatography (DCM/MeOH, 1:0 to 9:1) to give **8a** (237 mg, 0.28 mmol, 65%) as a yellowish solid. During concentration after the flash chromatography a few drops of 0.1 M aq NaOH were added.

$[\alpha]_D^{20}$ -10.4 (*c* 1.01, MeOH); ¹H NMR (500 MHz, CD₃OD): δ 1.89, 2.03, 2.06 (3s, 9H, 3 OAc), 3.48 (dd, *J* = 7.4, 10.4 Hz, 1H, H-6a), 3.59 (dd, *J* = 4.4, 10.5 Hz, 1H, H-6b), 3.69, 3.72

(2s, 6H, 2 OMe), 3.77 (dd, $J = 7.8, 9.6$ Hz, 1H, H-2), 3.98 (dd, $J = 4.5, 7.4$ Hz, 1H, H-5), 4.03 (m, 1H, H-3), 4.05 (d, $J = 10.2$ Hz, 1H, H-5'), 4.46, 4.49 (A, B of AB, $J = 11.6$ Hz, 2H, CH_2Ph), 4.60 (t, $J = 9.3$ Hz, 1H, H-3'), 4.73, 4.92 (A, B of AB, $J = 11.8$ Hz, 2H, CH_2Ph), 4.94 (d, $J = 7.5$ Hz, 1H, H-2'), 4.96 (d, $J = 7.9$ Hz, 1H, H-1'), 4.99 (d, $J = 8.0$ Hz, 1H, H-1), 5.06 (m, 1H, H-4'), 5.40 (d, $J = 3.6$ Hz, 1H, H-4), 6.77, 7.00 (AA', BB' of AA'BB', $J = 9.1$ Hz, 4H, C_6H_4), 7.23-7.35 (m, 8H, 2 C_6H_5), 7.39 (d, $J = 7.2$ Hz, 2H, 2 C_6H_5); ^{13}C NMR (126 MHz, CD_3OD): δ 19.32, 19.23, 19.64 (3 COCH_3), 51.68, 54.52 (2 OMe), 68.73 (C-6), 69.50 (C-4), 69.80 (C-4'), 71.36 (C-2'), 71.91 (C-5'), 72.52 (C-5), 72.83, 74.69 (2 CH_2Ph), 77.50 (C-3'), 78.57 (C-3), 78.59 (C-2), 100.04 (C-1), 102.01 (C-1'), 114.03, 117.64 (4C, C_6H_4), 127.14, 127.23, 127.36, 127.57, 127.81, 127.89, 138.02, 138.23 (12C, 2 C_6H_5), 151.29, 155.26 (2C, C_6H_4), 167.77, 170.07, 170.17, 170.64 (4 CO); ESI-MS: m/z : calcd for $\text{C}_{40}\text{H}_{46}\text{O}_{19}\text{S} [\text{M}]^+$: 862.24, found: 862.42.

Methyl (methyl 2,4-di-O-acetyl-3-O-sulfo- β -D-glucopyranuronate)-(1 \rightarrow 3)-4-O-acetyl-2,6-di-O-benzyl- β -D-galactopyranoside, sodium salt (8b).

Compound **7b** (90 mg, 0.130 mmol) was dissolved in dry DMF (1 mL) and $\text{SO}_3 \cdot \text{Py}$ (114 mg, 0.717 mmol) was added. The mixture was stirred for 2 h to give a clean conversion monitored by TLC (DCM/MeOH 9/1). The reaction was quenched by addition of NaHCO_3 (100 mg, 1.19 mmol), and then was stirred for 2 h. The solid was filtered off and the filter was washed with DCM (30 mL) and then with MeOH (30 mL). The filtrate was passed through a Dowex 50 X 8 (Na^+) cation-exchange column, and was then concentrated and the residue was purified by flash chromatography (DCM/MeOH 1:0 – 9:1) to give **8b** (78 mg, 0.098 mmol, 76%) as a yellowish solid. During concentration after the flash chromatography a drop of 0.1M NaHCO_3 aqueous solution was added.

$[\alpha]_D^{20} +4.47^\circ$ (c 1.0, CHCl_3); ^1H -NMR (500 MHz, CDCl_3): δ 7.30 (m, 10H, Ar), 5.37 (m, 2H), 5.04 (m, 2H), 4.84 (d, $J = 10.6$, 1H), 4.57 (m, 2H), 4.52 (d, $J = 11.8$, 1H, CH_2 in Bn), 4.46 (d, $J = 11.8$, 1H, CH_2 in Bn), 4.30 (d, $J = 7.8$, 1H), 4.04 (d, $J = 8.6$, 1H), 3.89 (dd, $J = 9.6, 3.4$, 1H), 3.71 (m, 3H), 3.56 (m, 6H), 2.07 (s, 3H), 2.05 (s, 3H), 1.97 (s, 3H); ^{13}C -NMR (125 MHz, CDCl_3) δ 171.27, 171.11, 170.82, 167.99, 137.81, 137.52, 128.24, 128.11, 127.66, 127.56, 104.33, 99.45, 79.26, 74.70, 73.32, 72.27, 71.94, 71.31, 69.44, 69.02, 68.39, 56.96, 52.81, 20.66, 20.60, 20.44; ESI-MS calcd for $\text{C}_{34}\text{H}_{41}\text{O}_{18}\text{S}^- [\text{M}-\text{H}]^-$ (M for free acid): 769.20, Found: 769.34.

4-Methoxyphenyl (disodium-3-O-sulfo- β -D-glucofuranuronate)-(1 \rightarrow 3)- β -D-galactopyranoside (1a).

Compound **8a** (237 mg, 0.28 mmol) and Pd(OH)₂/C (48 mg, 20%) were suspended in MeOH/H₂O (10:1, 5 mL) under argon. The reaction mixture was stirred for 9 h under an atmosphere of hydrogen (1 atm). The catalyst was filtered off through a pad of Celite and the pad was washed with a MeOH/H₂O gradient (6 \times 10 mL, 10:0, 8:2, 6:4, 4:6, 2:8, 0:10). The filtrate was concentrated and the residue was dissolved in MeOH/H₂O (1:1, 8 mL). Then 1 M aq LiOH (6.5 mL) was added at -10 °C and the reaction mixture was allowed to warm to rt over 3 h, neutralized with Amberlyste 15 (H⁺) ion-exchange resin, filtered and concentrated. The residue was purified by reversed-phase chromatography (RP-18, water) and passed over a Dowex 50X8 (Na⁺) ion-exchange column. Final purification by P2 size-exclusion chromatography yielded **1a** (142 mg, 0.24 mmol, 88%) as a solid.

[α]_D²⁰ -19.2 (c 1.00, H₂O); ¹H NMR (500 MHz, D₂O): δ 3.63 (dd, J = 8.0, 9.2 Hz, 1H, H-2'), 3.73 (m, 1H, H-4'), 3.75-3.81 (m, 6H, H-5, H-6, OMe), 3.85 (d, J = 10.0 Hz, 1H, H-5'), 3.89 (dd, J = 3.2, 9.9 Hz, 1H, H-3), 3.94 (dd, J = 7.7, 9.8 Hz, 1H, H-2), 4.24 (d, J = 3.1 Hz, 1H, H-4), 4.40 (t, J = 9.2 Hz, 1H, H-3'), 4.81 (d, J = 7.9 Hz, 1H, H-1'), 4.97 (d, J = 7.7 Hz, 1H, H-1), 6.96, 7.11 (AA', BB' of AA'BB', J = 9.2 Hz, 4H, C₆H₄); ¹³C NMR (126 MHz, D₂O): δ 55.82 (OMe), 60.62 (C-6), 67.95 (C-4), 69.55 (C-2), 70.42 (C-4'), 71.86 (C-2'), 74.92 (C-5), 75.82 (C-5'), 82.49 (C-3), 83.30 (C-3'), 101.43 (C-1), 103.17 (C-1'), 115.02, 118.14, 150.89, 154.59 (6C, C₆H₄), 175.48 (CO); HRMS: m/z : calcd for C₁₉H₂₅Na₂O₁₆S [M + H]⁺: 587.0659, found: 587.0665.

4-Methoxyphenyl (disodium-3-O-sulfo- β -D-glucofuranuronate)-(1 \rightarrow 3)- β -D-galactopyranoside (1b).

Compound **8b** (20 mg, 0.0252 mmol) was dissolved in MeOH/H₂O (1:1, 1 mL). Then 1M LiOH_{aq} (0.80 mL) was added at -10 °C and the reaction mixture was allowed to warm to R.T. over 3 h. The mixture was neutralized with Amberlyste 15 (H⁺) cation-exchange resin. The resin was filtered off, the filtrate was concentrated and the residue was purified by reversed-phase chromatography (RP-18, water) to give the free acid, which was passed through a Dowex 50 X 8 (Na⁺) cation-exchange column to give the intermediate as a white solid (11 mg, 0.0163 mmol, yield = 65%) as the Na⁺ form.

[α]_D²⁰ -25.83° (c 0.27, MeOH:H₂O 4:1); ¹H-NMR (500 MHz, D₂O): δ 7.38 (m, 10H), 4.81 (d, J = 10.3, 1H, CH₂ in Bn), 4.72 (d, J = 2.9, 1H, CH₂ in Bn), 4.57 (q, J = 11.7, 2H, CH₂ in Bn), 4.34 (d, J = 8.2, 1H, Gal-H-1), 4.25 (m, 1H, Glu-H-4), 4.07 (d, J = 3.3, 1H, Gal-H-4), 3.82

(dd, $J = 9.8, 3.3$, 1H, Gal-H-3), 3.72 (m, 3H), 3.65 (s, 1H), 3.64 (d, $J = 1.2$, 1H), 3.59 (dd, $J = 9.7, .0$, 1H, Gal-H-2), 3.54 (dd, $J = 7.6, 6.5$, 1H), 3.52 (s, 3H, 1-OMe); ^{13}C -NMR (125 MHz, D_2O): δ 175.45, 137.31, 137.24, 128.96, 128.75, 128.69, 128.46, 128.34, 103.70, 103.04, 83.94, 81.25, 78.23, 76.04, 74.99, 73.13, 73.06, 71.91, 70.47, 69.45, 68.75, 57.37; ESI-MS calcd for $\text{C}_{27}\text{H}_{33}\text{O}_{15}\text{S}^-$ [M-H] $^-$ (M for free acids): 629.15, Found: 629.15.

The above intermediate was concentrated, and was then dissolved in MeOH/ H_2O (10:1, 2 mL). $\text{Pd}(\text{OH})_2/\text{C}$ (8 mg, 10%) was added under argon. The reaction mixture was stirred vigorously for 48 h under hydrogen (1 atm). The catalyst was filtered off through a pad of Celite and the pad was washed with a MeOH/ H_2O gradient (6 x 10 mL, 10:0, 8:2, 6:4, 4:6, 2:8, 0:10). The filtrate was concentrated and the residue was purified by reversed-phase chromatography (RP-18, water) and then by P2 size-exclusion chromatography (water) to afford the product **1b** as a white solid (7.5 mg, 0.0152mmol, yield = 93%)

$[\alpha]_{\text{D}}^{20} -13.4^\circ$ (c 0.2, MeOH: H_2O 3:1); ^1H -NMR (500 MHz, D_2O): δ 4.69 (1H, partially overlapped with HDO), 4.31 (d, $J = 8.0$, 1H), 4.27 (t, $J = 9.1$, 1H), 4.12 (d, $J = 3.2$, 1H), 3.69 (m, 6H), 3.60 (dd, $J = 9.8, 8.0$, 1H), 3.54 (dd, $J = 9.2, 8.0$, 1H), 3.51 (s, 3H). ^{13}C -NMR (125 MHz, D_2O): δ 175.39, 103.40, 103.24, 83.60, 82.83, 76.10, 74.86, 71.98, 70.43, 69.69, 68.19, 61.01, 57.08; ESI-MS calcd for $\text{C}_{13}\text{H}_{21}\text{O}_{15}\text{S}^-$ [M-H] $^-$ (M for free acids): 449.06, Found: 448.95

4-(2-Azidoethyl)phenol (**9**).

Tyramine (3.43 g, 25.0 mmol), NaHCO_3 (7.80 g, 92.8 mmol) and $\text{CuSO}_4 \cdot 5\text{H}_2\text{O}$ (0.22 g, 0.9 mmol) were dissolved in water (30 mL). Triflic azide stock solution (40 mL), which was prepared according Titz *et al.* (186), and MeOH (190 mL) were added to give a homogeneous mixture. The mixture was stirred at rt overnight, then diluted with water (150 mL) and extracted with EtOAc (3 x 150 mL). The organic layer was dried over Na_2SO_4 and the solvents were evaporated. The residue was purified by flash chromatography (petroleum ether/EtOAc, 1:0 to 4:1) to yield **9** (quant.) as colorless oil.

^1H NMR (500 MHz, CDCl_3): δ 2.81 (t, $J = 7.3$ Hz, 2H, $\text{CH}_2\text{CH}_2\text{N}_3$), 3.44 (t, $J = 7.2$ Hz, 2H, $\text{CH}_2\text{CH}_2\text{N}_3$), 6.77, 7.07 (AA', BB' of AA'BB', $J = 8.5$ Hz, 4H, C_6H_4); ^{13}C NMR (126 MHz, CDCl_3): δ 34.50 ($\text{CH}_2\text{CH}_2\text{N}_3$), 52.72 ($\text{CH}_2\text{CH}_2\text{N}_3$), 115.53, 129.96, 130.22, 154.39 (6C, C_6H_4); IR (film): 2105 cm^{-1} (N_3).

4-(2-Azidoethyl)phenyl 2,3,4,6-tetra-O-acetyl- β -D-galactopyranoside (11).

To an ice-cooled suspension of **10** (8.30 g, 17.5 mmol) (**187**) and 4 Å molecular sieves (3 g) in DCM (40 mL) was added **9** (4.00 g, 24.5 mmol) in DCM (40 mL) under argon. TfOH (0.45 mL, 2.5 mmol) was added dropwise and the reaction mixture was allowed to warm to rt overnight. After quenching with TEA (0.8 mL) the suspension was filtered and the filtrate was concentrated. The residue was purified by flash chromatography (petroleum ether/EtOAc, 9:1 to 3:2) to yield **11** (4.58 g, 9.28 mmol, 53%) as oil.

$[\alpha]_{\text{D}}^{20} +6.1$ (*c* 1.10, CHCl₃); ¹H NMR (500 MHz, CDCl₃): δ 1.98, 2.02, 2.06, 2.15 (4s, 12H, 4 OAc), 2.82 (t, *J* = 7.2 Hz, 2H, CH₂CH₂N₃), 3.45 (t, *J* = 7.1 Hz, 2H, CH₂CH₂N₃), 4.02 (t, *J* = 6.6 Hz, 1H, H-5), 4.13 (dd, *J* = 6.3, 11.3 Hz, 1H, H-6a), 4.20 (dd, *J* = 6.9, 11.2 Hz, 1H, H-6b), 4.99 (d, *J* = 8.0 Hz, 1H, H-1), 5.08 (dd, *J* = 3.4, 10.5 Hz, 1H, H-3), 5.40-5.48 (m, 2H, H-2, H-4), 6.93, 7.12 (AA', BB' of AA'BB', *J* = 8.6 Hz, 4H, C₆H₄); ¹³C NMR (126 MHz, CDCl₃): δ 20.58, 20.65, 20.65, 20.73 (4 COCH₃), 34.52 (CH₂CH₂N₃), 52.51 (CH₂CH₂N₃), 61.36 (C-6), 66.89 (C-4), 68.67 (C-2), 70.85 (C-3), 71.01 (C-5), 99.78 (C-1), 117.19, 129.87, 133.01, 155.85 (6C, C₆H₄), 169.40, 170.13, 170.26, 170.36 (4 CO); ESI-MS: *m/z*: calcd for C₂₂H₂₇N₃NaO₁₀ [M+Na]⁺: 516.17, found: 516.19; IR (film): 2101 cm⁻¹ (N₃).

4-(2-Azidoethyl)phenyl β -D-galactopyranoside (12).

A solution of **11** (4.58 g, 9.28 mmol) in MeOH (45 mL) was treated with 1 M NaOMe/MeOH (4.5 mL) under argon overnight. After neutralization with Amberlite IR-120 (H⁺) ion-exchange resin, the solvent was evaporated and the residue was purified by flash chromatography (DCM/MeOH, 1:0 to 4:1) to give **12** (2.86g, 8.79 mmol, 95%) as an oil.

$[\alpha]_{\text{D}}^{20} -38.1$ (*c* 1.00, MeOH); ¹H NMR (500 MHz, CD₃OD): δ 2.85 (t, *J* = 7.1 Hz, 2H, CH₂CH₂N₃), 3.49 (t, *J* = 7.1 Hz, 2H, CH₂CH₂N₃), 3.60 (dd, *J* = 3.4, 9.7 Hz, 1H, H-3), 3.70 (m, 1H, H-5), 3.75-3.85 (m, 3H, H-2, H-6), 3.93 (d, *J* = 3.2 Hz, 1H, H-4), 4.86 (d, *J* = 7.8 Hz, 1H, H-1), 7.09, 7.20 (AA', BB' of AA'BB', *J* = 8.6 Hz, 4H, C₆H₄); ¹³C NMR (126 MHz, CD₃OD): δ 35.49 (CH₂CH₂N₃), 53.75 (CH₂CH₂N₃), 62.44 (C-6), 70.25 (C-4), 72.34 (C-2), 74.89 (C-3), 76.96 (C-5), 103.11 (C-1), 118.00, 130.82, 133.65, 158.08 (6C, C₆H₄); ESI-MS: *m/z*: calcd for C₁₄H₁₉N₃NaO₆ [M+Na]⁺: 348.13, found: 348.04; IR (film): 2112 cm⁻¹ (N₃).

4-(2-Azidoethyl)phenyl 3,4-isopropylidene- β -D-galactopyranoside (13).

To a solution of **12** (2.86 g, 8.79 mmol) in DMF (30 mL) were added 2,2-dimethoxypropane (2.50 mL, 19.3 mmol) and *p*-TsOH (37 mg) under argon. After stirring overnight at 80 °C, the

reaction mixture was neutralized with TEA (0.5 mL) and the solvents were evaporated. The residue was purified by flash chromatography (petroleum ether + 0.5% TEA/EtOAc, 1:2 to 0:1) to yield **13** (2.39 g, 6.55 mmol, 75%) as an oil.

$[\alpha]_D^{20}$ -22.4 (*c* 1.10, CHCl₃); ¹H NMR (500 MHz, CDCl₃): δ 1.34, 1.53 (2s, 6H, Me₂C), 2.42 (s, 2H, 2 OH), 2.81 (t, *J* = 7.1 Hz, 2H, CH₂CH₂N₃), 3.44 (t, *J* = 7.2 Hz, 2H, CH₂CH₂N₃), 3.78-3.85 (m, 2H, H-2, H-6a), 3.93-4.00 (m, 2H, H-6b, H-5), 4.14-4.21 (m, 2H, H-3, H-4), 4.78 (d, *J* = 8.2 Hz, 1H, H-1), 6.95, 7.12 (AA', BB' of AA'BB', *J* = 8.5 Hz, 4H, C₆H₄); ¹³C NMR (126 MHz, CDCl₃): δ 26.33, 28.10 (C(CH₃)₂), 34.54 (CH₂CH₂N₃), 52.53 (CH₂CH₂N₃), 62.29 (C-6), 73.31 (C-2), 73.69 (C-5), 73.87 (C-4), 78.89 (C-3), 100.33 (C-1), 110.69 (C(CH₃)₂), 116.89, 129.95, 132.63, 155.78 (6C, C₆H₄); ESI-MS: *m/z*: calcd for C₁₇H₂₃N₃NaO₆ [M+Na]⁺: 388.16, found: 388.06; IR (film): 2099 cm⁻¹ (N₃).

4-(2-Azidoethyl)phenyl 2,6-di-O-benzyl-3,4-isopropylidene-β-D-galactopyranoside (14).

Compound **13** (1.02 g, 2.78 mmol) was dissolved in DCM (15 mL). 15-Crown-5 (55 μL, 0.28 mmol), 50% aq NaOH (37.5 mL) and benzylbromide (3.30 mL, 27.8 mmol) were added and the biphasic mixture was stirred overnight under reflux at 60 °C. The reaction mixture was neutralized with 4 M aq HCl. The organic layer was separated and the aqueous phase extracted with DCM (2 × 50 mL) and. The combined organic layers were concentrated and the residue was purified by flash chromatography (petroleum ether + 0.5% TEA/EtOAc, 1:0 to 3:1) to give **14** (1.26 g, 2.31 mmol, 83%) as a white solid.

$[\alpha]_D^{20}$ +8.4 (*c* 1.00, CHCl₃); ¹H NMR (500 MHz, CDCl₃): δ 1.28, 1.34 (2s, 6H, Me₂C), 2.76 (t, *J* = 7.3 Hz, 2H, CH₂CH₂N₃), 3.37 (t, *J* = 7.3 Hz, 2H, CH₂CH₂N₃), 3.60 (dd, *J* = 6.8, 7.9 Hz, 1H, H-2), 3.69-3.80 (m, 2H, H-6), 3.97 (ddd, *J* = 1.8, 4.7, 6.8 Hz, 1H, H-5), 4.13 (dd, *J* = 2.0, 5.7 Hz, 1H, H-4), 4.18 (m, 1H, H-3), 4.46, 4.54 (A, B of AB, *J* = 11.8 Hz, 2H, CH₂Ph), 4.78-4.85 (m, 3H, CH₂Ph, H-1), 6.69, 7.03 (AA', BB' of AA'BB', *J* = 8.6 Hz, 4H, C₆H₄), 7.15-7.28 (m, 8H, 2 C₆H₅), 7.34 (d, *J* = 7.4 Hz, 2H, 2 C₆H₅); ¹³C NMR (126 MHz, CDCl₃): δ 26.41, 27.81 (C(CH₃)₂), 34.62 (CH₂CH₂N₃), 52.62 (CH₂CH₂N₃), 69.60 (C-6), 72.72 (C-5), 73.67 (C-4), 73.69 (2C, 2 CH₂Ph), 79.08 (C-3), 79.26 (C-2), 101.09 (C-1), 110.27 (C(CH₃)₂), 117.23 (2C, C₆H₄), 127.63, 127.69, 127.72, 128.26, 128.32, 128.40 (8C, 2 C₆H₅), 129.80 (2C, C₆H₄), 132.19, 138.14 (2 C₆H₅), 138.29, 156.26 (C₆H₄); ESI-MS: *m/z*: calcd for C₃₁H₃₅N₃NaO₆ [M+Na]⁺: 568.25, found: 568.21; IR (KBr): 2096 cm⁻¹ (N₃).

4-(2-Azidoethyl)phenyl 2,6-di-O-benzyl-β-D-galactopyranoside (15).

A solution of **14** (1.26 g, 2.31 mmol) in 90% aq AcOH (50 mL) was stirred at 60 °C overnight. The solvents were evaporated and the residue was purified by flash chromatography (DCM/MeOH, 1:0 to 9:1) to give **15** (1.17 g, 2.31 mmol, quant) as an oil.

$[\alpha]_D^{20}$ -9.9 (*c* 1.10, CHCl₃); ¹H NMR (500 MHz, CDCl₃): δ 2.76 (t, *J* = 7.3 Hz, 2H, CH₂CH₂N₃), 3.38 (t, *J* = 7.3 Hz, 2H, CH₂CH₂N₃), 3.59 (dd, *J* = 3.3, 9.5 Hz, 1H, H-3), 3.62-3.76 (m, 4H, H-2, H-5, H6), 3.92 (d, *J* = 3.2 Hz, 1H, H-4), 4.48 (s, 2H, CH₂Ph), 4.69 (A of AB, *J* = 11.5 Hz, 1H, CH₂Ph), 4.87 (d, *J* = 7.7 Hz, 1H, H-1), 4.96 (B of AB, *J* = 11.5 Hz, 1H, CH₂Ph), 6.97, 7.05 (AA', BB' of AA'BB', *J* = 8.5 Hz, 4H, C₆H₄), 7.15-7.31 (m, 10H, 2 C₆H₅); ¹³C NMR (126 MHz, CDCl₃): δ 34.58 (CH₂CH₂N₃), 52.59 (CH₂CH₂N₃), 68.92 (C-4), 69.41 (C-6), 73.20 (C-3), 73.74 (C-5), 73.81, 74.91 (2 CH₂Ph), 78.87 (C-2), 101.86 (C-1), 117.19 (2C, C₆H₄), 127.75, 127.83, 128.03, 128.27, 128.47, 128.60 (8C, 2 C₆H₅), 129.83 (2C, C₆H₄), 132.33, 137.87 (2 C₆H₅), 138.14, 156.13 (C₆H₄); ESI-MS: *m/z*: calcd for C₂₈H₃₁N₃NaO₆ [M+Na]⁺: 528.22, found: 528.22; IR (film): 2098 cm⁻¹ (N₃).

4-(2-Azidoethyl)phenyl 4-O-benzoyl-2,6-di-O-benzyl-β-D-galactopyranoside (16).

To a solution of **55** (1.17 g, 2.31 mmol) in toluene (15 mL) were added trimethylortho-benzoate (0.64 mL, 3.72 mmol) and *p*-TsOH (118 mg, 0.62 mmol). The mixture was stirred at 45 °C overnight, then concentrated and the residue dissolved in 90% aq AcOH (15 mL). The solution was stirred for 2 h at 60 °C, concentrated and the residue was purified by flash chromatography (petroleum ether/EtOAc, 9:1 to 7:3) to yield **16** (1.30 g, 2.14 mmol, 93%) as a colorless oil.

$[\alpha]_D^{20}$ -8.4 (*c* 1.00, CHCl₃); ¹H NMR (500 MHz, CDCl₃): δ 2.83 (t, *J* = 7.3 Hz, 2H, CH₂CH₂N₃), 3.44 (t, *J* = 7.3 Hz, 2H, CH₂CH₂N₃), 3.60-3.66 (m, 2H, H-6), 3.87 (dd, *J* = 7.4, 9.6 Hz, 1H, H-2), 3.92 (dd, *J* = 3.5, 9.6 Hz, 1H, H-3), 3.96 (t, *J* = 6.2 Hz, 1H, H-5), 4.41, 4.48 (A, B of AB, *J* = 11.7 Hz, 2H, CH₂Ph), 4.78 (A of AB, *J* = 11.2 Hz, 1H, CH₂Ph), 4.99-5.07 (m, 2H, H-1, CH₂Ph), 5.63 (d, *J* = 2.8 Hz, 1H, H-4), 7.06, 7.12 (AA', BB' of AA'BB', *J* = 8.5 Hz, 4H, C₆H₄), 7.18-7.35 (m, 10H, 2 C₆H₅), 7.43 (t, *J* = 7.8 Hz, 2H, C₆H₅), 7.56 (t, *J* = 7.4 Hz, 1H, C₆H₅), 8.04-8.09 (m, 2H, C₆H₅); ¹³C NMR (126 MHz, CDCl₃): δ 34.62 (CH₂CH₂N₃), 52.63 (CH₂CH₂N₃), 68.61 (C-6), 70.25 (C-4), 72.21 (C-3), 73.28 (C-5), 73.71, 75.13 (2 CH₂Ph), 79.15 (C-2), 101.89 (C-1), 117.07 (2C, C₆H₄), 127.76, 127.78, 128.04, 128.29, 128.39, 128.49, 128.58, 129.57 (12C, 3 C₆H₅), 129.93 (2C, C₆H₄), 130.10, 132.46, 133.38,

137.79 (6C, 3 C₆H₅), 138.06, 156.17 (C₆H₄), 166.38 (CO); ESI-MS: *m/z*: calcd for C₃₅H₃₅N₃NaO₇ [M+Na]⁺: 532.24, found: 532.28; IR (film): 2102 cm⁻¹ (N₃).

4-(2-Azidoethyl)phenyl (methyl 2,3,4-tri-O-benzoyl-β-D-glucopyranuronate)-(1→3)-4-O-benzoyl-2,6-di-O-benzyl-β-D-galactopyranoside (17).

Under argon trichloroacetimidate **3** (1.75 g, 2.63 mmol), **16** (1.30 g, 2.14 mmol) and activated 4 Å molecular sieves (2 g) were suspended in DCM (25 mL). The mixture was stirred for 1 h at rt and then cooled to 0 °C. TMSOTf (58.4 μL, 0.32 mmol) was added dropwise. The reaction mixture was allowed to warm to rt overnight, and was then neutralized with TEA (150 μL) and concentrated. The residue was purified by chromatography (petroleum ether/EtOAc, 9:1 to 7:3) to yield **17** (2.04 g, 1.84 mmol, 86%) as a white solid.

[α]_D²⁰ +25.2 (*c* 1.10, CHCl₃); ¹H NMR (500 MHz, CDCl₃): δ 2.84 (t, *J* = 7.3 Hz, 2H, CH₂CH₂N₃), 3.46 (t, *J* = 7.2 Hz, 2H, CH₂CH₂N₃), 3.61 (dd, *J* = 7.3, 10.1 Hz, 1H, H-6a), 3.67 (s, 3H, OMe), 3.72 (dd, *J* = 4.7, 10.2 Hz, 1H, H-6b), 3.98 (dd, *J* = 7.9, 9.5 Hz, 1H, H-2), 4.02 (dd, *J* = 5.3, 6.5 Hz, 1H, H-5), 4.15 (d, *J* = 9.8 Hz, 1H, H-5'), 4.24 (dd, *J* = 3.4, 9.5 Hz, 1H, H-3), 4.48 (A, B of AB, *J* = 11.5 Hz, 2H, CH₂Ph), 4.55, 4.91 (A, B of AB, *J* = 10.7 Hz, 2H, CH₂Ph), 5.02 (d, *J* = 7.7 Hz, 1H, H-1), 5.39 (d, *J* = 7.4 Hz, 1H, H-1'), 5.47 (dd, *J* = 7.4, 9.1 Hz, 1H, H-2'), 5.69 (t, *J* = 9.5 Hz, 1H, H-4'), 5.77 (t, *J* = 9.3 Hz, 1H, H-3'), 5.81 (d, *J* = 3.3 Hz, 1H, H-4), 7.02, 7.10 (AA', BB' of AA'BB', *J* = 8.7 Hz, 4H, C₆H₄), 7.22-7.46, 7.48-7.53, 7.56-7.66, 7.76-7.81, 7.88-7.93, 8.05-8.10 (m, 30H, 6 C₆H₅); ¹³C NMR (126 MHz, CDCl₃): δ 34.60 (CH₂CH₂N₃), 52.59 (CH₂CH₂N₃), 52.86 (OMe), 69.06 (C-6), 70.01 (C-4), 70.06 (C-4'), 71.83 (C-2'), 72.24 (C-3'), 72.94 (C-5'), 73.67 (C-5), 73.73, 75.25 (2 CH₂Ph), 76.26 (C-3), 79.77 (C-2), 100.3 (C-1'), 101.81 (C-1), 117.02 (2C, C₆H₄), 127.69, 127.76, 127.98, 128.10, 128.30, 128.37, 128.43, 128.56, 128.75, 128.94, 129.09, 129.60, 129.77, 129.82, 129.87, 129.94, 130.10, 132.39, 132.92, 133.08, 133.26, 133.38, 137.85, 137.92, 156.09 (40C, 6 C₆H₅, C₆H₄), 164.47, 165.00, 165.51, 165.64, 167.16 (5 CO); ESI-MS: *m/z*: calcd for C₆₃H₅₇N₃NaO₁₆ [M+Na]⁺: 1134.36, found: 1134.47; IR (KBr): 2099 cm⁻¹ (N₃).

4-(2-Azidoethyl)phenyl (β-D-glucopyranuronate)-(1→3)-2,6-di-O-benzyl-β-D-galactopyranoside (18).

Compound **17** (2.04 g, 1.84 mmol) was suspended in THF (14 mL) and the suspension was cooled to -10 °C. Then 2 M aq LiOH (10 mL) was added dropwise. The reaction mixture was stirred overnight and allowed to warm to rt. After neutralization with Amberlite IR-120 (H⁺) ion-exchange resin and filtration, the solvents were evaporated, the residue was dissolved in

THF/H₂O (2:3, 16 mL) and treated with TFA (8 mL) for 30 min. The mixture was evaporated to dryness and the residue was purified by reversed-phase chromatography (RP-18, MeOH/water, 0:1 to 3:1) to give **18** (1.12 g, 1.64 mmol, 89%) as a solid

$[\alpha]_D^{20}$ -48.1 (*c* 1.00, MeOH); ¹H NMR (500 MHz, CD₃OD): δ 2.79 (t, *J* = 7.0 Hz, 2H, CH₂CH₂N₃), 3.35-3.47 (m, 4H, H-2', H-3', CH₂CH₂N₃), 3.53 (t, *J* = 9.1 Hz, 1H, H-4'), 3.73 (m, 2H, H-6), 3.77 (d, *J* = 9.8 Hz, 1H, H-5'), 3.81-3.89 (m, 2H, H-3, H-5), 3.94 (m, 1H, H-2), 4.06 (d, *J* = 2.5 Hz, 1H, H-4), 4.53 (s, 2H, CH₂Ph), 4.74 (d, *J* = 7.3 Hz, 1H, H-1'), 4.88-4.95 (m, 2H, CH₂Ph), 4.99 (d, *J* = 7.7 Hz, 1H, H-1), 7.02, 7.12 (AA', BB' of AA'BB', *J* = 8.5 Hz, 4H, C₆H₄), 7.20-7.34 (m, 8H, 2 C₆H₅), 7.41 (d, *J* = 7.1 Hz, 2H, 2 C₆H₅); ¹³C NMR (126 MHz, CD₃OD): δ 33.97 (CH₂CH₂N₃), 52.19 (CH₂CH₂N₃), 68.85 (C-4), 69.18 (C-6), 71.78 (C-4'), 72.86 (CH₂Ph), 73.32 (C-2'), 73.58 (C-5), 74.69 (CH₂Ph), 74.93 (C-5'), 75.83 (C-3'), 78.50 (C-2), 80.64 (C-3), 101.39 (C-1), 104.07 (C-1'), 116.43 (2C, C₆H₄), 127.12, 127.21, 127.25, 127.75, 127.87, 128.23 (10C, 2 C₆H₅), 129.44, 132.31 (3C, C₆H₄), 138.22, 138.38 (2 C₆H₅), 156.25 (C₆H₄), 171.27 (CO); ESI-MS: *m/z*: calcd for C₃₄H₃₉N₃NaO₁₂ [M+Na]⁺: 704.24, found: 704.30; IR (KBr): 2099 cm⁻¹ (N₃).

4-(2-Azidoethyl)phenyl (methyl 2,4-di-O-acetyl- β -D-glucopyranuronate)-(1 \rightarrow 3)-4-O-acetyl-2,6-di-O-benzyl- β -D-galactopyranoside (19).

A solution of **18** (900 mg, 1.32 mmol) in Ac₂O (15 mL) was stirred at 80 °C for 1 h and then cooled to rt. Pyridine (9 mL) and DMAP (25 mg) were added and the reaction mixture was stirred for 3 d. The solvents were co-evaporated with toluene (5 \times 5 mL). The residue was dissolved in DCM (50 mL) and extracted with brine (50 mL) and water (50 mL). The organic phase was dried over Na₂SO₄ and filtered through cotton wool. After evaporation of the solvent the residue was dissolved in dry MeOH (20 mL) and anhydrous NaOAc (100 mg) was added. The mixture was stirred overnight, neutralized with Amberlyste 15 (H⁺) ion-exchange resin and filtered. The filtrate was concentrated and the residue purified by flash chromatography (petroleum ether/EtOAc, 2:1 to 2:3) to yield **19** (794 mg, 0.97 mmol, 73%) as a yellowish solid.

$[\alpha]_D^{20}$ -32.6 (*c* 1.00, CHCl₃); ¹H NMR (500 MHz, CDCl₃): δ 1.92, 2.01, 2.04 (3s, 9H, 3 OAc), 2.77 (t, *J* = 7.2 Hz, 2H, CH₂CH₂N₃), 3.40 (t, *J* = 7.2 Hz, 2H, CH₂CH₂N₃), 3.48 (dd, *J* = 7.1, 10.1 Hz, 1H, H-6a), 3.55 (dd, *J* = 4.8, 10.2 Hz, 1H, H-6b), 3.61 (m, 1H, H-3'), 3.67 (s, 3H, OMe), 3.78-3.83 (m, 2H, H-5, H-5'), 3.86 (dd, *J* = 7.6, 9.7 Hz, 1H, H-2), 3.91 (dd, *J* = 3.3, 9.6 Hz, 1H, H-3), 4.43 (A, B of AB, *J* = 11.7 Hz, 2H, CH₂Ph), 4.64 (A of AB, *J* = 11.6 Hz, 1H, CH₂Ph), 4.81-4.88 (m, 2H, H-1, H-2), 4.91 (d, *J* = 7.6 Hz, 1H, H-1'), 4.95 (B of AB, *J* = 10.6

Hz, 1H, CH_2Ph), 5.07 (t, $J = 9.5$ Hz, 1H, H-4'), 5.38 (d, $J = 3.0$ Hz, 1H, H-4), 6.96, 7.04 (AA', BB' of AA'BB', $J = 8.5$ Hz, 4H, C_6H_4), 7.18-7.31 (m, 10H, 2 C_6H_5); ^{13}C NMR (126 MHz, $CDCl_3$): δ 20.69, 20.72, 20.76 (3 $COCH_3$), 34.59 ($CH_2CH_2N_3$), 52.58 ($CH_2CH_2N_3$), 52.79 (OCH_3), 68.93 (C-6), 69.30 (C-4), 71.91 (C-4'), 72.53 (C-5), 73.10 (C-5'), 73.38 (C-3'), 73.70 (CH_2Ph), 73.87 (C-2'), 75.31 (CH_2Ph), 77.24 (C-3), 79.19 (C-2), 100.10 (C-1'), 101.71 (C-1), 117.04 (2C, C_6H_4), 127.76, 127.80, 127.96, 128.01, 128.40, 128.49 (10C, 2 C_6H_5), 129.85, 132.41 (3C, C_6H_4), 137.87, 137.96 (2 C_6H_5), 156.08 (C_6H_4), 167.42, 170.11, 170.29, 170.32 (4 CO); ESI-MS: m/z : calcd for $C_{41}H_{47}N_3NaO_{15}$ $[M+Na]^+$: 844.29, found: 844.39; IR (KBr): 2101 cm^{-1} (N_3).

4-(2-Azidoethyl)phenyl (methyl 2,4-di-O-acetyl-3-O-sulfo- β -D-glucopyranuronate)-(1 \rightarrow 3)-4-O-acetyl-2,6-di-O-benzyl- β -D-galactopyranoside, sodium salt (20).

Compound **19** (794 mg, 0.97 mmol) was dissolved in dry DMF (10 mL) and $SO_3 \cdot Py$ (846 mg, 5.31 mmol) was added. The mixture was stirred for 2 h at rt and quenched by stirring with $NaHCO_3$ (719 mg, 8.56 mmol) for 2 h. The solid was filtered off and the filter was washed with MeOH. The filtrate was passed over a Dowex 50X8 (Na^+) ion-exchange column. The filtrate was concentrated and the residue was purified by flash chromatography (DCM/MeOH, 1:0 to 9:1) to give **20** (808 mg, 0.88 mmol, 91%) as a yellowish solid. During concentration after the flash chromatography a few drops of 0.1 M aq NaOH were added.

$[\alpha]_D^{20}$ -18.3 (c 1.00, MeOH); 1H NMR (500 MHz, CD_3OD): δ 1.97, 2.09, 2.11 (3s, 9H, 3 OAc), 2.86 (t, $J = 7.0$ Hz, 2H, $CH_2CH_2N_3$), 3.50 (t, $J = 7.0$ Hz, 2H, $CH_2CH_2N_3$), 3.54 (dd, $J = 7.4, 10.4$ Hz, 1H, H-6a), 3.65 (dd, $J = 4.4, 10.4$ Hz, 1H, H-6b), 3.75 (s, 3H, OMe), 3.86 (dd, $J = 7.9, 9.5$ Hz, 1H, H-2), 4.07 (dd, $J = 4.6, 7.1$ Hz, 1H, H-5), 4.09-4.14 (m, 2H, H-3, H-5'), 4.49-4.57 (m, 2H, CH_2Ph), 4.66 (t, $J = 9.2$ Hz, 1H, H-3'), 4.80 (A of AB, $J = 10.7$ Hz, 1H, CH_2Ph), 4.96-5.03 (m, 2H, CH_2Ph , H-2'), 5.06 (d, $J = 7.9$ Hz, 1H, H-1'), 5.11-5.17 (m, 2H, $J = 8.2$ Hz, H-1, H-4') 5.48 (d, $J = 3.6$ Hz, 1H, H-4), 7.07, 7.18 (AA', BB' of AA'BB', $J = 8.5$ Hz, 4H, C_6H_4), 7.29-7.44 (m, 10H, 2 C_6H_5); ^{13}C NMR (126 MHz, CD_3OD): δ 20.87, 21.20 (3C, 3 $COCH_3$), 35.50 ($CH_2CH_2N_3$), 53.24 ($CH_2CH_2N_3$), 53.71 (OMe), 70.27 (C-6), 71.08 (C-4), 71.37 (C-4'), 72.95 (C-2'), 73.50 (C-5'), 74.14 (C-5), 74.41, 76.26 (2 CH_2Ph), 78.98 (C-3'), 80.02 (C-3), 80.11 (C-2), 101.62 (C-1'), 102.61 (C-1), 117.93 (2C, C_6H_4), 128.69, 128.79, 128.90, 129.17, 129.37, 129.43 (10C, 2 C_6H_5), 131.02, 134.06 (3C, C_6H_4), 139.56, 139.72 (2 C_6H_5), 157.58 (C_6H_4), 164.89, 169.39, 171.64, 171.75 (4 CO); ESI-MS: m/z : calcd for $C_{41}H_{46}N_3O_{18}S$ $[M-H]^-$: 900.25, found: 900.42; IR (KBr): 2101 cm^{-1} (N_3).

4-(2-Aminoethyl)phenyl (disodium 3-O-sulfo- β -D-glucopyranuronate)-(1 \rightarrow 3)- β -D-galactopyranoside (21).

To a solution of **20** (470 mg, 0.51 mmol) in THF/H₂O (10:1, 10 mL) was added 2 M aq LiOH (2 mL) at -10°C. The reaction mixture was allowed to warm to rt and was stirred overnight. The mixture was neutralized with Amberlyste 15 (H⁺) ion-exchange resin and filtered. The filtrate was passed over a Dowex 50X8 (Na⁺) ion-exchange column with MeOH and concentrated. The residue was purified by flash chromatography (DCM/MeOH/H₂O, 10:3:0.3). A few drops of 0.1 M aq NaOH were added during concentration of the product, which was then dissolved in MeOH (4.5 mL) and H₂O (3.75 mL). AcOH (0.2 mL) and Pd(OH)₂/C (94 mg, 20%) were added under argon and the reaction mixture was stirred overnight under an atmosphere of hydrogen (1 atm). The catalyst was filtered off through a pad of Celite and the pad was washed with MeOH and a few drops of H₂O. The filtrate was concentrated and the residue purified by P2 size-exclusion chromatography to yield **21** (238 mg, 0.40 mmol, 78%) as a colorless solid after lyophilization.

$[\alpha]_D^{20}$ -25.6 (*c* 1.00, H₂O); ¹H NMR (500 MHz, D₂O): δ 2.99 (t, *J* = 7.0 Hz, 2H, CH₂CH₂NH₂), 3.28 (t, *J* = 7.1 Hz, 2H, CH₂CH₂NH₂), 3.66 (t, *J* = 8.4 Hz, 1H, H-2'), 3.71-3.88 (m, 5H, H5, H-6, H-4', H-5'), 3.92 (dd, *J* = 3.2, 9.9 Hz, 1H, H-3), 3.99 (t, *J* = 8.6 Hz, 1H, H-2), 4.26 (d, *J* = 3.1 Hz, 1H, H-4), 4.39 (t, *J* = 9.0 Hz, 1H, H-3'), 4.82 (d, *J* = 7.9 Hz, 1H, H-1'), 5.12 (d, *J* = 7.7 Hz, 1H, H-1), 7.17, 7.32 (AA', BB' of AA'BB', *J* = 8.0 Hz, 4H, C₆H₄); ¹³C NMR (126 MHz, D₂O): δ 31.97 (CH₂CH₂NH₂), 40.65 (CH₂CH₂NH₂), 60.78 (C-6), 68.05 (C-4), 69.02 (C-2), 70.50 (C-4'), 72.03 (C-2'), 75.10 (2C, C-5, C-5'), 82.43 (C-3), 83.60 (C-3'), 100.46 (C-1), 103.24 (C-1'), 117.01, 130.30, 131.29, 155.75 (6C, C₆H₄), 175.45 (CO); ESI-MS: *m/z*: calcd for C₂₀H₂₇NNa₂O₁₅S [M-2Na+H]⁺: 554.12, found: 554.07.

4-(2-(4-Mercaptobutanamido)ethyl)phenyl (disodium-3-O-sulfo- β -D-glucopyranuronate)-(1 \rightarrow 3)- β -D-galactopyranoside (22).

To a suspension of **21** (238 mg, 0.40 mmol) in DMF (8 mL) were added dithiothreitol (112 mg, 0.72 mmol), thiobutylolactone (343 μ L, 4 mmol), and TEA (552 μ L, 4 mmol). The mixture was stirred for 18 h at 85 °C. The solvent was co-evaporated with toluene (3 \times 5 mL) and the residue purified by flash chromatography (DCM/MeOH/H₂O, 10:5:1). A few drops of 0.1 M aq NaOH were added during concentration of the product. Lyophilization gave **22** (164 mg, 0.234 mmol, 59%) as a colorless solid.

$[\alpha]_D^{20}$ -20.2 (c 1.00, H₂O); ¹H NMR (500 MHz, D₂O): δ 1.72-1.85 (m, 2H, CH₂CH₂CH₂SH), 2.28 (t, J = 7.2 Hz, 2H, CH₂CH₂CH₂SH), 2.37 (t, J = 7.2 Hz, 2H, CH₂CH₂CH₂SH), 2.83 (t, J = 6.5 Hz, 2H, CH₂CH₂NH), 3.49 (t, J = 6.5 Hz, 2H, CH₂CH₂NH), 3.67 (dd, J = 8.1, 9.1 Hz, 1H, H-2'), 3.73-3.91 (m, 5H, H-5, H6, H-4', H-5'), 3.94-4.02 (m, 2H, H-2, H-3), 4.29 (d, J = 2.7 Hz, 1H, H-4), 4.39 (t, J = 9.1 Hz, 1H, H-3'), 4.84 (d, J = 7.9 Hz, 1H, H-1'), 5.13 (d, J = 7.4 Hz, 1H, H-1), 7.14, 7.27 (AA', BB' of AA'BB', J = 8.5 Hz, 4H, C₆H₄); ¹³C NMR (126 MHz, D₂O): δ 22.87 (CH₂CH₂CH₂SH), 29.44 (CH₂CH₂CH₂SH), 33.63 (CH₂CH₂NH), 34.34 (CH₂CH₂CH₂SH), 40.25 (CH₂CH₂NH), 60.77 (C-6), 68.04 (C-4), 69.03 (C-2), 70.47 (C-4'), 72.02 (C-2'), 75.10 (C-5), 76.10 (C-5'), 82.48 (C-3), 83.62 (C-3'), 100.67 (C-1), 103.26 (C-1'), 116.72, 130.19, 133.93, 155.24 (6C, C₆H₄), 175.43, 175.79 (2 CO); HRMS: m/z : calcd for C₂₄H₃₃NNa₂O₁₆S₂ [M+H]⁺: 702.1109, found: 702.1104.

Chloroacetylated polylysine (24).

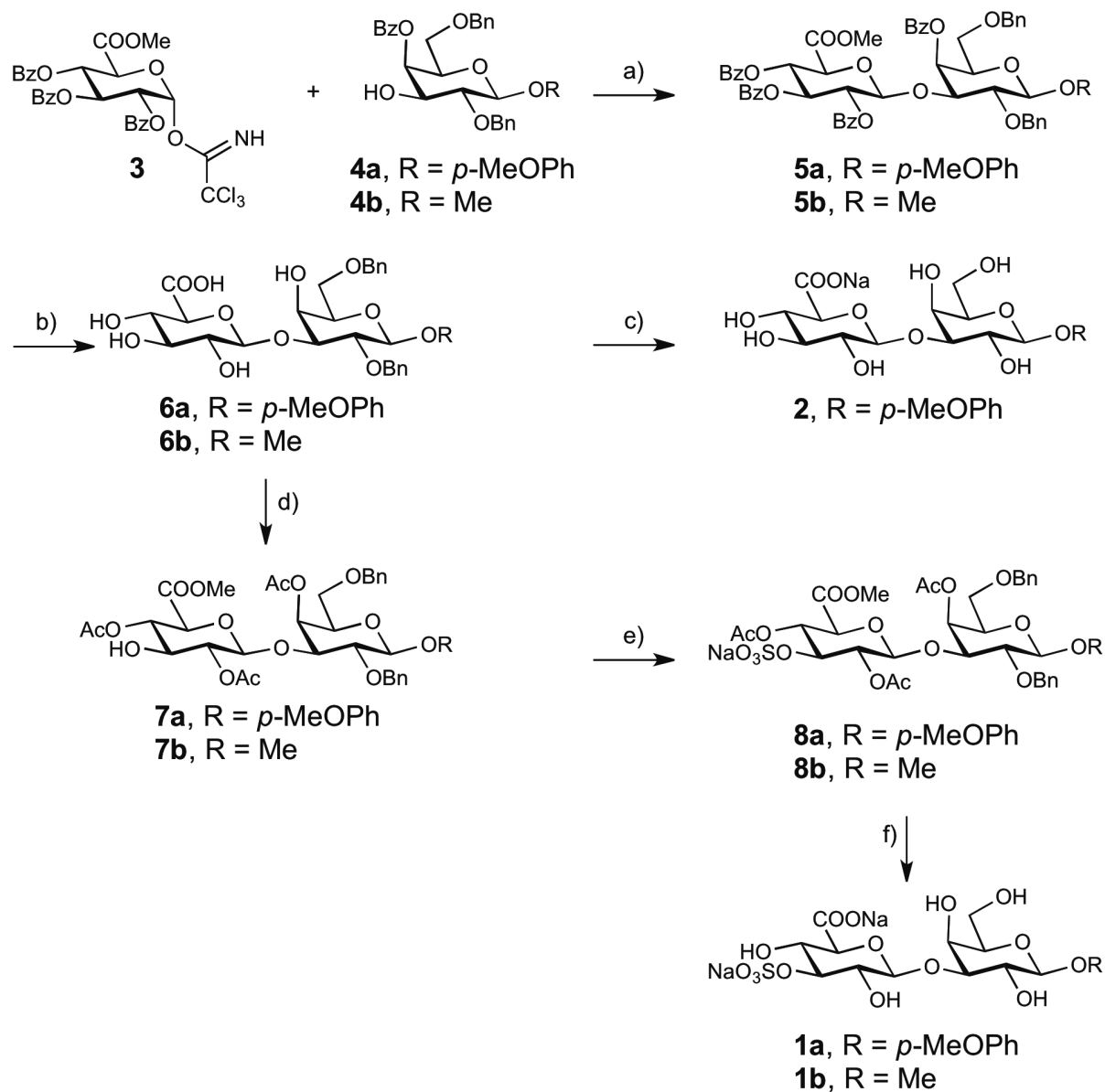
Poly-L-lysine hydrobromide (**23**) (P3995, Sigma-Aldrich) (0.50 g, 2.4 mmol) was suspended in a mixture of DMF (5 mL) and 2,6-lutidine (1.25 mL) under argon. The suspension was cooled to 0 °C and a solution of chloroacetic anhydride (513 mg, 3.00 mmol) in DMF (1 mL) was added slowly. The resulting clear solution was stirred for 16 h at 0 °C. The product was precipitated by dropwise addition of the reaction mixture to a stirred solution of ethanol/ether (1:1, 40 mL). The precipitate was filtered off, washed with ethanol/ether (1:1, 20 mL) and concentrated to give **24** (449 mg, 96%). The ¹H NMR data were in accordance with literature values (196).

Minimal HNK-1 polymer (25).

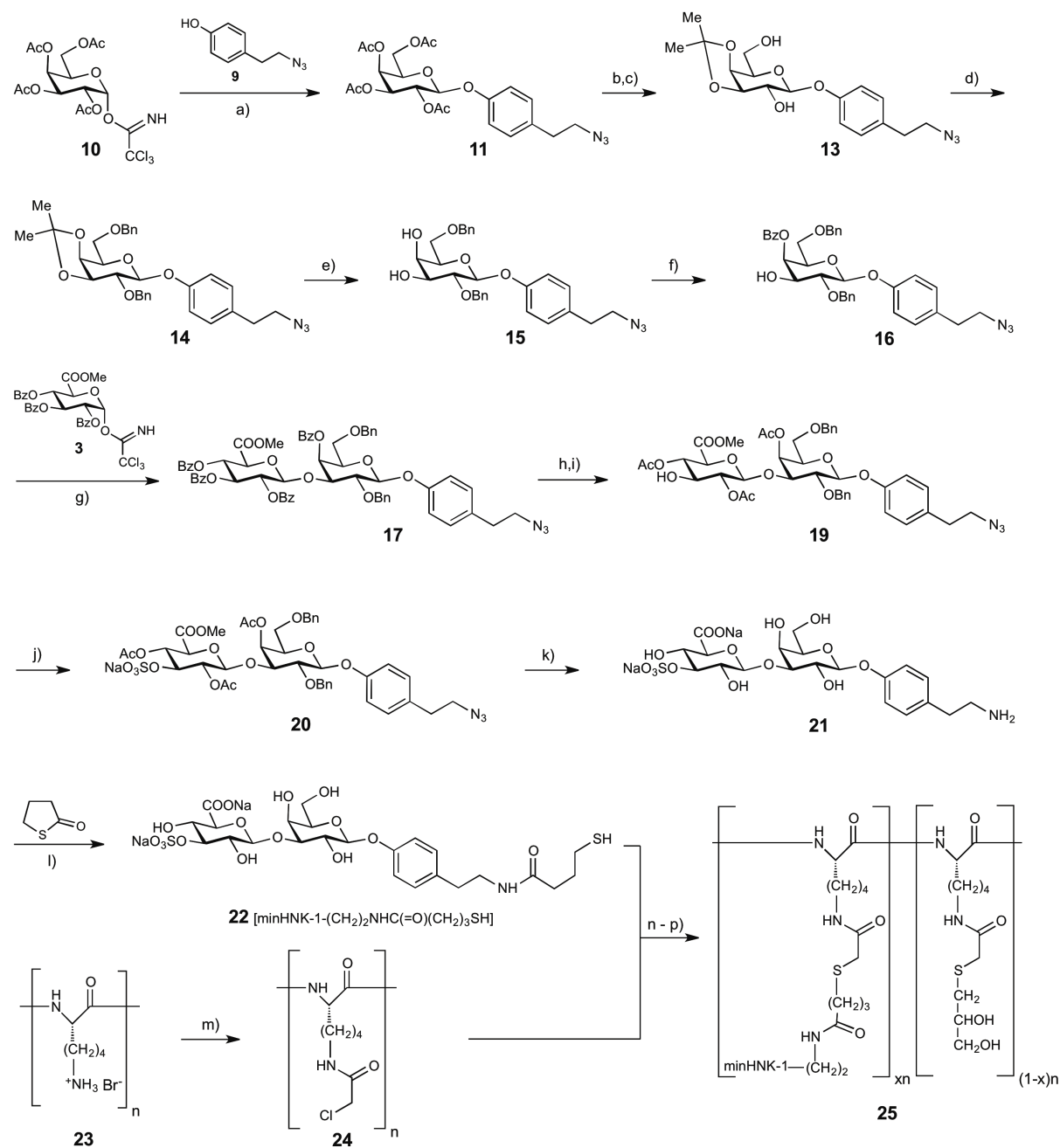
To a solution of **24** (80.2 mg, 0.39 mmol) in DMF (4 mL) were subsequently added **22** (110 mg, 0.16 mmol), water (200 μ L) and DBU (88 μ L, 0.59 mmol) in DMF (0.8 mL). After stirring for 1 h thioglycerol (102 μ L, 1.18 mmol) and TEA (164 μ L, 1.18 mmol) were added and the reaction mixture was stirred for 18 h. The product was precipitated by dropwise addition of the reaction mixture to a stirred solution of ethanol/ether (1:1, 30 mL). The precipitate was filtered off, washed with ethanol/ether (1:1, 15 mL) and dried. Further purification was achieved by means of ultrafiltration. The dried product was dissolved in water (10 mL) and ultracentrifugation was performed using two Sartorius Stedim Vivaspin 6 tubes (volume, 6 mL, diameter, 17 mm, molecular weight cutoff 5000). The ultrafiltration was repeated four times from 10 mL down to 3 mL, on each occasion the volume was filled up with water.

Lyophilization gave the HNK-1 polymer **25** (139 mg, 70%) According to ^1H NMR, the product contained approximately 50% monomer carbohydrate units linked to the polymer.

Schemes, figures, tables and legends



Scheme 2 (III 1): Synthesis of the minimal HNK-1 epitope in sulfated (**1a,b**) and unsulfated form (**2**). Reagents and conditions: a) TMSOTf, molecular sieves 4 Å, DCM, 0 °C to rt, (**5a**: 81%; **5b**: 84%) b) LiOH, THF/H₂O (**6a**: 97%; **6b**: 86%); c) Pd(OH)₂/C, H₂, MeOH/H₂O (**2**: 96%); d) Ac₂O, 80°C, pyr, DMAP; MeOH, anhyd AcONa (**7a**: 57%; **7b**: 50%); e) SO₃·Py, DMF (**8a**: 65%; **8b**: 76%); f) Pd(OH)₂/C, H₂, MeOH/H₂O, LiOH, MeOH/H₂O (**1a**: 88%; **1b**: 93%).



Scheme 3 (III 2): Synthesis of the minHNK-1 polymer **25**. Reagents and conditions: a) TMSOTf, molecular sieves 4 Å, DCM, 0 °C to rt (→ **11**: 53%); b) MeOH, NaOMe, rt, overnight (→ **12**, 95%); c) 2,2-dimethoxypropane, *p*-TsOH (Ts: toluylsulfonyl), DMF, rt, overnight (→ **13**: 75%); d) Crown ether 15-crown-5, BnBr, 50% aq NaOH, DCM, overnight, 60 °C (→ **14**: 83%); e) AcOH, H₂O, 60°C, overnight (→ **15**: quant.); f) trimethylorthobenzoate, *p*-TsOH, toluene, 45°C, overnight; AcOH, H₂O, 60°C, 2 h (→ **16**: 93%); g) TMSOTf, molecular sieves 4 Å, DCM, 0 °C to rt, (→ **17**: 86%); h) LiOH in THF/H₂O (→ **18**: 89%); i) Ac₂O, DMAP, pyr; MeOH, NaOAc MeOH (→ **19**, 73%); j) SO₃·Py, DMF (→ **20**: 91%); k) LiOH, THF/H₂O; Pd(OH)₂/C, H₂, MeOH/H₂O (→ **21**: 78%); l) dithiotreitol, thiobutylolactone, TEA, DMF, 85 °C (→ **22**: 59%); m) chloroacetic anhydride, 2,6-lutidine, DMF (→ **24**: 96%); n) DMF, H₂O, DBU; thioglycerol, TEA; ultracentrifugation (→ **25**: 70%).

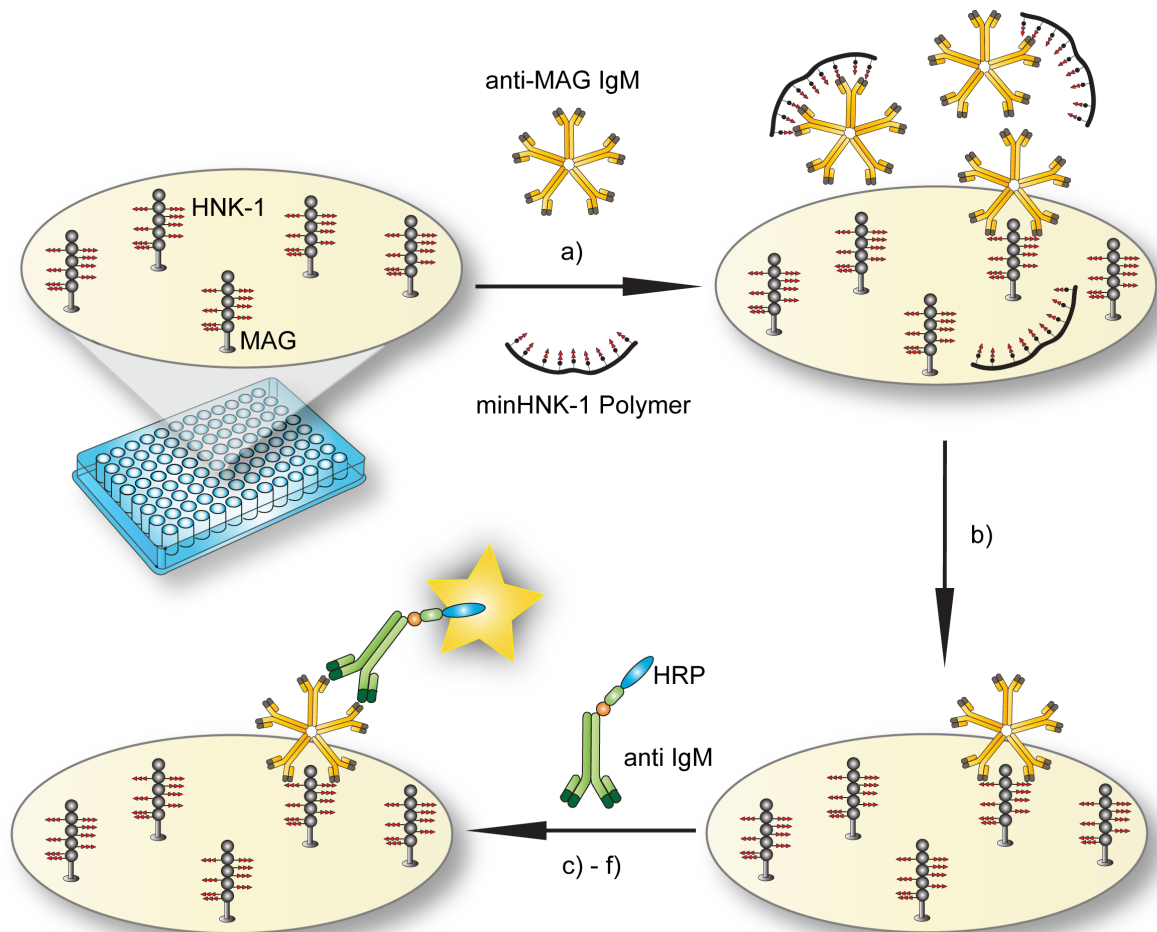


Figure 15 (III 1): Representative competitive binding ELISA. (a) Incubation of MAG-coated plates with anti-MAG IgM (patient sera) and minHNK-1 polymer **25** (or ligands **1a,b** or **2**). (b) Wash step. (c) Incubation with anti-human IgM antibody coupled to horseradish peroxidase. (d) Wash step. (e) Addition of tetramethylbenzidine (TMB) substrate. (f) Addition of acidic stop solution and measurement of the optical density.

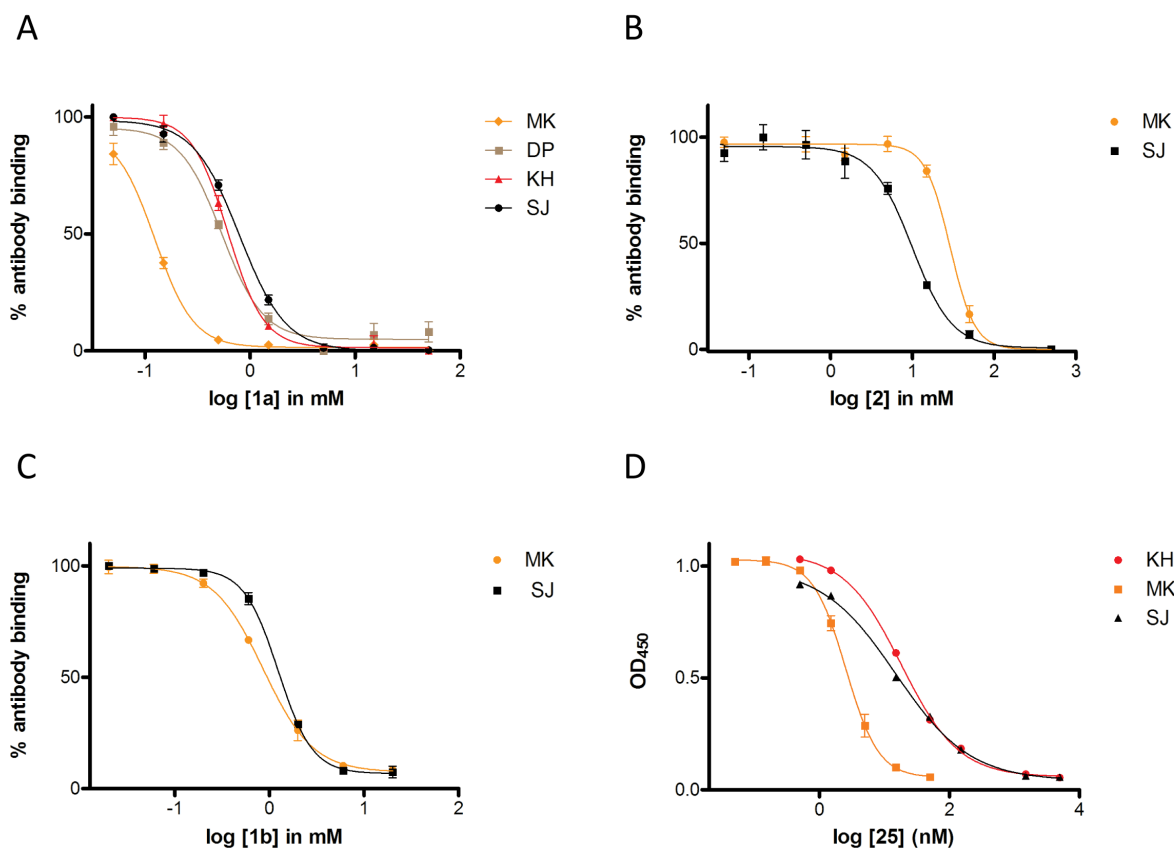


Figure16 (III 2): A-D: Binding curves for compounds **1a**, **1b** and **2**, and polymer **25**. The MAG-coated wells were co-incubated with the HNK-1 mimetics (highest concentrations: 50 mM for **1a** and **2**, 20 mM for **1b** and 0.005 mM for **25**) and the four patient sera: MK, DP, KH and SJ.

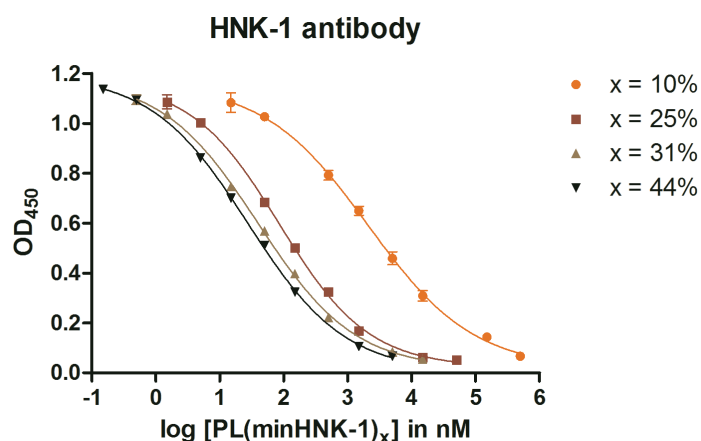


Figure 17 (III 3): Inhibition curves of PL(minHNK-1)₁₀₋₄₄ with the HNK-1 reference antibody (119). Inhibitory activity of polymers approaches a maximum with increasing epitope loading.

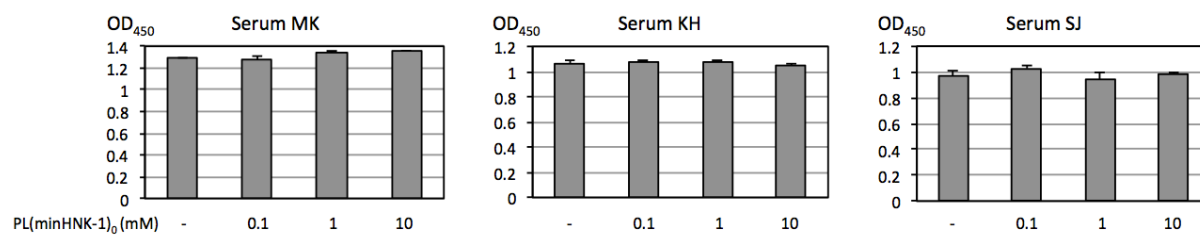


Figure 18 (III 4): Control polymer PL(minHNK-1)₀ without minHNK-1 epitope loading does not inhibit IgM antibody binding from patient sera MK, KH, and SJ to MAG.

Table 4 (III 1): IC₅₀ values of compounds **1a**, **1b**, **2** and the minHNK-1 polymer (**25**) for the four patient sera MK, DP, KH and SJ.

Serum	Compound 1a IC ₅₀ (μM)	Compound 1b IC ₅₀ (μM)	Compound 2 IC ₅₀ (μM)	Polymer (25) IC ₅₀ (μM)
MK	124. ± 9.5	860.0 ± 58.2	28967.3 ± 533.0	0.0025 ± 0.0001
DP	536.1 ± 23.5	n.d.	n.d.	n.d.
KH	614.2 ± 20.1	n.d.	n.d.	0.0183 ± 0.0022
SJ	793.1 ± 24.0	1237.0 ± 56.0	9981.1 ± 1002.2	0.0148 ± 0.0006

Table 5 (III 2): IC₅₀ values of PL(minHNK-1)₁₀₋₄₄ for patient sera KH, MK and SJ, and the monoclonal HNK-1 antibody (*119*).

Serum/Antibody	PL(minHNK-1) ₁₀ IC ₅₀ (nM)	PL(minHNK-1) ₂₅ IC ₅₀ (nM)	PL(minHNK-1) ₃₁ IC ₅₀ (nM)	PL(minHNK-1) ₄₄ IC ₅₀ (nM)
MK	10.0 ± 0.7	5.0 ± 0.2	4.0 ± 0.2	4.6 ± 0.1
KH	1936.7 ± 595.9	87.4 ± 2.0	34.0 ± 0.5	24.5 ± 2.5
SJ	27228.7 ± 4066.1	182.7 ± 16.4	47.5 ± 12.6	31.6 ± 6.7
HNK-1	2124.7 ± 443.8	85.6 ± 11.9	39.5 ± 4.0	27.6 ± 2.0

3.5 Discussion

The scope of this discussion is to draw the main conclusions from our study on anti-MAG neuropathy and to evaluate the potential of our investigated new therapeutic approach.

Characteristics of anti-MAG neuropathy and current treatments

Anti-MAG neuropathy is a rare peripheral neuropathy with currently no approved and no satisfactorily effective treatment available. The disease develops in MGUS patients with an IgM antibody with autoreactivity against MAG and other myelin components carrying the HNK-1 carbohydrate epitope. The anti-MAG IgM autoantibodies are thought to be pathogenic (8, 106). The neuropathy is associated with an underlying lymphoproliferative disorder, characterized by monoclonal gammopathy, that is to say that monoclonal anti-MAG IgM antibodies are produced by a pathogenically proliferating B-cell clone (109, 110). The majority of current immunosuppressive therapies aim at reducing anti-MAG IgM load via antibody removal or inhibition of its production (174). There seems to be a correlation between clinical improvement and lowering of anti-MAG IgM titer and of IgM memory B cell load (110, 142). Immunosuppressive treatments are mostly nonselective in their mode of action and immunosuppression comes at a high risk of side effects. Such treatments for anti-MAG neuropathy, e.g. PE, cytotoxic drugs, corticosteroids, and interferon, are prime examples of a “baseball bat hit-like treatment”, in the words of Prof. M. Dalakas at the ICNMD 2014 conference. Rituximab is currently the most promising treatment as it depletes a subpopulation of B cells, CD20+ B cells (110). Yet, rituximab inhibits production of antibodies in a non-selective manner, and some patients have been reported to clinically worsen under treatment (182). Overall, side effects are commonly associated with immunosuppressive treatments. Antigen-specific immunomodulatory treatments might offer a substantial benefit with regard to treatment effectiveness and more importantly to reduced risk of treatment side effects.

Design of small molecular weight inhibitors of anti-MAG IgM binding to MAG

The aim of our study was to find antigen-specific inhibitors for the interaction of pathogenic anti-MAG IgM antibodies and MAG. Based on the structure of the natural HNK-1 carbohydrate epitope, we synthesized carbohydrate-based small molecular weight inhibitors and evaluated their inhibitory effect on the binding of anti-MAG IgM antibodies from patient sera to MAG in an ELISA assay. We showed that disaccharide mimetics of the natural epitope

retain affinity for the IgM antibodies, supporting previous findings, defining the SO₃-3-GlcA(β1-3)Gal disaccharide as the minimal requirement for binding (130). Monosaccharide ligands, including only the terminal SO₃-3-GlcA (non-reducing end), are not expected to retain affinity for the IgM antibodies. From three synthesized HNK-1 mimetics the compound structurally closest to the natural trisaccharide epitope displayed best inhibitory activity on IgM antibody binding to MAG with micromolar IC₅₀ values. We defined this molecule as the minimal HNK-1 epitope (minHNK-1). Deletion of the sulfate group in position 3 of GlcA resulted in decreased inhibitory activity. Deletion of the *para*-methoxyphenyl group at the reducing end of our minHNK-1 disaccharide also resulted in decreased inhibitory activity. We suggest, that the minHNK-1 epitope with the terminal aromatic *para*-methoxyphenyl group acts as a pseudo-trisaccharide, mimicking the natural HNK-1 trisaccharide epitope. Involvement of aromatic groups in the binding of carbohydrate-based ligands to lectins has been described before (194). With respect to the complexity of the synthetic route and scale-up synthesis, disaccharide ligands are of more value than longer, structurally more complex oligosaccharides. It is reasonable that the closer HNK-1 mimetics are to the natural epitope in structure, the higher is also their binding affinity to anti-MAG antibodies. Furthermore, the structurally closer mimetics retain affinity towards anti-MAG IgM antibodies from various patients, as the antibodies all share the same epitope. Conventional lead optimization does not make sense for the HNK-1 mimetics, as the natural epitope serves as the “perfect” template. Chemical optimization of epitope mimetics for the IgM antibodies of one patient will likely result in decreased binding affinity for IgM antibodies of another patient. Chemical optimization makes more sense when aimed at defining a minimal carbohydrate epitope, which is synthetically more easily available than the whole epitope. Furthermore, the replacement of single monosaccharides can be considered, such as with lipophilic cyclohexane or aromatic groups (e.g. *para*-methoxyphenyl).

Design of an antigen-specific glycopolymer

Carbohydrate-protein interactions are often of a multivalent nature (195). A multivalent interaction most likely happens in anti-MAG neuropathy, whereby patients’ IgM antibody molecules with ten binding sites bind to the HNK-1 epitope, which is densely displayed on MAG at up to eight glycosylation sites (153). The study by Ogino *et al.* describes significantly decreased binding of anti-MAG IgM antibodies to MAG upon either breaking pentameric IgM into their monomers or by digesting MAG into peptides with monomeric HNK-1 oligosaccharides. We therefore hypothesized that a polymer that presents the minHNK-1 epitope in

a multivalent manner might display significantly increased IgM antibody binding affinity. Synthesis of a minHNK-1 polylysine polymer yielded a high molecular weight glycopolymer with a dramatically increased binding affinity towards the IgM antibodies compared to the corresponding monomeric molecule. IC_{50} values were determined for three patient sera already used in previous assays with the minHNK-1 monomer. Testing of an additional fourth patient serum confirmed the strong inhibition of IgM antibody binding to MAG *in vitro*, at low nanomolar polymer concentrations. Also, the monoclonal HNK-1 mouse IgM antibody (119) was tested and its binding to MAG was successfully inhibited at low nanomolar glycopolymer concentrations. A control polymer with no minHNK-1 epitope loading did not inhibit patient IgM antibody binding to MAG.

Therapeutic potential of the minHNK-1 glycopolymer

An ideal polymer-based drug candidate could be administered to the patient via infusion or as an injectable. Therefore, besides good inhibitory activity and selectivity for anti-MAG IgM, the compound should be readily water-soluble, sufficiently stable in solution, and biodegradable. Non-biodegradable polymers will accumulate in the body and are of little therapeutic value. The investigated minHNK-1 epitope polymer investigated in this study displayed good water solubility and its peptide backbone is biodegradable. As outlined earlier, it has shown very strong inhibition of anti-MAG IgM antibody binding to MAG *in vitro*. Through structural similarity of the polymer warhead (minHNK-1 epitope) with the natural HNK-1 epitope this polymer might act as an antigen specific immunomodulatory agent that blocks anti-MAG IgM antibody binding to MAG *in vivo*. Besides blocking circulating anti-MAG antibodies in the patients, the polymer might also induce a down-regulation of anti-MAG IgM production via binding to the specific B cells, as indicated by a previous study with a similar glycopolymer (188). Sustained down-regulation of the anti-MAG IgM titers and concomitant remyelination of the affected peripheral nerves would be expected if long term therapy is feasible. Taken together, the described minHNK-1 glycopolymer has significant therapeutic potential. In addition to therapeutic applications, diagnostic applications are also possible, i.e. for detection of anti-MAG antibodies in patient sera. In fact, the company Bühlmann AG successfully incorporated our polymer in a diagnostic ELISA assay kit that detects antibody reactivity in patient sera against several myelin carbohydrate epitopes. The next steps towards a therapeutic application for this polymer will be discussed in the outlook section.

3.6 Outlook

The most important next step towards a therapeutic application of the minHNK-1 glycopolymer will be its evaluation in an animal model. As outlined earlier, there are a few animal models described for anti-MAG neuropathy: passive transfer of patients' IgM antibodies into healthy experimental animals, including cats (143, 144) and chicks (145); and active immunization of cats with the glycolipid SGPG (147). All of these three animal models display aspects of human myelin/nerve pathology. Rats and mice do not express the HNK-1 epitope and are therefore less suitable as a neuropathy model (197). However, to study depletion and down-regulation of anti-MAG antibodies by the glycopolymer, three mouse models are of particular interest: (i) passive transfer of the HNK-1 mouse IgM antibody to mice, (ii) injection of the HNK-1 IgM producing hybridoma clone into the peritoneum of mice, and (iii) active immunization of mice with SGPG. All of these models should result in circulating anti-HNK-1 antibodies, and titers could be measured before, during, and after treatment with the glycopolymer by ELISA. Models (ii) and (iii) mimic constant antibody production, as in the human disease, and are thus preferable. Model (ii) could be problematic, as produced antibodies might not reach the circulation from the peritoneum.

In addition to the animal model experiments, immunohistochemistry of human nerve biopsies (skin biopsies) could be used to study whether HNK-1-binding of IgM antibodies from anti-MAG neuropathy patients is inhibited in the presence of the glycopolymer.

Furthermore, the selectivity for anti-MAG antibodies will have to be investigated. Data from Bühlmann AG suggest that the minHNK-1 polymer is very selective for anti-MAG IgM antibodies in the IgM subgroup of immunoglobulins, but also displays a certain degree of nonspecific IgG binding. This nonspecificity could be chemically optimized.

In order to be able to use a chemically defined polymeric molecule (in terms of molecular weight, the polylysine polymer is not clearly defined) it might be worth to synthesize polymer backbones with defined polypeptide lengths.

Eventually, polymers such as the minHNK-1 glycopolymer could be designed for neuropathies associated with autoantibodies against other carbohydrate epitopes (see section 3.1). The proposed therapeutic approach might pave the way for the first antigen-specific treatment for anti-MAG neuropathy, and potentially for other antibody-mediated neuropathies.

4 Closing Words

This doctoral thesis presents novel therapeutic approaches for two NMDs. In a drug discovery project for DM1 we identified new potent small molecular weight inhibitors of the CUG₇₈-MBNL1 complex. The concept of searching for small molecules that displace MBNL1 from DMPK CUG_n RNA to treat DM1 is not new (51). However, our approach and methodology to identify small molecules were new. The format of the developed CUG₇₈-MBNL1 inhibition assay might be used for drug screenings in other RNA-mediated neuromuscular diseases, in particular for other TREDs with pathogenic RNA-protein interactions (e.g. DM2).

With regard to a successful *in vivo* application of small molecules currently being investigated in the DM1 field, including ours, particularly issues with target CUG_n-RNA selectivity, toxicity, and poor pharmacokinetic properties will have to be resolved over the coming years. Eventually, continued effort might result in an effective small molecule treatment for DM1. According to comments by Prof. Charles Thornton (ICNMD 2014) a small molecule treatment is the desired DM1 therapy. For the moment, however, the small molecules will have to leave the stage to antisense oligonucleotides (46, 48), until the small molecules will be suited for a therapeutic application. As kinase inhibitors are being increasingly investigated for DM1 and show ameliorating effects in DM1 cell models (60, 61, 67), the first small molecular therapeutic agent reaching the patients might be a kinase inhibitor.

The investigated novel therapeutic approach for the autoimmune disorder anti-MAG neuropathy with the minHNK-1 glycopolymer could pave the way for the first antigen-specific treatment for anti-MAG neuropathy and might provide an example for other antibody-mediated autoimmune diseases. As a targeted immunomodulatory treatment the new therapeutic approach might provide substantial benefit over current immunosuppressive therapies (174).

The drug discovery projects for both diseases were made possible by many studies elucidating the molecular disease mechanisms and therefore clearly owe to these previous basic studies. Hopefully, both drug discovery projects will contribute to the development of new therapies for both of these disabling NMDs. Indeed, “it is an exciting time to work in the field of neuromuscular disorders”, as mentioned in the preface, where better understanding of neuromuscular disease mechanisms fosters the development of new therapies.

References

1. C. M. McDonald, Clinical Approach to the Diagnostic Evaluation of Hereditary and Acquired Neuromuscular Diseases. *Physical Medicine and Rehabilitation Clinics of North America* **23**, 495-+ (2012).
2. F. Muntoni, M. J. A. Wood, Targeting RNA to treat neuromuscular disease. *Nature Reviews Drug Discovery* **10**, 621-637 (2011).
3. J. T. Caroscio, M. N. Mulvihill, R. Sterling, B. Abrams, AMYOTROPHIC-LATERAL-SCLEROSIS - ITS NATURAL-HISTORY. *Neurologic Clinics* **5**, 1-8 (1987).
4. K. E. Davies, K. J. Nowak, Molecular mechanisms of muscular dystrophies: old and new players. *Nature Reviews Molecular Cell Biology* **7**, 762-773 (2006).
5. H. Azhary, M. U. Farooq, M. Bhanushali, A. Majid, M. Y. Kassab, Peripheral Neuropathy: Differential Diagnosis and Management. *American Family Physician* **81**, 887-892 (2010).
6. F. Rahimov, L. M. Kunkel, Cellular and molecular mechanisms underlying muscular dystrophy. *Journal of Cell Biology* **201**, 499-510 (2013).
7. J. Kinter, M. Sinnreich, Molecular targets to treat muscular dystrophies. *Swiss Medical Weekly* **144**, (2014).
8. A. J. Steck, A. K. Stalder, S. Renaud, Anti-myelin-associated glycoprotein neuropathy. *Current Opinion in Neurology* **19**, 458-463 (2006).
9. J. D. Brook *et al.*, Molecular basis of myotonic dystrophy: expansion of a trinucleotide (CTG) repeat at the 3' end of a transcript encoding a protein kinase family member. *Cell* **69**, 385-385 (1992).
10. C. L. Liquori *et al.*, Myotonic dystrophy type 2 caused by a CCTG expansion in intron 1 of ZNF9. *Science* **293**, 864-867 (2001).
11. L. Machuca-Tzili, D. Brook, D. Hilton-Jones, Clinical and molecular aspects of the myotonic dystrophies: A review. *Muscle & Nerve* **32**, 1-18 (2005).
12. A. Mankodi *et al.*, Myotonic dystrophy in transgenic mice expressing an expanded CUG repeat. *Science* **289**, 1769-1772 (2000).
13. T. M. Wheeler *et al.*, Reversal of RNA Dominance by Displacement of Protein Sequestered on Triplet Repeat RNA. *Science* **325**, 336-339 (2009).
14. M. Mahadevan *et al.*, MYOTONIC-DYSTROPHY MUTATION - AN UNSTABLE CTG REPEAT IN THE 3' UNTRANSLATED REGION OF THE GENE. *Science* **255**, 1253-1255 (1992).
15. A. Hunter *et al.*, THE CORRELATION OF AGE OF ONSET WITH CTG TRINUCLEOTIDE REPEAT AMPLIFICATION IN MYOTONIC-DYSTROPHY. *Journal of Medical Genetics* **29**, 774-779 (1992).
16. E. B. Gharehbaghi-Schnell, J. Finsterer, I. Korschineck, B. Mamoli, B. R. Binder, Genotype-phenotype correlation in myotonic dystrophy. *Clinical Genetics* **53**, 20-26 (1998).
17. D. G. Monckton, L. J. C. Wong, T. Ashizawa, C. T. Caskey, SOMATIC MOSAICISM, GERMLINE EXPANSIONS, GERMLINE REVERSIONS AND INTERGENERATIONAL REDUCTIONS IN MYOTONIC-DYSTROPHY MALES - SMALL POOL PCR ANALYSES. *Human Molecular Genetics* **4**, 1-8 (1995).
18. I. V. Kovtun, C. T. McMurray, Trinucleotide expansion in haploid germ cells by gap repair. *Nature Genetics* **27**, 407-411 (2001).

19. Y. H. Fu *et al.*, DECREASED EXPRESSION OF MYOTONIN PROTEIN-KINASE MESSENGER-RNA AND PROTEIN IN ADULT FORM OF MYOTONIC-DYSTROPHY. *Science* **260**, 235-238 (1993).
20. S. Reddy *et al.*, Mice lacking the myotonic dystrophy protein kinase develop a late onset progressive myopathy. *Nature Genetics* **13**, 325-335 (1996).
21. G. Jansen *et al.*, Abnormal myotonic dystrophy protein kinase levels produce only mild myopathy in mice. *Nature Genetics* **13**, 316-324 (1996).
22. H. Seznec *et al.*, Mice transgenic for the human myotonic dystrophy region with expanded CTG repeats display muscular and brain abnormalities. *Human Molecular Genetics* **10**, 2717-2726 (2001).
23. M. Gomes-Pereira, T. A. Cooper, G. Gourdon, Myotonic dystrophy mouse models: towards rational therapy development. *Trends in Molecular Medicine* **17**, 506-517 (2011).
24. J. W. Miller *et al.*, Recruitment of human muscleblind proteins to (CUG)(n) expansions associated with myotonic dystrophy. *Embo Journal* **19**, 4439-4448 (2000).
25. Y. Yuan *et al.*, Muscleblind-like 1 interacts with RNA hairpins in splicing target and pathogenic RNAs. *Nucleic Acids Research* **35**, 5474-5486 (2007).
26. B. M. Davis, M. E. McCurrach, K. L. Taneja, R. H. Singer, D. E. Housman, Expansion of a CUG trinucleotide repeat in the 3' untranslated region of myotonic dystrophy protein kinase transcripts results in nuclear retention of transcripts. *Proceedings of the National Academy of Sciences of the United States of America* **94**, 7388-7393 (1997).
27. K. L. Taneja, M. McCurrach, M. Schalling, D. Housman, R. H. Singer, FOCI OF TRINUCLEOTIDE REPEAT TRANSCRIPTS IN NUCLEI OF MYOTONIC-DYSTROPHY CELLS AND TISSUES. *Journal of Cell Biology* **128**, 995-1002 (1995).
28. A. Mankodi *et al.*, Ribonuclear inclusions in skeletal muscle in myotonic dystrophy types 1 and 2. *Annals of Neurology* **54**, 760-768 (2003).
29. A. Mankodi *et al.*, Expanded CUG repeats trigger aberrant splicing of CIC-1 chloride channel pre-mRNA and hyperexcitability of skeletal muscle in myotonic dystrophy. *Molecular Cell* **10**, 35-44 (2002).
30. N. Charlet-B *et al.*, Loss of the muscle-specific chloride channel in type 1 myotonic dystrophy due to misregulated alternative splicing. *Molecular Cell* **10**, 45-53 (2002).
31. Y. Kino *et al.*, MBNL and CELF proteins regulate alternative splicing of the skeletal muscle chloride channel CLCN1. *Nucleic Acids Research* **37**, 6477-6490 (2009).
32. R. S. Savkur, A. V. Philips, T. A. Cooper, Aberrant regulation of insulin receptor alternative splicing is associated with insulin resistance in myotonic dystrophy. *Nature Genetics* **29**, 40-47 (2001).
33. W. Dansithong, S. Paul, L. Comai, S. Reddy, MBNL1 is the primary determinant of focus formation and aberrant insulin receptor splicing in DM1. *Journal of Biological Chemistry* **280**, 5773-5780 (2005).
34. S.-i. Hino *et al.*, Molecular mechanisms responsible for aberrant splicing of SERCA1 in myotonic dystrophy type 1. *Human Molecular Genetics* **16**, 2834-2843 (2007).
35. T. H. Ho *et al.*, Muscleblind proteins regulate alternative splicing. *Embo Journal* **23**, 3103-3112 (2004).
36. J. D. Lueck *et al.*, Chloride channelopathy in myotonic dystrophy resulting from loss of posttranscriptional regulation for CLCN1. *American Journal of Physiology-Cell Physiology* **292**, C1291-C1297 (2007).
37. R. N. Kanadia *et al.*, A muscleblind knockout model for myotonic dystrophy. *Science* **302**, 1978-1980 (2003).

38. R. N. Kanadia *et al.*, Reversal of RNA missplicing and myotonia after muscleblind overexpression in a mouse poly(CUG) model for myotonic dystrophy. *Proceedings of the National Academy of Sciences of the United States of America* **103**, 11748-11753 (2006).
39. X. Y. Lin *et al.*, Failure of MBNL1-dependent post-natal splicing transitions in myotonic dystrophy. *Human Molecular Genetics* **15**, 2087-2097 (2006).
40. D. L. Black, Mechanisms of alternative pre-messenger RNA splicing. *Annual Review of Biochemistry* **72**, 291-336 (2003).
41. N. M. Kuyumcu-Martinez, G.-S. Wang, T. A. Cooper, Increased steady-state in levels of CUGBP1 in myotonic dystrophy 1 are due to PKC-mediated hyperphosphorylation. *Molecular Cell* **28**, 68-78 (2007).
42. T. Yamamoto *et al.*, Long-term treatment of diabetes mellitus in myotonic dystrophy with pioglitazone. *Rinsho shinkeigaku = Clinical neurology* **45**, 287-292 (2005).
43. M. S. Damian, A. Gerlach, F. Schmidt, E. Lehmann, H. Reichmann, Modafinil for excessive daytime sleepiness in myotonic dystrophy. *Neurology* **56**, 794-796 (2001).
44. D. Furling *et al.*, Viral vector producing antisense RNA restores myotonic dystrophy myoblast functions. *Gene Therapy* **10**, 795-802 (2003).
45. M. A. Langlois *et al.*, Cytoplasmic and nuclear retained DMPK mRNAs are targets for RNA interference in myotonic dystrophy cells. *Journal of Biological Chemistry* **280**, 16949-16954 (2005).
46. A. J. Leger *et al.*, Systemic Delivery of a Peptide-Linked Morpholino Oligonucleotide Neutralizes Mutant RNA Toxicity in a Mouse Model of Myotonic Dystrophy. *Molecular Therapy* **21**, S175-S175 (2013).
47. J. E. Lee, C. F. Bennett, T. A. Cooper, RNase H-mediated degradation of toxic RNA in myotonic dystrophy type 1. *Proceedings of the National Academy of Sciences of the United States of America* **109**, 4221-4226 (2012).
48. T. M. Wheeler *et al.*, Targeting nuclear RNA for in vivo correction of myotonic dystrophy. *Nature* **488**, 111-+ (2012).
49. M. A. Langlois, N. S. Lee, J. J. Rossi, J. Puymirat, Hammerhead ribozyme-mediated destruction of nuclear foci in myotonic dystrophy myoblasts. *Molecular Therapy* **7**, 670-680 (2003).
50. W. Zhang *et al.*, Treatment of Type 1 Myotonic Dystrophy by Engineering Site-specific RNA Endonucleases that Target (CUG)(n) Repeats. *Molecular Therapy* **22**, 312-320 (2014).
51. M. B. Warf, M. Nakamori, C. M. Matthys, C. A. Thornton, J. A. Berglund, Pentamidine reverses the splicing defects associated with myotonic dystrophy. *Proceedings of the National Academy of Sciences of the United States of America* **106**, 18551-18556 (2009).
52. J. F. Arambula, S. R. Ramisetty, A. M. Baranger, S. C. Zimmerman, A simple ligand that selectively targets CUG trinucleotide repeats and inhibits MBNL protein binding. *Proceedings of the National Academy of Sciences of the United States of America* **106**, 16068-16073 (2009).
53. A. Pushechnikov *et al.*, Rational Design of Ligands Targeting Triplet Repeating Transcripts That Cause RNA Dominant Disease: Application to Myotonic Muscular Dystrophy Type 1 and Spinocerebellar Ataxia Type 3. *Journal of the American Chemical Society* **131**, 9767-9779 (2009).
54. J. L. Childs-Disney, J. Hoskins, S. G. Rzuczek, C. A. Thornton, M. D. Disney, Rationally Designed Small Molecules Targeting the RNA That Causes Myotonic Dystrophy Type 1 Are Potently Bioactive. *Acs Chemical Biology* **7**, 856-862 (2012).
55. P. C. Gareiss *et al.*, Dynamic Combinatorial Selection of Molecules Capable of Inhibiting the (CUG) Repeat RNA-MBNL1 Interaction In Vitro: Discovery of Lead

- Compounds Targeting Myotonic Dystrophy (DM1). *Journal of the American Chemical Society* **130**, 16254-16261 (2008).
56. L. O. Ofori, J. Hoskins, M. Nakamori, C. A. Thornton, B. L. Miller, From dynamic combinatorial 'hit' to lead: in vitro and in vivo activity of compounds targeting the pathogenic RNAs that cause myotonic dystrophy. *Nucleic Acids Research* **40**, 6380-6390 (2012).
57. J. W. Hoskins *et al.*, Lomofungin and dilomofungin: inhibitors of MBNL1-CUG RNA binding with distinct cellular effects. *Nucleic acids research* **42**, 6591-6602 (2014).
58. C. Z. Chen *et al.*, Two high-throughput screening assays for aberrant RNA-protein interactions in myotonic dystrophy type 1. *Analytical and Bioanalytical Chemistry* **402**, 1889-1898 (2012).
59. L. A. Coonrod *et al.*, Reducing Levels of Toxic RNA with Small Molecules. *Acs Chemical Biology* **8**, 2528-2537 (2013).
60. A. Ketley *et al.*, High-content screening identifies small molecules that remove nuclear foci, affect MBNL distribution and CELF1 protein levels via a PKC-independent pathway in myotonic dystrophy cell lines. *Human Molecular Genetics* **23**, 1551-1562 (2014).
61. C. Wei, K. Jones, N. A. Timchenko, L. Timchenko, GSK3beta is a new therapeutic target for myotonic dystrophy type 1. *Rare diseases (Austin, Tex.)* **1**, e26555-e26555 (2013).
62. K. Oana *et al.*, Manumycin A corrects aberrant splicing of Clcn1 in myotonic dystrophy type 1 (DM1) mice. *Scientific Reports* **3**, (2013).
63. J. R. Thomas, P. J. Hergenrother, Targeting RNA with small molecules. *Chemical Reviews* **108**, 1171-1224 (2008).
64. A. V. Philips, L. T. Timchenko, T. A. Cooper, Disruption of splicing regulated by a CUG-binding protein in myotonic dystrophy. *Science* **280**, 737-741 (1998).
65. J. Berg, H. Jiang, C. A. Thornton, S. C. Cannon, Truncated CIC-1 mRNA in myotonic dystrophy exerts a dominant-negative effect on the Cl current. *Neurology* **63**, 2371-2375 (2004).
66. W. J. Krzyzosiak *et al.*, Triplet repeat RNA structure and its role as pathogenic agent and therapeutic target. *Nucleic Acids Research* **40**, 11-26 (2012).
67. M. Wojciechowska, K. Taylor, K. Sobczak, M. Napierala, W. J. Krzyzosiak, Small molecule kinase inhibitors alleviate different molecular features of myotonic dystrophy type 1. *RNA biology* **11**, (2014).
68. F. E. Koehn, G. T. Carter, The evolving role of natural products in drug discovery. *Nature Reviews Drug Discovery* **4**, 206-220 (2005).
69. O. Potterat, M. Hamburger, Combined Use of Extract Libraries and HPLC-Based Activity Profiling for Lead Discovery: Potential, Challenges, and Practical Considerations. *Planta Med* **80**, 1171-1181 (2014).
70. R. A. Collins, T. B. Ng, W. P. Fong, C. C. Wan, H. W. Yeung, Removal of polyphenolic compounds from aqueous plant extracts using polyamide minicolumns. *Biochemistry and Molecular Biology International* **45**, 791-796 (1998).
71. S. Chaouch *et al.*, Immortalized Skin Fibroblasts Expressing Conditional MyoD as a Renewable and Reliable Source of Converted Human Muscle Cells to Assess Therapeutic Strategies for Muscular Dystrophies: Validation of an Exon-Skipping Approach to Restore Dystrophin in Duchenne Muscular Dystrophy Cells. *Human Gene Therapy* **20**, 784-790 (2009).
72. A. Mykowska, K. Sobczak, M. Wojciechowska, P. Kozlowski, W. J. Krzyzosiak, CAG repeats mimic CUG repeats in the misregulation of alternative splicing. *Nucleic Acids Research* **39**, 8938-8951 (2011).

73. D. N. Wilson, Ribosome-targeting antibiotics and mechanisms of bacterial resistance. *Nature Reviews Microbiology* **12**, 35-48 (2014).
74. M. M. Islam, S. R. Chowdhury, G. S. Kumar, Spectroscopic and Calorimetric Studies on the Binding of Alkaloids Berberine, Palmatine and Coralyne to Double Stranded RNA Polynucleotides. *Journal of Physical Chemistry B* **113**, 1210-1224 (2009).
75. G. S. Kumar, RNA targeting by small molecules: Binding of protoberberine, benzophenanthridine and aristolochia alkaloids to various RNA structures. *Journal of Biosciences* **37**, 539-552 (2012).
76. S. Nafisi, Z. M. Malekabad, M. A. Khalilzadeh, Interaction of beta-Carboline Alkaloids with RNA. *DNA and Cell Biology* **29**, 753-761 (2010).
77. O. P. Cetinkol, N. V. Hud, Molecular recognition of poly(A) by small ligands: an alternative method of analysis reveals nanomolar, cooperative and shape-selective binding. *Nucleic Acids Research* **37**, 611-621 (2009).
78. M. B. Warf, J. A. Berglund, MBNL binds similar RNA structures in the CUG repeats of myotonic dystrophy and its pre-mRNA substrate cardiac troponin T. *Rna-a Publication of the Rna Society* **13**, 2238-2251 (2007).
79. Y. B. Guan, E. D. Louis, W. Zheng, Toxicokinetics of tremorogenic natural products, harmine and harmaline, in male Sprague-Dawley rats. *Journal of Toxicology and Environmental Health-Part A* **64**, 645-660 (2001).
80. J. Lutes, J. F. Lorden, M. Beales, G. A. Oltmans, TOLERANCE TO THE TREMOROGENIC EFFECTS OF HARMALINE - EVIDENCE FOR ALTERED OLIVO-CEREBELLAR FUNCTION. *Neuropharmacology* **27**, 849-855 (1988).
81. N. Turner *et al.*, Berberine and its more biologically available derivative, dihydroberberine, inhibit mitochondrial respiratory complex I: A mechanism for the action of berberine to activate AMP-Activated protein kinase and improve insulin action. *Diabetes* **57**, 1414-1418 (2008).
82. J.-F. Jiang *et al.*, Novel Effect of Berberine on Thermoregulation in Mice Model Induced by Hot and Cold Environmental Stimulation. *Plos One* **8**, (2013).
83. Y. S. Lee *et al.*, Berberine, a natural plant product, activates AMP-activated protein kinase with beneficial metabolic effects in diabetic and insulin-resistant states. *Diabetes* **55**, 2256-2264 (2006).
84. N. Goeckler *et al.*, Harmine specifically inhibits protein kinase DYRK1A and interferes with neurite formation. *Febs Journal* **276**, 6324-6337 (2009).
85. S. S. Lee, M. Kai, M. K. Lee, Effects of natural isoquinoline alkaloids on monoamine oxidase activity in mouse brain: inhibition by berberine and palmatine. *Medical Science Research* **27**, 749-751 (1999).
86. T. Herraiz, D. Gonzalez, C. Ancin-Azpilicueta, V. J. Aran, H. Guillen, beta-Carboline alkaloids in *Peganum harmala* and inhibition of human monoamine oxidase (MAO). *Food and Chemical Toxicology* **48**, 839-845 (2010).
87. Y. N. Zhao *et al.*, A new approach to investigate the pharmacokinetics of Traditional Chinese Medicine YL2000. *American Journal of Chinese Medicine* **32**, 921-929 (2004).
88. G. Zetler, G. Back, H. Iven, PHARMACOKINETICS IN RAT OF HALLUCINOGENIC ALKALOIDS HARMINE AND HARMALINE. *Naunyn-Schmiedebergs Archives of Pharmacology* **285**, 273-292 (1974).
89. I. Dimauro, T. Pearson, D. Caporossi, M. J. Jackson, A simple protocol for the subcellular fractionation of skeletal muscle cells and tissue. *BMC research notes* **5**, 513-513 (2012).
90. M. M. Lee *et al.*, Controlling the Specificity of Modularly Assembled Small Molecules for RNA via Ligand Module Spacing: Targeting the RNAs That Cause

- Myotonic Muscular Dystrophy. *Journal of the American Chemical Society* **131**, 17464-17472 (2009).
91. A. Garcia-Lopez, B. Llamusi, M. Orzaez, E. Perez-Paya, R. D. Artero, In vivo discovery of a peptide that prevents CUG-RNA hairpin formation and reverses RNA toxicity in myotonic dystrophy models. *Proceedings of the National Academy of Sciences of the United States of America* **108**, 11866-11871 (2011).
 92. R. Parkesh *et al.*, Design of a Bioactive Small Molecule That Targets the Myotonic Dystrophy Type 1 RNA via an RNA Motif-Ligand Database and Chemical Similarity Searching. *Journal of the American Chemical Society* **134**, 4731-4742 (2012).
 93. W. D. Wilson, L. Ratmeyer, M. Zhao, L. Strekowski, D. Boykin, THE SEARCH FOR STRUCTURE-SPECIFIC NUCLEIC-ACID INTERACTIVE DRUGS - EFFECTS OF COMPOUND STRUCTURE ON RNA VERSUS DNA INTERACTION STRENGTH. *Biochemistry* **32**, 4098-4104 (1993).
 94. D. A. Patrick *et al.*, Anti-Pneumocystic carinii pneumonia activity of dicationic carbazoles. *European Journal of Medicinal Chemistry* **32**, 781-793 (1997).
 95. A. Kumar, M. Say, D. W. Boykin, Synthesis of new substituted 2-(trimethylstannyl)indoles. *Synthesis-Stuttgart*, 707-710 (2008).
 96. J. Bezencon *et al.*, pK(a) determination by H-1 NMR spectroscopy - An old methodology revisited. *Journal of Pharmaceutical and Biomedical Analysis* **93**, 147-155 (2014).
 97. M. Kansy, F. Senner, K. Gubernator, Physicochemical high throughput screening: Parallel artificial membrane permeation assay in the description of passive absorption processes. *Journal of Medicinal Chemistry* **41**, 1007-1010 (1998).
 98. L. Sanderson, M. Dogruel, J. Rodgers, H. P. De Koning, S. A. Thomas, Pentamidine Movement across the Murine Blood-Brain and Blood-Cerebrospinal Fluid Barriers: Effect of Trypanosome Infection, Combination Therapy, P-Glycoprotein, and Multidrug Resistance-Associated Protein. *Journal of Pharmacology and Experimental Therapeutics* **329**, 967-977 (2009).
 99. L. R. Guan, M. D. Disney, Recent Advances in Developing Small Molecules Targeting RNA. *Acs Chemical Biology* **7**, 73-86 (2012).
 100. M. Zhao *et al.*, SMALL CHANGES IN CATIONIC SUBSTITUENTS OF DIPHENYLFURAN DERIVATIVES HAVE MAJOR EFFECTS ON THE BINDING-AFFINITY AND THE BINDING MODE WITH RNA HELICAL DUPLEXES. *Bioorganic & Medicinal Chemistry* **3**, 785-794 (1995).
 101. M. N. C. Soeiro *et al.*, Novel amidines and analogues as promising agents against intracellular parasites: a systematic review. *Parasitology* **140**, 929-951 (2013).
 102. L. Pang *et al.*, FimH Antagonists: Structure-Activity and Structure-Property Relationships for Biphenyl α -D-Mannopyranosides. *Chemmedchem* **7**, 1404-1422 (2012).
 103. M. W. Pantoliano *et al.*, High-density miniaturized thermal shift assays as a general strategy for drug discovery. *Journal of Biomolecular Screening* **6**, 429-440 (2001).
 104. E. S. Goers, J. Purcell, R. B. Voelker, D. P. Gates, J. A. Berglund, MBNL1 binds GC motifs embedded in pyrimidines to regulate alternative splicing. *Nucleic Acids Research* **38**, 2467-2484 (2010).
 105. Z. Yong, H. Meirong, Z. Jianping, X. Shaofei, PKSolver: an add-in program for pharmacokinetic and pharmacodynamic data analysis in Microsoft Excel. *Computer Methods and Programs in Biomedicine* **99**, 306-314 (2010).
 106. M. C. Dalakas, Pathogenesis and Treatment of Anti-MAG Neuropathy. *Current Treatment Options in Neurology* **12**, 71-83 (2010).
 107. V. Chaudhry, M. Swash, Multifocal motor neuropathy - Is conduction block essential? *Neurology* **67**, 558-559 (2006).

108. E. Nobile-Orazio, Antigenic Determinants in IgM Paraprotein-Related Neuropathies. *Clinical Lymphoma & Myeloma* **9**, 107-109 (2009).
109. J. Kriangkum *et al.*, Clonotypic IgM V/D/J sequence analysis in Waldenstrom macroglobulinemia suggests an unusual B-cell origin and an expansion of polyclonal B cells in peripheral blood. *Blood* **104**, 2134-2142 (2004).
110. M. A. Maurer *et al.*, Rituximab induces sustained reduction of pathogenic B cells in patients with peripheral nervous system autoimmunity. *Journal of Clinical Investigation* **122**, 1393-1402 (2012).
111. A. Steck, N. Yuki, F. Graus, Antibody testing in peripheral nerve disorders. *Handbook of clinical neurology* **115**, 189-212 (2013).
112. M. C. Dalakas, Clinical trials in CIDP and chronic autoimmune demyelinating polyneuropathies. *Journal of the Peripheral Nervous System* **17**, 34-39 (2012).
113. R. A. Kyle, J. P. Garton, THE SPECTRUM OF IGM MONOCLONAL GAMMOPATHY IN 430 CASES. *Mayo Clinic Proceedings* **62**, 719-731 (1987).
114. E. Nobileorazio *et al.*, PERIPHERAL NEUROPATHY IN MONOCLONAL GAMMOPATHY OF UNDETERMINED SIGNIFICANCE - PREVALENCE AND IMMUNOPATHOGENETIC STUDIES. *Acta Neurologica Scandinavica* **85**, 383-390 (1992).
115. R. A. Kyle, S. V. Rajkumar, Monoclonal gammopathies of undetermined significance: a review. *Immunological Reviews* **194**, 112-139 (2003).
116. E. Nobileorazio *et al.*, FREQUENCY AND CLINICAL CORRELATES OF ANTI-NEURAL IGM ANTIBODIES IN NEUROPATHY ASSOCIATED WITH IGM MONOCLONAL GAMMOPATHY. *Annals of Neurology* **36**, 416-424 (1994).
117. P. E. Braun, D. E. Frail, N. Latov, MYELIN-ASSOCIATED GLYCOPROTEIN IS THE ANTIGEN FOR A MONOCLONAL IGM IN POLYNEUROPATHY. *Journal of Neurochemistry* **39**, 1261-1265 (1982).
118. A. J. Steck, N. Murray, C. Meier, N. Page, G. Perruisseau, DEMYELINATING NEUROPATHY AND MONOCLONAL IGM ANTIBODY TO MYELIN-ASSOCIATED GLYCOPROTEIN. *Neurology* **33**, 19-23 (1983).
119. T. Abo, C. M. Balch, A DIFFERENTIATION ANTIGEN OF HUMAN NK-CELLS AND K-CELLS IDENTIFIED BY A MONOCLONAL-ANTIBODY (HNK-1). *Journal of Immunology* **127**, 1024-1029 (1981).
120. R. C. McGarry, S. L. Helfand, R. H. Quarles, J. C. Roder, RECOGNITION OF MYELIN-ASSOCIATED GLYCOPROTEIN BY THE MONOCLONAL-ANTIBODY HNK-1. *Nature* **306**, 376-378 (1983).
121. A. A. Ilyas *et al.*, IGM IN A HUMAN NEUROPATHY RELATED TO PARAPROTEINEMIA BINDS TO A CARBOHYDRATE DETERMINANT IN THE MYELIN-ASSOCIATED GLYCOPROTEIN AND TO A GANGLIOSIDE. *Proceedings of the National Academy of Sciences of the United States of America-Biological Sciences* **81**, 1225-1229 (1984).
122. K. H. Chou, A. A. Ilyas, J. E. Evans, R. H. Quarles, F. B. Jungalwala, STRUCTURE OF A GLYCOLIPID REACTING WITH MONOCLONAL IGM IN NEUROPATHY AND WITH HNK-1. *Biochemical and Biophysical Research Communications* **128**, 383-388 (1985).
123. D. K. H. Chou *et al.*, STRUCTURE OF SULFATED GLUCURONYL GLYCOLIPIDS IN THE NERVOUS-SYSTEM REACTING WITH HNK-1 ANTIBODY AND SOME IGM PARAPROTEINS IN NEUROPATHY. *Journal of Biological Chemistry* **261**, 1717-1725 (1986).
124. T. Ariga *et al.*, CHARACTERIZATION OF SULFATED GLUCURONIC-ACID CONTAINING GLYCOLIPIDS REACTING WITH IGM M-PROTEINS IN

- PATIENTS WITH NEUROPATHY. *Journal of Biological Chemistry* **262**, 848-853 (1987).
125. H. Voshol, W. E. M. vanZuylen, G. Orberger, J. F. G. Vliegthart, M. Schachner, Structure of the HNK-1 carbohydrate epitope on bovine peripheral myelin glycoprotein P0. *Journal of Biological Chemistry* **271**, 22957-22960 (1996).
126. R. H. Quarles, Myelin-associated glycoprotein (MAG): past, present and beyond. *Journal of Neurochemistry* **100**, 1431-1448 (2007).
127. F. Fluri, F. Ferracin, B. Erne, A. J. Steck, Microheterogeneity of anti-myelin-associated glycoprotein antibodies. *Journal of the Neurological Sciences* **207**, 43-49 (2003).
128. A. A. Ilyas, D. K. H. Chou, F. B. Jungalwala, C. Costello, R. H. Quarles, VARIABILITY IN THE STRUCTURAL REQUIREMENTS FOR BINDING OF HUMAN MONOCLONAL ANTI-MYELIN-ASSOCIATED GLYCOPROTEIN IMMUNOGLOBULIN-M ANTIBODIES AND HNK-1 TO SPHINGOGLYCOLIPID ANTIGENS. *Journal of Neurochemistry* **55**, 594-601 (1990).
129. B. Schmitz, M. Schachner, Y. Ito, T. Nakano, T. Ogawa, DETERMINATION OF STRUCTURAL ELEMENTS OF THE L2/HNK-1 CARBOHYDRATE EPITOPE REQUIRED FOR ITS FUNCTION. *Glycoconjugate Journal* **11**, 345-352 (1994).
130. A. Tokuda *et al.*, On the specificity of anti-sulfoglucuronosyl glycolipid antibodies'. *Journal of Carbohydrate Chemistry* **17**, 535-546 (1998).
131. N. Page, N. Murray, G. Perruisseau, A. J. Steck, A MONOCLONAL ANTI-IDIOTYPIC ANTIBODY AGAINST A HUMAN MONOCLONAL IGM WITH SPECIFICITY FOR MYELIN-ASSOCIATED GLYCOPROTEIN. *Journal of Immunology* **134**, 3094-3099 (1985).
132. R. Lombardi *et al.*, IgM deposits on skin nerves in anti-myelin-associated glycoprotein neuropathy. *Annals of Neurology* **57**, 180-187 (2005).
133. M. Takatsu *et al.*, IMMUNOFLUORESCENCE STUDY OF PATIENTS WITH NEUROPATHY AND IGM M-PROTEINS. *Annals of Neurology* **18**, 173-181 (1985).
134. A. Vital, C. Vital, J. Julien, A. Baquey, A. J. Steck, POLYNEUROPATHY ASSOCIATED WITH IGM MONOCLONAL GAMMOPATHY - IMMUNOLOGICAL AND PATHOLOGICAL-STUDY IN 31 PATIENTS. *Acta Neuropathologica* **79**, 160-167 (1989).
135. J. R. Mendell *et al.*, POLYNEUROPATHY AND IGM MONOCLONAL GAMMOPATHY - STUDIES ON THE PATHOGENETIC ROLE OF ANTI-MYELIN-ASSOCIATED GLYCOPROTEIN ANTIBODY. *Annals of Neurology* **17**, 243-254 (1985).
136. A. P. Hays, S. S. L. Lee, N. Latov, IMMUNE REACTIVE C3D ON THE SURFACE OF MYELIN SHEATHS IN NEUROPATHY. *Journal of Neuroimmunology* **18**, 231-244 (1988).
137. S. Monaco *et al.*, COMPLEMENT-MEDIATED DEMYELINATION IN PATIENTS WITH IGM MONOCLONAL GAMMOPATHY AND POLYNEUROPATHY. *New England Journal of Medicine* **322**, 649-652 (1990).
138. E. Nobileorazio *et al.*, TREATMENT OF PATIENTS WITH NEUROPATHY AND ANTI-MAG IGM M-PROTEINS. *Annals of Neurology* **24**, 93-97 (1988).
139. D. C. Haas, A. H. Tatum, PLASMAPHERESIS ALLEVIATES NEUROPATHY ACCOMPANYING IGM ANTI-MYELIN-ASSOCIATED GLYCOPROTEIN PARAPROTEINEMIA. *Annals of Neurology* **23**, 394-396 (1988).
140. S. Renaud *et al.*, Rituximab in the treatment of polyneuropathy associated with anti-MAG antibodies. *Muscle & Nerve* **27**, 611-615 (2003).
141. A. Pestronk *et al.*, Treatment of IgM antibody associated polyneuropathies using rituximab. *Journal of Neurology Neurosurgery and Psychiatry* **74**, 485-489 (2003).

142. L. Benedetti *et al.*, Predictors of response to rituximab in patients with neuropathy and anti-myelin associated glycoprotein immunoglobulin M. *Journal of the Peripheral Nervous System* **12**, 102-107 (2007).
143. A. P. Hays, N. Latov, M. Takatsu, W. H. Sherman, EXPERIMENTAL DEMYELINATION OF NERVE INDUCED BY SERUM OF PATIENTS WITH NEUROPATHY AND AN ANTI-MAG IGM M-PROTEIN. *Neurology* **37**, 242-256 (1987).
144. H. J. Willison *et al.*, DEMYELINATION INDUCED BY INTRANEURAL INJECTION OF HUMAN ANTIMYELIN-ASSOCIATED GLYCOPROTEIN ANTIBODIES. *Muscle & Nerve* **11**, 1169-1176 (1988).
145. A. H. Tatum, EXPERIMENTAL PARAPROTEIN NEUROPATHY, DEMYELINATION BY PASSIVE TRANSFER OF HUMAN-IGM ANTI-MYELIN-ASSOCIATED GLYCOPROTEIN. *Annals of Neurology* **33**, 502-506 (1993).
146. W. Trojaborg *et al.*, ELECTROPHYSIOLOGIC STUDY OF EXPERIMENTAL DEMYELINATION INDUCED BY SERUM OF PATIENTS WITH IGM-M PROTEINS AND NEUROPATHY. *Neurology* **39**, 1581-1586 (1989).
147. A. A. Ilyas, Y. Gu, M. C. Dalakas, R. H. Quarles, S. Bhatt, Induction of experimental ataxic sensory neuronopathy in cats by immunization with purified SGPG. *Journal of Neuroimmunology* **193**, 87-93 (2008).
148. S. Kelm *et al.*, SIALOADHESIN, MYELIN-ASSOCIATED GLYCOPROTEIN AND CD22 DEFINE A NEW FAMILY OF SIALIC ACID-DEPENDENT ADHESION MOLECULES OF THE IMMUNOGLOBULIN SUPERFAMILY. *Current Biology* **4**, 965-972 (1994).
149. P. R. Crocker *et al.*, Siglecs: a family of sialic-acid binding lectins. *Glycobiology* **8**, v (1998).
150. R. O. Brady, R. H. Quarles, DEVELOPMENTAL AND PATHOPHYSIOLOGICAL ASPECTS OF THE MYELIN-ASSOCIATED GLYCOPROTEIN. *Cellular and Molecular Neurobiology* **8**, 139-148 (1988).
151. S. Sato *et al.*, CDNA CLONING AND AMINO-ACID SEQUENCE FOR HUMAN MYELIN-ASSOCIATED GLYCOPROTEIN. *Biochemical and Biophysical Research Communications* **163**, 1473-1480 (1989).
152. G. Spagnol *et al.*, MOLECULAR-CLONING OF HUMAN MYELIN-ASSOCIATED GLYCOPROTEIN. *Journal of Neuroscience Research* **24**, 137-142 (1989).
153. M. Ogino, A. H. Tatum, N. Latov, AFFINITY STUDIES OF HUMAN ANTI-MAG ANTIBODIES IN NEUROPATHY. *Journal of Neuroimmunology* **52**, 41-46 (1994).
154. N. H. Sternberger, R. H. Quarles, Y. Itoyama, H. D. Webster, MYELIN-ASSOCIATED GLYCOPROTEIN DEMONSTRATED IMMUNOCYTOCHEMICALLY IN MYELIN AND MYELIN-FORMING CELLS OF DEVELOPING RAT. *Proceedings of the National Academy of Sciences of the United States of America* **76**, 1510-1514 (1979).
155. M. Arquint *et al.*, MOLECULAR-CLONING AND PRIMARY STRUCTURE OF MYELIN-ASSOCIATED GLYCOPROTEIN. *Proceedings of the National Academy of Sciences of the United States of America* **84**, 600-604 (1987).
156. C. Lai *et al.*, 2 FORMS OF 1B236 MYELIN-ASSOCIATED GLYCOPROTEIN, A CELL-ADHESION MOLECULE FOR POSTNATAL NEURAL DEVELOPMENT, ARE PRODUCED BY ALTERNATIVE SPLICING. *Proceedings of the National Academy of Sciences of the United States of America* **84**, 4337-4341 (1987).
157. J. L. Salzer, W. P. Holmes, D. R. Colman, THE AMINO-ACID-SEQUENCES OF THE MYELIN-ASSOCIATED GLYCOPROTEINS - HOMOLOGY TO THE IMMUNOGLOBULIN GENE SUPERFAMILY. *Journal of Cell Biology* **104**, 957-965 (1987).

158. M. Erb *et al.*, Unraveling the differential expression of the two isoforms of myelin-associated glycoprotein in a mouse expressing GFP-tagged S-MAG specifically regulated and targeted into the different myelin compartments. *Molecular and Cellular Neuroscience* **31**, 613-627 (2006).
159. P. Kursula, V. P. Lehto, A. M. Heape, The small myelin-associated glycoprotein binds to tubulin and microtubules. *Brain Res Mol Brain Res* **87**, 22-30 (2001).
160. B. D. Trapp, S. B. Andrews, A. Wong, M. Oconnell, J. W. Griffin, CO-LOCALIZATION OF THE MYELIN-ASSOCIATED GLYCOPROTEIN AND THE MICROFILAMENT COMPONENTS, F-ACTIN AND SPECTRIN, IN SCHWANN-CELLS OF MYELINATED NERVE-FIBERS. *Journal of Neurocytology* **18**, 47-60 (1989).
161. M. P. T. Lunn, T. O. Crawford, R. A. C. Hughes, J. W. Griffin, K. A. Sheikh, Anti-myelin-associated glycoprotein antibodies alter neurofilament spacing. *Brain* **125**, 904-911 (2002).
162. X. H. Yin *et al.*, Myelin-associated glycoprotein is a myelin signal that modulates the caliber of myelinated axons. *Journal of Neuroscience* **18**, 1953-1962 (1998).
163. M. D. Weiss, C. A. Luciano, R. H. Quarles, Nerve conduction abnormalities in aging mice deficient for myelin-associated glycoprotein. *Muscle & Nerve* **24**, 1380-1387 (2001).
164. M. Schachner, U. Bartsch, Multiple functions of the myelin-associated glycoprotein MAG (siglec-4a) in formation and maintenance of myelin. *Glia* **29**, 154-165 (2000).
165. Z. Cai *et al.*, Focal myelin swellings and tomacula in anti-MAG IgM paraproteinaemic neuropathy: Novel teased nerve fiber studies. *Journal of the Peripheral Nervous System* **6**, 95-101 (2001).
166. J. M. Gabriel *et al.*, Confocal microscopic localization of anti-myelin-associated glycoprotein autoantibodies in a patient with peripheral neuropathy initially lacking a detectable IgM gammopathy. *Acta Neuropathologica* **95**, 540-546 (1998).
167. J. M. Gabriel *et al.*, Selective loss of myelin-associated glycoprotein from myelin correlates with anti-MAG antibody titre in demyelinating paraproteinaemic polyneuropathy. *Brain* **119**, 775-787 (1996).
168. H. C. Wilson, M. P. T. Lunn, S. Schey, R. A. C. Hughes, Successful treatment of IgM paraproteinaemic neuropathy with fludarabine. *Journal of Neurology Neurosurgery and Psychiatry* **66**, 575-580 (1999).
169. A. Ghosh, T. Littlewood, M. Donaghy, Cladribine in the treatment of IgM paraproteinemic polyneuropathy. *Neurology* **59**, 1290-1291 (2002).
170. G. Blume, A. Pestronk, L. T. Goodnough, ANTI-MAG ANTIBODY-ASSOCIATED POLYNEUROPATHIES - IMPROVEMENT FOLLOWING IMMUNOTHERAPY WITH MONTHLY PLASMA-EXCHANGE AND IV-CYCLOPHOSPHAMIDE. *Neurology* **45**, 1577-1580 (1995).
171. M.-A. Hospital *et al.*, Immunotherapy-based regimen in anti-MAG neuropathy: results in 45 patients. *Haematologica* **98**, E155-E157 (2013).
172. S. P. Treon, How I treat Waldenstrom macroglobulinemia. *Blood* **114**, 2375-2385 (2009).
173. E. Nobile-Orazio, N. Meucci, L. Baldini, A. Di Troia, G. Scarlato, Long-term prognosis of neuropathy associated with anti-MAG IgM M-proteins and its relationship to immune therapies. *Brain* **123**, 710-717 (2000).
174. M. P. T. Lunn, E. Nobile-Orazio, Immunotherapy for IgM anti-myelin-associated glycoprotein paraprotein-associated peripheral neuropathies. *Cochrane Database of Systematic Reviews*, (2012).

175. G. Comi *et al.*, A randomised controlled trial of intravenous immunoglobulin in IgM paraprotein associated demyelinating neuropathy. *Journal of Neurology* **249**, 1370-1377 (2002).
176. X. Mariette *et al.*, A randomised clinical trial comparing interferon-alpha and intravenous immunoglobulin in polyneuropathy associated with monoclonal IgM. *Journal of Neurology Neurosurgery and Psychiatry* **63**, 28-34 (1997).
177. X. Mariette *et al.*, A randomised double blind trial versus placebo does not confirm the benefit of alpha-interferon in polyneuropathy associated with monoclonal IgM. *Journal of Neurology Neurosurgery and Psychiatry* **69**, 279-280 (2000).
178. M. C. Dalakas *et al.*, Placebo-Controlled Trial of Rituximab in IgM Anti-Myelin-Associated Glycoprotein Antibody Demyelinating Neuropathy. *Annals of Neurology* **65**, 286-293 (2009).
179. J.-M. Leger *et al.*, Placebo-controlled trial of rituximab in IgM anti-myelin-associated glycoprotein neuropathy. *Neurology* **80**, 2217-2225 (2013).
180. L. Broglio, G. Lauria, Worsening after rituximab treatment in anti-MAG neuropathy. *Muscle & Nerve* **32**, 378-379 (2005).
181. A. C. J. Stork, N. C. Notermans, A. F. J. E. Vrancken, D. R. Cornblath, W. L. van der Pol, Rapid worsening of IgM anti-MAG demyelinating polyneuropathy during rituximab treatment. *Journal of the Peripheral Nervous System* **18**, 189-191 (2013).
182. M. D. Weiss, P. Becker, PARADOXICAL WORSENING OF ANTI-MYELIN-ASSOCIATED GLYCOPROTEIN POLYNEUROPATHY FOLLOWING RITUXIMAB. *Muscle & Nerve* **49**, 457-458 (2014).
183. F. Belot, A. Otter, M. Fukuda, O. Hindsgaul, Efficient synthesis of two HNK-1 related pentasaccharides. *Synlett*, 1315-1318 (2003).
184. C. Coutant, J. C. Jacquinet, 2-DEOXY-2-TRICHLOROACETAMIDO-D-GLUCOPYRANOSE DERIVATIVES IN OLIGOSACCHARIDE SYNTHESIS - FROM HYALURONIC-ACID TO CHONDROITIN 4-SULFATE TRISACCHARIDES. *Journal of the Chemical Society-Perkin Transactions 1*, 1573-1581 (1995).
185. A. V. Kornilov, A. A. Sherman, L. O. Kononov, A. S. Shashkov, N. E. Nifant'ev, Synthesis of oligosaccharides related to HNK-1 antigen, part 3 - Synthesis of 3-O-sulfoglucuronyl lacto-N-neotetraose 2-aminoethyl glycoside and biotinylated neoglycoconjugates thereof. *Carbohydrate Research* **329**, 717-730 (2000).
186. A. Titz, Z. Radic, O. Schwardt, B. Ernst, A safe and convenient method for the preparation of triflyl azide, and its use in diazo transfer reactions to primary amines. *Tetrahedron Letters* **47**, 2383-2385 (2006).
187. R. Bukowski, L. M. Morris, R. J. Woods, T. Weimar, Synthesis and conformational analysis of the T-antigen disaccharide (beta-D-Gal-(1 -> 3)-alpha-D-GalNAc-OMe). *European Journal of Organic Chemistry*, 2697-2705 (2001).
188. R. O. Duthaler *et al.*, In vivo Neutralization of Naturally Existing Antibodies against Linear alpha(1,3)-Galactosidic Carbohydrate Epitopes by Multivalent Antigen Presentation: A Solution for the First Hurdle of Pig-to-Human Xenotransplantation. *Chimia* **64**, 23-28 (2010).
189. T. Nakano, Y. Ito, T. Ogawa, SYNTHESIS OF SULFATED GLUCURONYL GLYCOSPHINGOLIPIDS - CARBOHYDRATE EPITOPES OF NEURAL CELL-ADHESION MOLECULES. *Carbohydrate Research* **243**, 43-69 (1993).
190. Y. E. Tsvetkov *et al.*, Synthesis and Molecular Recognition Studies of the HNK-1 Trisaccharide and Related Oligosaccharides. The Specificity of Monoclonal Anti-HNK-1 Antibodies as Assessed by Surface Plasmon Resonance and STD NMR. *Journal of the American Chemical Society* **134**, 426-435 (2012).

191. A. Bhunia *et al.*, Why Structurally Different Cyclic Peptides Can Be Glycomimetics of the HNK-1 Carbohydrate Antigen. *Journal of the American Chemical Society* **132**, 96-105 (2010).
192. T. D. Nelson *et al.*, Synthesis of a potent hNIK-1 receptor antagonist via an S(N)2 reaction of an enantiomerically pure alpha-alkoxy sulfonate. *Organic Letters* **7**, 55-58 (2005).
193. B. G. Davis, Recent developments in glycoconjugates. *Journal of the Chemical Society-Perkin Transactions 1*, 3215-3237 (1999).
194. C. T. Oberg, H. Leffler, U. J. Nilsson, Inhibition of Galectins with Small Molecules. *Chimia* **65**, 18-23 (2011).
195. B. Ernst, J. L. Magnani, From carbohydrate leads to glycomimetic drugs. *Nature Reviews Drug Discovery* **8**, 661-677 (2009).
196. G. Thoma *et al.*, Versatile functionalization of polylysine: Synthesis, characterization, and use of neoglycoconjugates. *Journal of the American Chemical Society* **121**, 5919-5929 (1999).
197. G. C. Tucker, M. Delarue, S. Zada, J. C. Boucaut, J. P. Thiery, EXPRESSION OF THE HNK-1/NC-1 EPITOPE IN EARLY VERTEBRATE NEUROGENESIS. *Cell and Tissue Research* **251**, 457-465 (1988).